

Reduced-Rank Tensor-on-Tensor Regression and Tensor-variate Analysis of Variance

Carlos Llosa-Vite and Ranjan Maitra

Abstract

Fitting regression models with many multivariate responses and covariates can be challenging, but such responses and covariates sometimes have tensor-variate structure. We extend the classical multivariate regression model to exploit such structure in two ways: first, we impose four types of low-rank tensor formats on the regression coefficients. Second, we model the errors using the tensor-variate normal distribution that imposes a Kronecker separable format on the covariance matrix. We obtain maximum likelihood estimators via block-relaxation algorithms and derive their computational complexity and asymptotic distributions. Our regression framework enables us to formulate tensor-variate analysis of variance (TANOVA) methodology. This methodology, when applied in a one-way TANOVA layout, enables us to identify cerebral regions significantly associated with the interaction of suicide attempters or non-attemptor ideators and positive-, negative- or death-connoting words in a functional Magnetic Resonance Imaging study. Another application uses three-way TANOVA on the Labeled Faces in the Wild image dataset to distinguish facial characteristics related to ethnic origin, age group and gender.

Index Terms

CP decomposition, HOLQ, HOSVD, Kronecker separable models, LFW dataset, Multilinear statistics, Multiway regression, Random tensors, Suicide ideation, Tensor Train format, Tensor Ring format, Tucker format

I. INTRODUCTION

The classical simple linear regression (SLR) model (without intercept) relates the response variable y_i to the explanatory variable x_i as $y_i = \beta x_i + e_i$ with $\text{Var}(e_i) = \sigma^2$ for $i = 1, 2, \dots, n$, where β is the regression coefficient parameter and σ^2 is the variance parameter. A natural extension of SLR for vector-valued responses and explanatory variables is the multivariate multiple linear regression (MVMLR) model

$$\mathbf{y}_i = B\mathbf{x}_i + \mathbf{e}_i, \quad \text{Var}(\mathbf{e}_i) = \Sigma, \quad (1)$$

where $(\mathbf{y}_1, \mathbf{x}_1), (\mathbf{y}_2, \mathbf{x}_2), \dots, (\mathbf{y}_n, \mathbf{x}_n)$ are vector-valued responses and covariates and (B, Σ) are parameters. The number of parameters relative to the sample size in (1) is greater in the MVMLR model than in its SLR counterpart because the parameters (B, Σ) are matrix-valued [1]. Several methodologies, for example, the lasso and graphical lasso [2], [3], envelope models [4] and reduced rank regression [5], have been proposed to alleviate issues arising from the large number of parameters in (1). However, these methodologies are only for vector-valued observations and do not exploit their underlying structure that may further reduce the number of necessary parameters, in some cases making computation feasible. Here we consider *tensor-* or *array-*structured responses and covariates that arise in many applications, such as the two motivating examples introduced next.

A. Illustrative Examples

1) *Cerebral activity in subjects at risk of suicide:* The United States Center for Disease Control and Prevention reports that 47173 Americans died by suicide in 2017, accounting for about two-thirds of all homicides in that year. Accurate suicide risk assessment is challenging, even for trained mental health professionals, as 78% of patients who commit suicide deny such ideation even in their last communication with professionals [6]. Understanding how subjects at risk of suicide respond to different stimuli is important to guide treatment and therapy. [7] provided data from a functional Magnetic Resonance Imaging (fMRI) study of nine suicide attempters and eight suicide non-attempter ideators (henceforth, ideators) upon exposing them to ten words each with positive, negative or death-related connotations. Our interest is in understanding brain regions associated with the interaction of a subject's attempter/ideator status and word type to inform diagnosis and treatment.

Traditional approaches fit separate regression models at each voxel without regard to spatial context that is only addressed post hoc at the time of inference. A more holistic strategy would use (1) with the response vector \mathbf{y}_i of size $30 \times 43 \times 56 \times 20 = 1444800$, which contains thirty $43 \times 56 \times 20$ image volumes, for each of the $i = 1, 2, \dots, 17$ subjects. The explanatory variable here is a 2D vector that indicates a subject's status as a suicide attempter or ideator. Under this framework, B and Σ have over 2.8 million and 1 trillion unconstrained parameters, making estimation with only 17 subjects impractical. Incorporating a 3D spatial autoregressive (AR) structure into the image volume, and another correlation structure between the words can allow estimation of the variance, but still needs additional methodology to accommodate the large sixth-order tensor-structured regression parameter B . We develop such methodology in this paper, and return to this dataset in Section IV-A.

2) *Distinguishing characteristics of faces*: Distinguishing the visual characteristics of faces is important for biometrics. The Labeled Faces in the Wild (LFW) database [8] is used for developing and testing facial recognition methods, and contains over 13000 250×250 color images of faces of different individuals along with their classification into ethnic origin, age group and gender [9], [10]. We use a subset, totalling 605 images, for which the three attributes of ethnic origin (African, European or Asian, as specified in the database), cohort (child, youth, middle-aged or senior) and gender (male or female) are unambiguous. The color at each pixel is a 3D RGB vector so each image (response) is a $250 \times 250 \times 3$ array. The three image attributes can each be represented by an indicator vector, so the covariates (attributes) have a three-way tensor-variate structure. Our objective is to train a linear model to help us distinguish the visual characteristics of different attributes. Transforming the 3D tensors into vectors and fitting (1) requires a B of $250 \times 250 \times 3 \times 2 \times 3 \times 4$ or 4.5 million unconstrained parameters and an error covariance matrix Σ of over 17 billion similar parameters, making accurate inference (from only 605 observed images) impractical. Methodology that incorporates the reductions afforded by the tensor-variate structures of the responses and the covariates can redeem the situation. We revisit this dataset in Section IV-B.

B. Related work and overview of our contributions

The previous examples show the inadequacy of training (1) on tensor-valued data without additional accommodation for structure, as the sizes of B and Σ in unconstrained vector-variate regression grow with the dimensions of the tensor-valued responses and explanatory variables. Several regression frameworks [11], [12] that efficiently allow for tensor responses [13]–[15] or covariates [16]–[28] have recently been considered. Tensor-on-tensor regression (ToTR) refers to the case where both the response and covariates are tensors. In this context, [13] proposed an outer matrix product (OP) factorization of B , [29] suggested *canonical polyadic* or CANDECOMP/PARAFAC (CP) decomposition [30], [31], while [32] and [33] factorized B using a tensor ring (TR) [34], [35] format. Finally, [36] considered a Tucker (TK) [37]–[39] framework but failed to include necessary constraints in their estimation algorithm. The CP, TR and OP formats on B allow for quantum dimension reduction without affecting prediction or discrimination ability of the regression model. However, these methodologies do not account for dependence within tensor observations, the sampling distribution of their estimated coefficients and the natural connection that exists between ToTR and the related analysis of variance (ANOVA). Here, we propose a general ToTR framework that renders four low-rank tensor formats on the coefficient B : CP, TK, TR and the OP, while simultaneously allowing the errors to follow a *tensor-variate normal (TVN) distribution* [40]–[43] that posits a Kronecker structure on the Σ of (1). Assuming TVN-distributed errors allows us to obtain the sampling distributions of the estimated coefficients under their assumed low-rank format. Indeed, Section IV-A uses our derived sampling distributions to produce statistical parametric maps to help detect significant neurological interactions between death-related words and suicide attempter/ideator status. The TVN assumption on the errors also allows us to consider dependence within the tensor-valued observations. The Kronecker structured Σ in the TVN model renders a different covariance matrix for each tensor dimension, allowing us to simultaneously study multiple dependence contexts within the same framework. Here we also introduce the notion of tensor-variate ANOVA (TANOVA) under the ToTR framework, which is analogous to ANOVA and multivariate ANOVA (MANOVA) being instances of multiple linear regression (MLR) and MVMLR.

The rest of the paper is structured as follows. Section II first presents notations and network diagrams, low-rank tensor formats, the TVN distribution and our preliminary results that we develop for use in this paper. We formulate ToTR and TANOVA methodology with low-rank tensor formats on the covariates, and TVN errors. We provide algorithms for finding maximum likelihood (ML) estimators and study their properties. Section III evaluates performance of our methods in two simulation scenarios while Section IV applies our methodology to the motivating applications of Sections I-A1 and I-A2. We conclude with some discussion. A supplementary appendix with sections, theorems, lemmas, figures and equations prefixed with “S” is also available.

II. THEORY AND METHODS

This section introduces a regression model with TVN errors and tensor-valued responses and covariates. We provide notations and definitions, then introduce our models and develop algorithms for ML estimation under the TK, CP, OP and TR low-rank formats. A special case leads us to TANOVA. We also derive asymptotic properties of our estimators and computational complexity of our algorithms.

A. Background and preliminary results

We provide a unified treatment of tensor reshapings and contractions by integrating the work of [44], [38], and [45] with our own results that we use later. We use $\text{tr}(\cdot)$, $(\cdot)'$, and $(\cdot)^-$ to denote the trace, transpose, and pseudo-inverse, I_n for the $n \times n$ identity matrix and \otimes for the Kronecker product (Section S1 has additional definitions and illustrations). We define tensors as multi-dimensional arrays of numbers. The total number of *modes* or sides of a tensor is called its *order*. We use lower-case letters (*i.e.* x) to specify scalars, bold lower-case italics (*i.e.* \mathbf{x}) for vectors, upper-case italics (*i.e.* \mathbf{X}) for matrices, and calligraphic scripts (*i.e.* \mathcal{X}) for higher-order tensors. Random matrices or vectors are denoted using \mathbf{X} and random tensors

by \mathcal{X} . We denote the (i_1, \dots, i_p) th element of a p th order tensor \mathcal{X} using $\mathcal{X}(i_1, \dots, i_p)$ or $\mathcal{X}(\mathbf{i})$ where $\mathbf{i} = [i_1, \dots, i_p]'$. The vector outer product, with notation \circ , of p vectors generates the p th-order tensor $\mathcal{X} = \circ_{j=1}^p \mathbf{x}_j$ with (i_1, \dots, i_p) th element $\mathcal{X}(\mathbf{i}) = \prod_{j=1}^p \mathbf{x}_j(i_j)$. Any p th-order tensor $\mathcal{X} \in \mathbb{R}^{m_1 \times \dots \times m_p}$ (or $\mathbb{R}^{\times_{j=1}^p m_j}$) can be expressed using the vector outer product as

$$\mathcal{X} = \sum_{i_1=1}^{m_1} \dots \sum_{i_p=1}^{m_p} \mathcal{X}(i_1, \dots, i_p) \left(\bigcirc_{q=1}^p \mathbf{e}_{i_q}^{m_q} \right), \quad (2)$$

where $\mathbf{e}_i^m \in \mathbb{R}^m$ is a unit basis vector with 1 as the i th element and 0 everywhere else. Equation (2) allows us to reshape a tensor by only manipulating the vector outer product. A p th-order diagonal tensor $\mathbb{I}_r^p \in \mathbb{R}^{\times_{i=1}^p r}$ has ones where the indices in each mode coincide, and zeroes elsewhere, that is,

$$\mathbb{I}_r^p = \sum_{i=1}^r \left(\bigcirc_{q=1}^p \mathbf{e}_i^r \right). \quad (3)$$

Tensor structures are conveniently represented by tensor network diagrams that are a recent adaptation [45] from quantum physics where they were originally introduced to visually describe many-body problems. Each node in a tensor network diagram corresponds to a tensor and each edge coming from the node represents a mode. A node with no edges is a scalar, a node with one edge is a vector and a node with two edges is a matrix. More generally, a node with p edges is a p th-order tensor

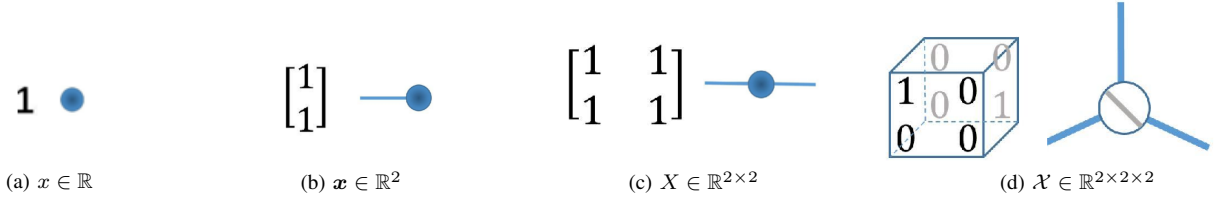


Fig. 1. Tensor network diagrams of a (a) scalar, (b) vector, (c) matrix and (d) third-order diagonal tensor.

(Figs. 1a–1d). (The angle between edges has no meaning beyond aesthetics.) Diagonal tensors as in (3) are represented by putting a diagonal across the node, as in Fig. 1d.

1) *Tensor reshapings, contractions, low-rank formats*: The matricization of a tensor is a matrix with its elements arranged differently. The following definition is from [44]

Definition II.1. Let $\mathcal{S} = \{r_1, \dots, r_L\}$ and $\mathcal{T} = \{m_1, \dots, m_M\}$ be ordered sets that partition the set of modes $\mathcal{M} = \{1, \dots, p\}$ of $\mathcal{X} \in \mathbb{R}^{\times_{j=1}^p m_j}$. Here $L + M = p$. Then if $\mathbf{i} = [i_1, \dots, i_p]'$, the matricization $\mathcal{X}_{(\mathcal{S} \times \mathcal{T})}$ is a matrix of size $(\prod_{q \in \mathcal{S}} m_q) \times (\prod_{q \in \mathcal{T}} m_q)$ defined as

$$\mathcal{X}_{(\mathcal{S} \times \mathcal{T})} = \sum_{i_1=1}^{m_1} \dots \sum_{i_p=1}^{m_p} \mathcal{X}(\mathbf{i}) \left(\bigotimes_{q \in \mathcal{S}} \mathbf{e}_{i_q}^{m_q} \right) \left(\bigotimes_{q \in \mathcal{T}} \mathbf{e}_{i_q}^{m_q} \right)'. \quad (4)$$

We define matricizations in *reverse lexicographic* order to be consistent with the traditional matrix vectorization. This means that the q modes in the multiple Kronecker product (4) are selected in reverse order. Table I defines several reshapings by

TABLE I
TENSOR RESHAPINGS DEFINED BY SPECIFYING PARTITIONS $(\mathcal{S}, \mathcal{T})$ OF \mathcal{M} IN (4).

Reshaping	Notation	\mathcal{S}	\mathcal{T}
k th mode matricization	$\mathcal{X}_{(k)}$	$\{k\}$	$\{1, \dots, k-1, k+1, \dots, p\}$
k th canonical matricization	$\mathcal{X}_{\langle k \rangle}$	$\{1, \dots, k\}$	$\{k+1, \dots, p\}$
vectorization	$\text{vec}(\mathcal{X})$	$\{1, \dots, p\}$	\emptyset

selecting different partitions $(\mathcal{S}, \mathcal{T})$ of \mathcal{M} . These definitions are clarified in (S3), (S4) and (S5).

Tensor contractions [45] generalize the matrix product to higher-ordered tensors. We use $\mathcal{X} \times_{k_1, \dots, k_a}^{l_1, \dots, l_a} \mathcal{Y}$ to denote the mode- $(\begin{smallmatrix} l_1, \dots, l_a \\ k_1, \dots, k_a \end{smallmatrix})$ product or contraction between the (k_1, \dots, k_a) modes of $\mathcal{X} \in \mathbb{R}^{\times_{j=1}^p m_j}$ and the (l_1, \dots, l_a) modes of $\mathcal{Y} \in \mathbb{R}^{\times_{j=1}^q n_j}$, where $m_{k_1} = n_{l_1}, \dots, m_{k_a} = n_{l_a}$. This contraction results in a tensor of order $p+q-2a$ where the a pairs of modes (l_j, k_j) get *contracted*. A simple contraction between the k th mode of \mathcal{X} and the l th mode of \mathcal{Y} has $(i_1, \dots, i_{k-1}, i_{k+1}, \dots, i_p, j_1, \dots, j_{l-1}, j_{l+1}, \dots, j_q)$ th element

$$\sum_{t=1}^{m_l} \mathcal{X}(i_1, \dots, i_{k-1}, t, i_{k+1}, \dots, i_p) \mathcal{Y}(j_1, \dots, j_{l-1}, t, j_{l+1}, \dots, j_q). \quad (5)$$

TABLE II
 TENSOR CONTRACTIONS, WHERE THE CONTRACTION ALONG ONE MODE IS DEFINED AS PER (5). HERE $\mathcal{X} \in \mathbb{R}^{\times_{j=1}^p m_j}$, $\mathcal{Y} \in \mathbb{R}^{\times_{j=1}^q n_j}$, AND X AND Y ARE THE CASES WHERE $p = 2$ AND $q = 2$ RESPECTIVELY.

Contraction	Notation	Definition	Conditions
matrix product	XY	$X \times_{\frac{1}{2}} Y$	$p = q = 2$
k th mode matrix product	$\mathcal{X} \times_k Y$	$\mathcal{X} \times_k^2 Y$	$q = 2$
k th mode vector product	$\mathcal{X} \bar{\times}_k \mathbf{y}$	$\mathcal{X} \times_k^1 \mathbf{y}$	$q = 1$
inner product	$\langle \mathcal{X}, \mathcal{Y} \rangle$	$\mathcal{X} \times_{1, \dots, p}^{1, \dots, q} \mathcal{Y}$	$p = q$
partial contraction	$\langle \mathcal{X} \mathcal{Y} \rangle$	$\mathcal{X} \times_{1, \dots, p}^{1, \dots, p} \mathcal{Y}$	$p < q$
last mode with first mode	$\mathcal{X} \times^1 \mathcal{Y}$	$\mathcal{X} \times_p^1 \mathcal{Y}$	—

Similarly, multiple contractions sum over multiple products of the elements of \mathcal{X} and \mathcal{Y} . Table II defines some contractions using this notation. An important special case is *partial contraction* that contracts all the $p < q$ modes of $\mathcal{X} \in \mathbb{R}^{\times_{j=1}^p m_j}$ with the first p modes of $\mathcal{Y} \in \mathbb{R}^{\times_{j=1}^q m_j}$ resulting in a tensor $\langle \mathcal{X} | \mathcal{Y} \rangle = \mathcal{X} \times_{1, \dots, p}^{1, \dots, p} \mathcal{Y}$ of size $\mathbb{R}^{\times_{j=p+1}^q m_j}$. The partial contraction helps define ToTR, and can also be written as a matrix-vector multiplication using Lemma II.1 (e) (below). The tensor trace is a self-contraction between the two outer-most modes of a tensor. If $m_1 = m_p$, then

$$\text{tr}(\mathcal{X}) = \sum_{i=1}^{m_1} \mathcal{X}(i, :, \dots, :, i), \quad (6)$$

whence $\text{tr}(\mathcal{X}) \in \mathbb{R}^{\times_{j=2}^{p+1} m_j}$. The contraction between two distinct modes (from possibly the same tensor) is represented in tensor network diagrams by joining the corresponding edges (see Fig. 2 for examples). Also, applying the k th mode matricization to

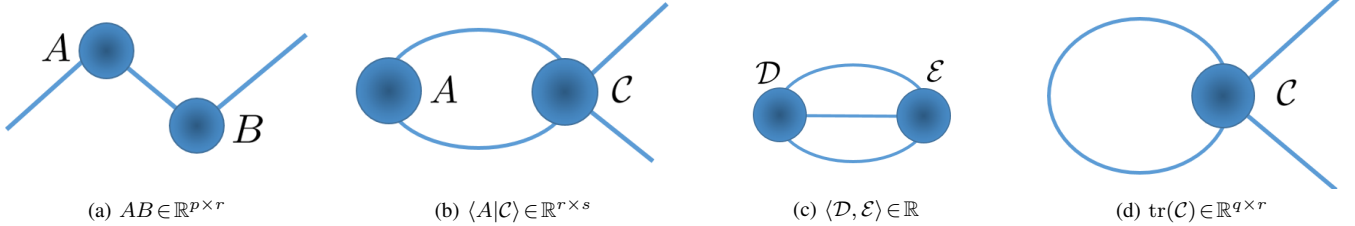


Fig. 2. Tensor network diagrams of (a) matrix product, (b) partial contraction, (c) inner product and (d) trace. Here $A \in \mathbb{R}^{p \times q}$, $B \in \mathbb{R}^{q \times r}$, $D, E \in \mathbb{R}^{p \times q \times r}$ and $C \in \mathbb{R}^{p \times q \times r \times p}$.

every mode of $\mathcal{V} \in \mathbb{R}^{\times_{j=1}^p g_j}$ with respect to (WRT) $A_i \in \mathbb{R}^{m_i \times g_i}$, $i = 1, 2, \dots, p$ results in the TK product $\mathcal{B} = \llbracket \mathcal{V}; A_1, \dots, A_p \rrbracket$ defined as

$$\mathcal{B} = \sum_{i_1=1}^{m_1} \dots \sum_{i_p=1}^{m_p} \mathcal{V}(i_1 \dots i_p) \left(\overset{p}{\underset{q=1}{\circ}} A_q(:, i_q) \right). \quad (7)$$

A tensor \mathcal{B} that can be written as the product in (7) is said to have a *TK format* with *TK rank* (g_1, \dots, g_p) . In this case, \mathcal{V} is called the *core tensor* and A_1, \dots, A_p are the *factor matrices*. When $g_i \ll m_i$ for $i = 1, \dots, p$, the TK format substantially reduces the number of unconstrained elements in a tensor and its complexity. TK formats are often fit by higher-order singular value (HOSVD) [46] or LQ (HOLQ) decomposition [47]. For a diagonal core tensor \mathcal{V} , as in (3), the TK format reduces to the CP format of rank r . This reduction is equivalent to setting the tensor \mathcal{B} as the sum of r vector outer products, where the vectors correspond to the columns of matrix factors $A_i \in \mathbb{R}^{m_i \times r}$, $i = 1, \dots, p$,

$$\mathcal{B} = \llbracket \boldsymbol{\lambda}; A_1, \dots, A_p \rrbracket = \sum_{i=1}^r \boldsymbol{\lambda}(i) \left(\overset{p}{\underset{q=1}{\circ}} A_q(:, i) \right). \quad (8)$$

The vector $\boldsymbol{\lambda} \in \mathbb{R}^r$ contains the diagonal entries of the core tensor, and is often set to the proportionality constants that make the matrix factors have unit column norms. When $\boldsymbol{\lambda}$ is ignored in the specification of (8), we assume that $\boldsymbol{\lambda} = [1, 1, \dots, 1]^T$. A tensor \mathcal{B} is said to have an OP format if it can be written as $\mathcal{B} = \circ \llbracket A_1, A_2, \dots, A_p \rrbracket$, or

$$\mathcal{B} = \sum_{\substack{i_1, \dots, i_p \\ j_1, \dots, j_p}} \left(\prod_{q=1}^p A_q[i_q, j_q] \right) \left\{ \left(\overset{p}{\underset{q=1}{\circ}} \mathbf{e}_{j_q}^{h_q} \right) \circ \left(\overset{p}{\underset{q=1}{\circ}} \mathbf{e}_{i_q}^{m_q} \right) \right\}, \quad (9)$$

where for all $q = 1, \dots, p$, we have $A_q \in \mathbb{R}^{m_q \times h_q}$ and the summation over i_q is from 1 through m_q , and that over j_q is from 1 through h_q . Our novel OP format is essentially the outer product of multiple matrices, and is useful for expressing the TK

product of (7) as a partial contraction between \mathcal{V} and $\circ[[A_1, A_2, \dots, A_p]]$, as we shortly state and prove in Theorem II.1(b). The derivation needs some properties of tensor products and reshapings that we prove first in Lemma II.1, along with several other properties that are useful for tensor manipulations. (Lemma II.1(a),(c) and (d) have been stated without proof in [44], [38], and [45] but we provide proofs here for completeness.)

Lemma II.1. Let $\mathcal{X} \in \mathbb{R}^{\times_{j=1}^p m_j}$. Then using the notation of Tables I and II, where $k = 1, \dots, p$,

- (a) $\mathcal{X}_{\langle p-1 \rangle} = \mathcal{X}'_{(p)}$.
- (b) $\text{vec}(\mathcal{X}) = \text{vec}(\mathcal{X}_{(1)}) = \text{vec}(\mathcal{X}_{\langle 1 \rangle}) = \dots = \text{vec}(\mathcal{X}_{\langle p \rangle})$.
- (c) $\langle \mathcal{X}, \mathcal{Y} \rangle = (\text{vec } \mathcal{X})' (\text{vec } \mathcal{Y}) = \text{tr}(\mathcal{X}_{(k)} \mathcal{Y}'_{(k)})$, $\mathcal{Y} \in \mathbb{R}^{\times_{j=1}^p m_j}$.
- (d) $\text{vec}[[\mathcal{X}; A_1, \dots, A_p]] = \left(\bigotimes_{i=p}^1 A_i \right) \text{vec}(\mathcal{X})$, where $A_i \in \mathbb{R}^{n_i \times m_i}$ for any $n_i \in \mathbb{N}$.
- (e) $\text{vec}(\mathcal{X}|\mathcal{B}) = \mathcal{B}'_{\langle p \rangle} \text{vec } \mathcal{X}$, $\mathcal{B} \in \mathbb{R}^{(\times_{j=1}^p m_j) \times (\times_{j=1}^q h_j)}$.
- (f) $\text{vec } \mathcal{X}_{(k)} = K_{(k)} \text{vec}(\mathcal{X})$, where $K_{(k)} = (I_{\prod_{i=k+1}^p m_i} \otimes K_{\prod_{i=1}^{k-1} m_i, m_k})$.

Proof. See Section S1-C. □

We now use Lemma II.1 to state and prove the following

Theorem II.1. Consider a p th-order tensor \mathcal{X} and matrices M_1, \dots, M_p such that the TK product with \mathcal{X} can be formed. Then

- (a) $\circ[[M_1, \dots, M_p]]_{\langle p \rangle} = \bigotimes_{q=p}^1 M'_q$.
- (b) $\langle \mathcal{X} | \circ[[M_1, \dots, M_p]] \rangle = [[\mathcal{X}; M_1, \dots, M_p]]$.
- (c) For any $k = 1, \dots, p$, let $\mathcal{S} = \{k, p+k\}$. Then

$$\begin{aligned} & \circ[[M_1, \dots, M_p]]_{(\mathcal{S} \times \mathcal{S}^c)} \\ &= (\text{vec } M'_k) (\text{vec } \circ[[M_1, \dots, M_{k-1}, M_{k+1}, \dots, M_p]])'. \end{aligned} \quad (10)$$

Proof. See Section S1-D. □

Remark: If $\mathcal{B} = \circ[[X', X']]$ for some matrix X , then Theorem II.1(a) implies that $\mathcal{B}_{\langle 2 \rangle} = X \otimes X$ while $\mathcal{B}_{(1,3) \times (2,4)} = (\text{vec } X)(\text{vec } X)'$ by Theorem II.1(c). In other words, $X \otimes X$ and $(\text{vec } X)(\text{vec } X)'$ are different matricizations of the same OP tensor \mathcal{B} , which formalizes our intuition because both $X \otimes X$ and $(\text{vec } X)(\text{vec } X)'$ have the same number of elements, and it motivates naming the format *outer product*.

Finally, a tensor \mathcal{B} is said to have a Tensor Ring (TR) format with TR rank (g_1, \dots, g_p) if it can be expressed as

$$\mathcal{B} = \text{tr}(\mathcal{G}_1 \times^1 \dots \times^1 \mathcal{G}_p), \quad (11)$$

where $\mathcal{G}_i \in \mathbb{R}^{g_{i-1} \times m_i \times g_i}$ for $i = 1, \dots, p$ and $g_0 = g_p$. The TR format is called the Matrix Product State (MPS) with closed boundary conditions in many-body physics [48]. When exactly one of the TR ranks is 1, the TR format is the same as the Tensor Train (TT) format [35] and is the MPS with open boundary conditions.

We conclude our discussion of low-rank tensor formats by using tensor network diagrams to illustrate in Fig. 3, a fourth-order tensor in the TK, CP and TR formats.

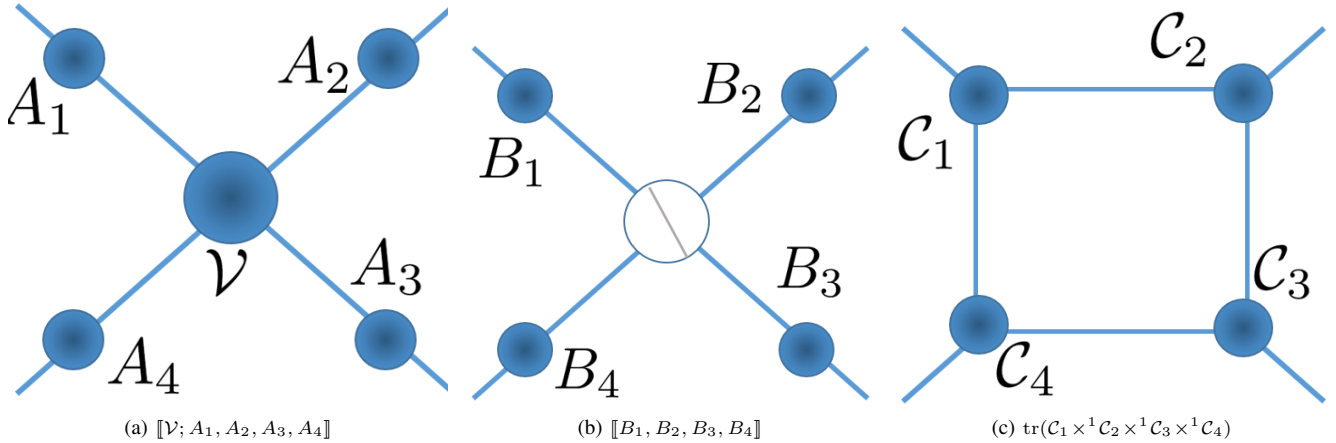


Fig. 3. Tensor network diagrams of example fourth-order tensor of (a) TK format (7), (b) CP format (8), and (c) TR format (11).

2) *The TVN Distribution*: The matrix-variate normal distribution, abbreviated in [49] as MxVN to distinguish it from the vector-variate multinormal distribution (MVN), was studied extensively in [50]. A random matrix $\mathbf{X} \in \mathbb{R}^{m_1 \times m_2}$ follows a MxVN distribution if $\text{vec}(\mathbf{X})$ is MVN with covariance matrix $\Sigma_2 \otimes \Sigma_1$, where $\Sigma_k \in \mathbb{R}^{m_k \times m_k}$ for $k = 1, 2$. Our TVN distribution, formulated in Definition II.2, extends this idea to the case of higher-order random tensors. For simplicity, we define the following notation for use in the rest of the paper:

$$m = \prod_{i=1}^p m_i, \quad m_{-k} = m/m_k, \quad \Sigma = \bigotimes_{i=p}^1 \Sigma_i, \quad \Sigma_{-k} = \bigotimes_{\substack{i=p \\ i \neq k}}^1 \Sigma_i.$$

Definition II.2. A random tensor $\mathcal{X} \in \mathbb{R}^{\times_{j=1}^p m_j}$ follows a p th-order TVN distribution with mean $\mathcal{M} \in \mathbb{R}^{\times_{j=1}^p m_j}$ and non-negative definite scale matrices $\Sigma_i \in \mathbb{R}^{m_i \times m_i}$ for $i = 1, 2, \dots, p$ (i.e., $\mathcal{X} \sim \mathcal{N}_{\mathbf{m}}(\mathcal{M}, \Sigma_1, \Sigma_2, \dots, \Sigma_p)$ where $\mathbf{m} = [m_1, m_2, \dots, m_p]'$) if $\text{vec}(\mathcal{X}) \sim \mathcal{N}_{\mathbf{m}}(\text{vec}(\mathcal{M}), \Sigma)$.

The Kronecker product in Definition II.2 is in reverse order because we have defined vectorization in reverse lexicographic order. Definition II.2 defines the TVN distribution in terms of a vectorization. We state and prove the distribution of other tensor reshaping in Theorem II.2. These results are essential in the development of ToTR models with TVN errors, as they allow us to model the vectorized tensor errors in terms of the MVN distribution.

Theorem II.2. The following statements are equivalent:

- (a) $\mathcal{Y} \sim \mathcal{N}_{\mathbf{m}}(\mathcal{M}, \Sigma_1, \Sigma_2, \dots, \Sigma_p)$
- (b) $\text{vec}(\mathcal{Y}) \sim \mathcal{N}_{\mathbf{m}}(\text{vec}(\mathcal{M}), \Sigma)$
- (c) $\mathcal{Y}_{(k)} \sim \mathcal{N}_{[m_k, m_{-k}]'}(\mathcal{M}_{(k)}, \Sigma_k, \Sigma_{-k}), \quad k = 1, 2, \dots, p$
- (d) For $k = 1, 2, \dots, p$ and $\mathbf{m}_k = [\prod_{i=1}^k m_i, \prod_{i=k+1}^p m_i]'$,
 $\mathcal{Y}_{\langle k \rangle} \sim \mathcal{N}_{\mathbf{m}_k}(\mathcal{M}_{\langle k \rangle}, \bigotimes_{i=k}^1 \Sigma_i, \bigotimes_{i=p}^{k+1} \Sigma_i)$

Proof. (a) and (b) are equivalent, following Definition II.2 while (b) and (c) are so from Lemma II.1(f) with $K_{(k)} \Sigma K_{(k)}' = \Sigma_{-k} \otimes \Sigma_k$. Further, (b) and (d) are equivalent because of Lemma II.1(b). \square

The density of $\mathcal{Y} \sim \mathcal{N}_{\mathbf{m}}(\mathcal{M}, \Sigma_1, \Sigma_2, \dots, \Sigma_p)$ is $f(\mathcal{Y}; \mathcal{M}, \Sigma) = |2\pi\Sigma|^{-1/2} \exp\left\{-\frac{1}{2}D_{\Sigma}^2(\mathcal{Y}, \mathcal{M})\right\}$, where $D_{\Sigma}^2(\mathcal{Y}, \mathcal{M})$ is the squared Mahalanobis distance between \mathcal{Y} and \mathcal{M} , and has the equivalent representation

$$\begin{aligned} D_{\Sigma}^2(\mathcal{Y}, \mathcal{M}) &= \text{vec}(\mathcal{Y} - \mathcal{M})' \Sigma^{-1} \text{vec}(\mathcal{Y} - \mathcal{M}) \\ &= \langle (\mathcal{Y} - \mathcal{M}), \llbracket (\mathcal{Y} - \mathcal{M}); \Sigma_1^{-1}, \Sigma_2^{-1}, \dots, \Sigma_p^{-1} \rrbracket \rangle, \end{aligned} \quad (12)$$

by Lemmas II.1(c) and II.1(d). Property S1.2 provides similar alternative expressions for the determinant $\det(\Sigma)$ of Σ .

B. Tensor-variate Linear Models with TVN Errors

1) *Tensor-on-Tensor Regression*: We formulate the ToTR model as

$$\mathcal{Y}_i = \Upsilon + \langle \mathcal{X}_i | \mathcal{B} \rangle + \mathcal{E}_i, \quad i = 1, 2, \dots, n, \quad (13)$$

where the response $\mathcal{Y}_i \in \mathbb{R}^{\times_{j=1}^p m_j}$ and the covariate $\mathcal{X}_i \in \mathbb{R}^{\times_{j=1}^l h_j}$ are both tensor-valued, $\mathcal{E}_i \stackrel{iid}{\sim} \mathcal{N}_{\mathbf{m}}(0, \sigma^2 \Sigma_1, \Sigma_2, \dots, \Sigma_p)$ is the TVN-distributed error, $\mathcal{B} \in \mathbb{R}^{(\times_{j=1}^l h_j) \times (\times_{j=1}^p m_j)}$ is the (tensor-valued) regression parameter and Υ is the (tensor-valued) intercept. This model is essentially the classical MVMLR model but exploits the tensor-variate structure of the covariates and responses to reduce the total number of parameters. To see this, we apply Lemma II.1(e) and Theorem II.2(b) to vectorize (13) as $\text{vec}(\mathcal{Y}_i) = \text{vec}(\Upsilon) + \mathcal{B}'_{\langle l \rangle} \text{vec}(\mathcal{X}_i) + e_i$, where $e_i \stackrel{iid}{\sim} \mathcal{N}_{\mathbf{m}}(0, \sigma^2 \Sigma)$ is the error. This formulation leads to a MVMLR model with intercept, which can be incorporated into the covariates as $[\text{vec}(\Upsilon) \mathcal{B}'_{\langle l \rangle}] [1, \text{vec}(\mathcal{X}_i)]'$. But the covariate $[1, \text{vec}(\mathcal{X}_i)]'$ is then no longer a vectorized tensor and we can not exploit the tensor structure of \mathcal{X}_i . To obviate this possibility, (13) includes a separate intercept term Υ .

Imposing a low-rank format on \mathcal{B} proffers several advantages. First, it makes the regression model practical to use, as accurate estimation of an unstructured version of \mathcal{B} may otherwise be prohibitive when dimensionality is high relative to sample size. Second, \mathcal{B} can be interpreted, in spite of its high dimensions, as being explainable through a few lower-dimensional tensor factor matrices (Fig. 4). These explanations mirror the many-body problem in physics, where weakly-coupled degrees of freedom are often embedded in ultra-high-dimensional Hilbert spaces [48], [51]. We now turn to the problem of learning \mathcal{B} in the given setup.

The dispersion matrix Σ in the TVN distribution specification of the \mathcal{E}_i s in (13) is Kronecker-separable and leads to the number of unconstrained parameters from $(\prod_{i=1}^p m_i) \times (\prod_{i=1}^p m_i + 1)/2$ to $\sum_{i=1}^p m_i(m_i + 1)/2$. Further, this Kronecker-separable structure is intuitive because it assigns a covariance matrix to each tensor-response dimension. This allows us to separately incorporate different dependence contexts that exist within a tensor. For example, a tensor may have temporal and

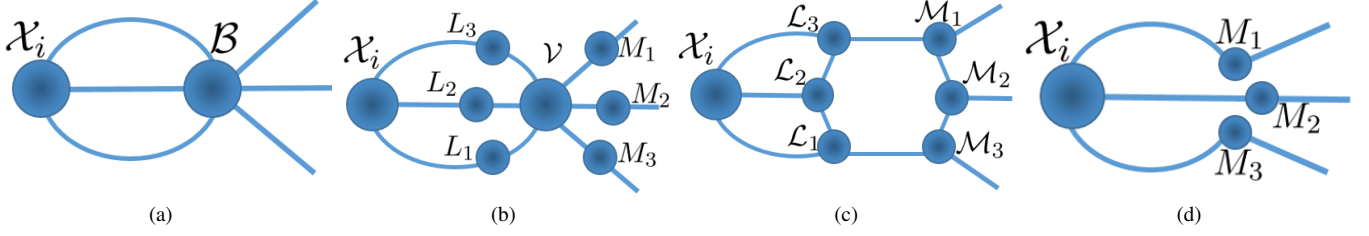


Fig. 4. Tensor network diagrams of tensor-on-tensor regression when both the response and the covariates are third-order tensors and for (a) $\mathcal{Y}_i = \langle \mathcal{X}_i | \mathcal{B} \rangle$ and (b-d) the special cases when the \mathcal{B} in $\langle \mathcal{X}_i | \mathcal{B} \rangle$ are of (b) Tucker, (c) TR and (d) OP formats (illustrated in Fig. 3).

spatial contexts in its modes. Kronecker separability allows us to assign a covariance matrix to each of these different contexts. However, Kronecker separability results in unidentifiable scale matrices (Σ_i), as $cA \otimes B = A \otimes cB$ for any matrices A, B and $c \neq 0$, so we constrain the scale matrices to each have $\Sigma_i(1, 1) = 1$, and introduce a parameter σ^2 to capture an overall proportional scalar variance. This approach further reduces the number of parameters by $p-1$ and imposes a curved exponential family distribution on the errors [52].

2) *The TANOVA model:* Suppose that we observe independent tensors $\mathcal{Y}_{j_1, \dots, j_l, i} \in \mathbb{R}^{\times_{j=1}^l m_j}$ ($i = 1, \dots, n_{j_1, \dots, j_l}$), where j_k ($k = 1, \dots, l$), indexes the k th categorical (factor) variable of h_k levels, that is, $j_k \in \{1, \dots, h_k\}$. The tensor-valued parameter \mathcal{B} encoding the dimensions of $\mathcal{Y}_{i, j_1, \dots, j_l}$ and all the possible factor classes is of size $h_1 \times \dots \times h_l \times m_1 \times \dots \times m_p$. To see this, consider the l th ordered single-entry tensor $\mathcal{X}_{j_1, \dots, j_l} = \circ_{q=1}^l e_{i_q}^{h_q}$ that is unity at (j_1, \dots, j_l) and zero everywhere else. Then $\langle \mathcal{X}_{j_1, \dots, j_l} | \mathcal{B} \rangle \in \mathbb{R}^{\times_{j=1}^l m_j}$ and

$$\langle \mathcal{X}_{j_1, \dots, j_l} | \mathcal{B} \rangle = \mathcal{B}[j_1, \dots, j_l, :, \dots, :]. \quad (14)$$

Therefore, modeling $\mathbb{E}(\mathcal{Y}_{i, j_1, \dots, j_l})$ as $\langle \mathcal{X}_{j_1, \dots, j_l} | \mathcal{B} \rangle$ results in each factor combination (j_1, \dots, j_p) getting assigned its own mean parameter as a sub-tensor of \mathcal{B} . This high-dimensional parameter \mathcal{B} is identical to cell-means MANOVA if we vectorize (14) using Lemma II.1(e) as $\mathcal{B}'_{<l>} \text{vec}(\mathcal{X}_{j_1, \dots, j_l}) = \text{vec}(\mathcal{B}[j_1, \dots, j_p, :, \dots, :])$, in which case $\text{vec}(\mathcal{X}_{j_1, \dots, j_p}) = \otimes_{q=1}^l e_{i_q}^{h_q}$ corresponds to a row in the MANOVA design matrix. Although this formulation is fundamentally the same as (14), the latter helps us visualize and formulate a low-rank format on \mathcal{B} . Based on the format, we refer to tensor-valued response regression models with the mean in (14) as TANOVA(l, p), where l is the number of different factors and p is the order of the tensor-valued response. In this way, because scalar and vector variables are tensors of order 0 and 1, ANOVA and MANOVA correspond to TANOVA(1, 0) and TANOVA(1, 1), respectively. In general, TANOVA(l, p) with TVN errors can be expressed as

$$\mathcal{Y}_i = \langle \mathcal{X}_i | \mathcal{B} \rangle + \mathcal{E}_i, \quad \mathcal{E}_i \stackrel{iid}{\sim} \mathcal{N}_m(0, \sigma^2 \Sigma_1, \Sigma_2, \dots, \Sigma_p), \quad (15)$$

where \mathcal{X}_i is the single-entry tensor that contains all the assigned factors of \mathcal{Y}_i , for $i = 1, \dots, n$. Model (15) is a ToTR model as in (13) with no intercept. This is analogous to ANOVA and MANOVA being special cases of univariate and multivariate multiple linear regressions, respectively. Further, the log-likelihood function of (15) is

$$\ell = -\frac{n}{2} \log |2\pi\sigma^2 \Sigma| - \frac{1}{2\sigma^2} \sum_{i=1}^n D_{\Sigma}^2(\mathcal{Y}_i, \langle \mathcal{X}_i | \mathcal{B} \rangle). \quad (16)$$

C. Parameter Estimation

We obtain estimators of (13) before deriving their properties.

1) *Profiling the intercept:* We first show that the intercept in (13) can be profiled out by centering the covariates and the responses. To see this, we express the loglikelihood in terms of Υ as

$$\ell = -\frac{1}{2\sigma^2} \sum_{i=1}^n D_{\Sigma}^2(\mathcal{Y}_i, \Upsilon + \langle \mathcal{X}_i | \mathcal{B} \rangle). \quad (17)$$

We define the tensor differential of an inner product WRT Υ using the matrix differential $\langle \partial \Upsilon, \mathcal{S} \rangle = \text{tr}(\partial \Upsilon_{(1)} \mathcal{S}'_{(1)})$. Applying it to (17) yields

$$\partial \ell(\Upsilon) = \frac{1}{\sigma^2} \langle \partial \Upsilon, \llbracket \mathcal{S}; \Sigma_1^{-1}, \dots, \Sigma_p^{-1} \rrbracket \rangle,$$

where $n^{-1} \mathcal{S} = \bar{\mathcal{Y}} - \langle \bar{\mathcal{X}} | \mathcal{B} \rangle - \Upsilon$ and $\bar{\mathcal{Y}}, \bar{\mathcal{X}}$ are the averaged responses and covariates. Now, $\partial \ell(\Upsilon) = 0$ if $\mathcal{S} = 0$, and after profiling on \mathcal{B} , the ML estimator (MLE) of Υ is $\hat{\Upsilon}(\mathcal{B}) = \bar{\mathcal{Y}} - \langle \bar{\mathcal{X}} | \mathcal{B} \rangle$. Setting Υ in (17) to be $\hat{\Upsilon}(\mathcal{B})$ yields (16) with centered responses and covariates, so we assume without loss of generality (WLOG) that (15) has no intercept, and estimate the other parameters. Our estimation uses block-relaxation [53] to optimize (16): we partition the parameter space into blocks and serially optimize the parameters in each block while holding fixed the other parameters.

2) *Estimation of $\mathcal{B}, \Sigma_1, \Sigma_2, \dots, \Sigma_p$ given σ^2* : Our estimates simplify as per the format of \mathcal{B} so we consider each case individually, before providing an overview.

a) *TK format*: Let \mathcal{B} have TK format of rank $(c_1, \dots, c_l, d_1, \dots, d_p)$:

$$\mathcal{B}_{TK} = \llbracket \mathcal{V}; L_1, \dots, L_l, M_1, \dots, M_p \rrbracket, \quad (18)$$

where $M'_k \Sigma_k^{-1} M_k = I_{d_k}$ for $k = 1, \dots, p$. Then the number of parameters to be estimated goes down from the unconstrained $\prod_{i=1}^l h_i \prod_{i=1}^p m_i$ to $\prod_{i=1}^l c_i \prod_{i=1}^p d_i + \sum_{i=1}^l c_i h_i + \sum_{i=1}^p d_i m_i$. The constraint $M'_k \Sigma_k^{-1} M_k = I_{d_k}$ greatly simplifies estimation and inference. Using (18), we vectorize (15) for any $k = 1, \dots, l$ as

$$\text{vec}(\mathcal{Y}_i) = \mathcal{H}_{ik < 2 >}^{TK} \text{vec}(L_k) + \mathbf{e}_i \quad (19)$$

where $\mathcal{H}_{ik < 2 >}^{TK}$ is the 2-canonical matricization of the tensor

$$\mathcal{H}_{ik}^{TK} = \mathcal{X}_i \times_{1, \dots, k-1, k+1, \dots, l} \llbracket \mathcal{V}; L_1, \dots, L_{k-1}, I_{h_k}, L_{k+1}, \dots, L_l, M_1, \dots, M_p \rrbracket \quad (20)$$

and \mathbf{e}_i s are i.i.d $\mathcal{N}_m(0, \sigma^2 \Sigma)$. Optimizing (16) WRT L_k forms its own block, which corresponds to a MVMLR model where, for $S_k^{TK} = \sum_{i=1}^n (\mathcal{H}_{ik < 2 >}^{TK} \Sigma^{-1} \mathcal{H}_{ik < 2 >}^{TK'})$,

$$\text{vec}(\widehat{L}_k) = (S_k^{TK})^{-1} \left(\sum_{i=1}^n \mathcal{H}_{ik < 2 >}^{TK} \Sigma^{-1} \text{vec}(\mathcal{Y}_i) \right). \quad (21)$$

The computation of S_k^{TK} is greatly simplified based on the constraint that $M'_k \Sigma_k^{-1} M_k = I_{d_k}$ for all $k = 1, 2, \dots, p$. For fixed $L_1, \dots, L_p, \Sigma_1, \dots, \Sigma_p$, we estimate $M_1, \dots, M_p, \mathcal{V}$. We first show that \mathcal{V} can be profiled from the loglikelihood for fixed M_1, \dots, M_p . To see this, we write an alternative vectorized form of (15) as

$$\text{vec}(\mathcal{Y}_i) = \left(\otimes_{i=p}^1 M_i \right) \mathcal{V}'_{< l >} \mathbf{w}_i + \mathbf{e}_i,$$

where $\mathbf{w}_i = \text{vec}[\mathcal{X}_i; L'_1, L'_2, \dots, L'_l]$. Letting $Z = Y - M \mathcal{V}'_{< l >} W$, for $M = \otimes_{k=p}^1 M_k$, $Y = [\text{vec } \mathcal{Y}_1 \dots \text{vec } \mathcal{Y}_n]$, and $W = [\mathbf{w}_1 \dots \mathbf{w}_n]$ simplifies (16) to

$$\ell = -\frac{n}{2} \log |\Sigma| - \frac{1}{2\sigma^2} \left\{ \text{tr}(Z' \Sigma^{-1} Z) \right\}. \quad (22)$$

Optimizing (22) for fixed M_1, \dots, M_p yields the profiled MLE

$$\widehat{\mathcal{V}}_{< l >}(M_1, \Sigma_1, \dots, M_p, \Sigma_p) = W^{-'} Y' \left(\bigotimes_{k=p}^1 \Sigma_k^{-1} M_k \right), \quad (23)$$

where W^{-} is the right inverse of W . Therefore, given values of all M_k s, we obtain $\widehat{\mathcal{V}}$ by simply inserting them in (23). To estimate M_k we profile $\widehat{\mathcal{V}}$ out of the loglikelihood by replacing (23) into (22), and expressing it up to a constant as

$$\ell(M_k, \Sigma_k) = \frac{1}{2\sigma^2} \|M'_k \Sigma_k^{-1} Q_k\|_2^2, \quad (24)$$

where $Q_k = \llbracket \mathcal{Y}_T; M'_1 \Sigma_1^{-1}, \dots, M'_{k-1} \Sigma_{k-1}^{-1}, I_{m_k}, M'_{k+1} \Sigma_{k+1}^{-1}, \dots, M'_p \Sigma_p^{-1}, W^{-} W \rrbracket_{(k)}$ and $\mathcal{Y}_T \in \mathbb{R}^{(\times_{j=1}^p m_j) \times n}$ is such that $\mathcal{Y}_T(:, \dots, :, i) = \mathcal{Y}_i$ for $i = 1, \dots, n$. From (24), the MLE of M_k is obtained via generalized SVD of Q_k [54]:

$$\widehat{M}_k(\Sigma_k) = \arg \max_{M_k: M'_k \Sigma_k^{-1} M_k = I_{d_k}} \|M'_k \Sigma_k^{-1} Q_k\|_2^2 = \Sigma_k^{1/2} U, \quad (25)$$

with the leading d_k left singular vectors of $\Sigma_k^{-1/2} Q_k$ as the columns of U . To estimate Σ_k at fixed \mathcal{B}_{TK} , we write (22) as

$$\ell(\Sigma_k) = -\frac{nm-k}{2} \log |\Sigma_k| - \frac{1}{2\sigma^2} \text{tr}(\Sigma_k^{-1} S_k), \quad (26)$$

where $S_k = \sum_{i=1}^n \mathcal{Z}_{i(k)} \Sigma_k^{-1} \mathcal{Z}'_{i(k)}$ and $\mathcal{Z}_{i(k)} = \mathcal{Y}_i - \langle \mathcal{X}_i | \mathcal{B} \rangle$. The MLE of Σ_k under the (TK format) constraint of (18) is

$$\widehat{\Sigma}_k = \arg \max_{\Sigma_k: \Sigma_k[1,1]=1} \ell(\Sigma_k) = ADJUST(nm-k, \sigma^2, S_k), \quad (27)$$

where the *ADJUST* procedure is as introduced in [55] and that was shown to satisfy the Karush-Kuhn-TK (KKT) conditions. Without this constraint, the MLE is $S_k / (nm-k\sigma^2)$. Further reductions can be obtained by imposing additional parameterized structures on Σ_k s, as needed. Our block relaxation algorithm, detailed in Algorithm 1, is initialized by methods discussed in Section II-C4.

Algorithm 1: Block-relaxation algorithm for ToTR (13) with TK formatted \mathcal{B}

Initial values: $k = 0$, $\hat{\sigma}^{2(0)}$, $\hat{L}_1^{(0)}, \dots, \hat{L}_l^{(0)}$, $(\hat{M}_1^{(0)}, \hat{\Sigma}_1^{(0)}), \dots, (\hat{M}_p^{(0)}, \hat{\Sigma}_p^{(0)})$

- 1 Center the data while saving the means $\bar{\mathcal{X}}, \bar{\mathcal{Y}}$.
- 2 **while** convergence criteria is not met **do**
- 3 **for** $j = 1, 2, \dots, p$ **do**
- 4 $\hat{M}_j^{(k+1)}$ as per (25)
- 5 **end**
- 6 $\hat{\mathcal{Y}}^{(k+1)}$ as per (23)
- 7 **for** $j = 1, 2, \dots, l$ **do**
- 8 $\hat{L}_j^{(k+1)}$ as per (21)
- 9 **end**
- 10 **for** $j = 1, 2, \dots, p$ **do**
- 11 $\hat{\Sigma}_j^{(k+1)}$ as per (27)
- 12 $\hat{\sigma}^{2(k+1)}$ as per (39)
- 13 **end**
- 14 $k \leftarrow k + 1$
- 15 **end**
- 16 $\hat{\Upsilon} = \bar{\mathcal{Y}} - \langle \bar{\mathcal{X}} | \hat{\mathcal{B}}_{TK} \rangle$

b) CP format: We now optimize (16) when \mathcal{B} is

$$\mathcal{B}_{CP} = \llbracket \boldsymbol{\lambda}; L_1, L_2, \dots, L_l, M_1, M_2, \dots, M_p \rrbracket, \quad (28)$$

that is, of CP format of rank r . Then, with $\Sigma_k = I_{m_k}$ for $k = 1, 2, \dots, p$, (15) reduces to the framework of [29]. The CP format reduces the number of parameters in \mathcal{B} from $\prod_{i=1}^p m_i \prod_{i=1}^l h_i$ to $r(\sum_{i=1}^p m_i + \sum_{i=1}^l h_i)$. Here also, we optimize (16) via a block-relaxation algorithm. The k th block corresponds to (M_k, Σ_k) for $k = 1, 2, \dots, p$ and can be estimated in a MVMLR framework by applying Theorem II.2(c) on the k th mode matricized form of (15):

$$\mathcal{Y}_{i(k)} = M_k G_{ik}^{CP} + E_i, \quad E_i \stackrel{iid}{\sim} \mathcal{N}_{[m_k, m_{-k}]'}(0, \sigma^2 \Sigma_k, \Sigma_{-k}), \quad (29)$$

where $G_{ik}^{CP} \equiv \mathcal{G}_{ik}^{CP}$ is the k th mode matricization of $\mathcal{G}^{CP} = \llbracket \llbracket \mathcal{X}; L'_1, \dots, L'_l \rrbracket | \mathcal{I}_r^{p+l} \rrbracket; M_1, \dots, M_{k-1}, I_{m_k}, M_{k+1}, \dots, M_p \rrbracket$. Additional simplifications of G_{ik}^{CP} are possible, for example, using (Section S1-E1) the Khatri-Rao product (\odot) [38]. When all parameters except (M_k, Σ_k) are held fixed, (29) matches a MVMLR model with loglikelihood

$$\ell(\Sigma_k, M_k) = \frac{nm_{-k}}{2} \log |\Sigma_k^{-1}| - \frac{1}{2\sigma^2} \text{tr}(\Sigma_k^{-1} S_k), \quad (30)$$

with $S_k = \sum_{i=1}^n Z_{ik} \Sigma_{-k}^{-1} Z'_{ik}$, where $Z_{ik} = \mathcal{Y}_{i(k)} - M_k G_{ik}^{CP}$. Then the MLEs are

$$\begin{aligned} \hat{M}_k &= \sum_{i=1}^n \mathcal{Y}_{i(k)} \Sigma_{-k}^{-1} G_{ik}^{CP'} \left[\sum_{i=1}^n G_{ik}^{CP} \Sigma_{-k}^{-1} G_{ik}^{CP'} \right]^{-1}, \\ \hat{\Sigma}_k(M_k) &= ADJUST(nm_{-k}, \sigma^2, S_k). \end{aligned} \quad (31)$$

The matrices $\sum_{i=1}^n \mathcal{Y}_{i(k)} \Sigma_{-k}^{-1} G_{ik}^{CP'}$, $\sum_{i=1}^n G_{ik}^{CP} \Sigma_{-k}^{-1} G_{ik}^{CP'}$ are substantially simplified in Section S1-E1. We estimate Σ_k by directly optimizing (30). The other l blocks in the block-relaxation algorithm correspond to L_1, \dots, L_l and are each MVMLR models obtained by vectorizing (15) as:

$$\text{vec}(\mathcal{Y}_i) = H_{ik}^{CP} \text{vec}(L_k) + e_i, \quad e_i \stackrel{iid}{\sim} \mathcal{N}_m(0, \sigma^2 \Sigma), \quad (32)$$

where $H_{ik}^{CP} = \mathcal{H}_{ik < 2}^{CP}$ and \mathcal{H}_{ik}^{CP} is identical to the \mathcal{H}_{ik}^{TK} of (20), but for the fact that \mathcal{V} is the diagonal tensor \mathcal{I}_r^{p+l} . (Fig. 5 displays \mathcal{H}_{ik}^{CP} for when $p=l=3$.) For $k = 1, \dots, l$, holding all parameters except L_k fixed makes (32) a MVMLR model with the MLE of L_k obtained as

$$\text{vec}(\hat{L}_k) = \left(\sum_{i=1}^n H_{ik}^{CP} \Sigma^{-1} H_{ik}^{CP'} \right)^{-1} \left(\sum_{i=1}^n H_{ik}^{CP} \Sigma^{-1} \text{vec}(\mathcal{Y}_i) \right). \quad (33)$$

The matrices $\sum_{i=1}^n H_{ik}^{CP} \Sigma^{-1} \text{vec}(\mathcal{Y}_i)$, $\sum_{i=1}^n H_{ik}^{CP} \Sigma^{-1} H_{ik}^{CP'}$ are substantially simplified in Section S1-E1. As summarized in Fig. 5, the tensors \mathcal{H}_{ik}^{CP} and \mathcal{G}_{ik}^{CP} play a critical role in the estimation of M_k and L_k through (29) and (32), permitting the use of standard MVMLR and MLR estimation methods. From (8), we deduce that the j th columns of all the factor matrices in the CP decomposition (28) are identifiable only up to a constant. So we constrain the columns to have unit norm. The MLEs of our parameters are obtained using a block-relaxation algorithm, as outlined in Algorithm 2.

Algorithm 2: Block-relaxation algorithm for ToTR (13) with CP formatted \mathcal{B}

Initial Values: $k = 0, \hat{\sigma}^{2(0)}, \hat{L}_2^{(0)}, \hat{L}_3^{(0)}, \dots, \hat{L}_l^{(0)}, \hat{M}_1^{(0)}, \hat{M}_2^{(0)}, \dots, \hat{M}_p^{(0)}$

- 1 Center the data while saving the means $\bar{\mathcal{X}}, \bar{\mathcal{Y}}$.
- 2 **while** convergence criteria is not met **do**
- 3 **for** $j = 1, 2, \dots, l$ **do**
- 4 $\hat{L}_j^{(k+1)}$ as per (33) and normalize its columns
- 5 **end**
- 6 **for** $j = 1, 2, \dots, p-1$ **do**
- 7 $(\hat{M}_k^{(k+1)}, \hat{\Sigma}_k^{(k+1)})$ as per (31) and normalize the columns of $\hat{M}_k^{(k+1)}$
- 8 **end**
- 9 $(\hat{M}_p^{(k+1)}, \hat{\Sigma}_p^{(k+1)})$ as per (31)
- 10 $\hat{\sigma}^{2(k+1)}$ as per (39)
- 11 Normalize the columns of $\hat{M}_p^{(k+1)}$ while setting $\hat{\lambda}^{(k+1)}$ to those norms
- 12 $k = k + 1$
- 13 **end**
- 14 $\hat{\Upsilon} = \bar{\mathcal{Y}} - \langle \bar{\mathcal{X}} | \hat{\mathcal{B}}_{CP} \rangle$

c) OP format: For an OP-formatted \mathcal{B} , i.e.,

$$\mathcal{B}_{OP} = \circ[[M_1, \dots, M_p]], \quad (34)$$

we use Theorem II.1(b) to express (15) as

$$\mathcal{Y}_i = [[\mathcal{X}_i; M_1, \dots, M_p]] + \mathcal{E}_i. \quad (35)$$

We estimate the parameters in (35) by applying the k th mode matricization for each $k = 1, \dots, p$ on both sides as $\mathcal{Y}_{i(k)} = M_k G_{ik}^{OP} + E_i$, where $G_{ik}^{OP} = \mathcal{X}_{i(k)} \left(\bigotimes_{j=p, j \neq k}^1 M_j' \right)$ and $E_i \stackrel{iid}{\sim} \mathcal{N}_{[m_k, m_{-k}]'}(0, \sigma^2 \Sigma_k, \Sigma_{-k})$. Given the similarities between this formulation and (29), the MLEs of the factor matrices are as in (33) but with G_{ik}^{OP} instead of G_{ik}^{CP} . The optimization procedure is similar to Algorithm 2, with the difference again that M_1, \dots, M_{p-1} are normalized to have unit Frobenius norm. We conclude by noting that (35) is the multilinear tensor regression setup of [13], and for $p = 2$ is the matrix-variate regression framework of [56] and [57]. So the OP format frames existing methodology within the ToTR framework.

d) TR format: Let \mathcal{B} have TR format (11), i.e.

$$\mathcal{B}_{TR} = \text{tr}(\mathcal{L}_1 \times^1 \mathcal{L}_2 \times^1 \dots \times^1 \mathcal{L}_l \times^1 \mathcal{M}_1 \times^1 \mathcal{M}_2 \times^1 \dots \times^1 \mathcal{M}_p), \quad (36)$$

of TR rank $(s_1, \dots, s_l, g_1, \dots, g_p)$, where \mathcal{L}_j and \mathcal{M}_k are third order tensor of sizes $(s_{j-1} \times h_j \times s_j)$ and $(g_{k-1} \times m_k \times g_k)$ respectively, for all $j = 1, \dots, l$ and $k = 1, \dots, p$, and where $g_0 = s_l$ and $s_0 = g_p$. The TR format reduces the number of unconstrained parameters in \mathcal{B} from $\prod_{i=1}^l h_i \prod_{i=1}^p m_i$ to $\sum_{j=1}^l s_{j-1} h_j s_j + \sum_{k=1}^p g_{k-1} m_k g_k$. To estimate parameters, we apply the k th mode matricization for $k = 1, \dots, p$ on both sides of (13), yielding

$$\mathcal{Y}_{i(k)} = \mathcal{M}_{k(2)} G_{ik}^{TR} + E_i, \quad E_i \stackrel{iid}{\sim} \mathcal{N}_{[m_k, m_{-k}]'}(0, \sigma^2 \Sigma_k, \Sigma_{-k}), \quad (37)$$

and the vectorization for $k = 1, \dots, l$, which gives us

$$\text{vec}(\mathcal{Y}_i) = H_{ik}^{TR} \text{vec}(\mathcal{L}_k) + \mathbf{e}_i, \quad \mathbf{e}_i \stackrel{iid}{\sim} \mathcal{N}_m(0, \sigma^2 \Sigma), \quad (38)$$

where G_{ik}^{TR} and H_{ik}^{TR} are matrices as defined in Section S1-E2. Fig. 5 represents tensor-variate versions of H_{ik}^{TR} and G_{ik}^{TR} for when $p=l=3$. Because (29) and (32) are similar to (37) and (38), our ML estimators mirror the CP format case but by replacing $(H_{ik}^{CP}, G_{ik}^{CP})$ with $(H_{ik}^{TR}, G_{ik}^{TR})$. In this case, estimating $(M_k, \text{vec}(L_k))$ corresponds to estimating $(\mathcal{M}_{k(2)}, \text{vec}(\mathcal{L}_k))$. The optimization procedure is similar to Algorithm 2, with the difference in this case being that each factor tensor, other than \mathcal{M}_p , is scaled to have unit Frobenius norm. We end here by noting that the special TR case of TT format has been used for ToTR in [32], with $\Sigma = I$, and hence $\Sigma_k = I$ for all k .

Concluding Remarks: Fig. 5 summarizes our estimation methods for \mathcal{B} of different formats. We see that in many cases, an algorithmic block can be made to correspond to a linear model by appropriate choice of \mathcal{G}_{ik} or \mathcal{H}_{ik} . Then, fitting a tensor-response linear model involves sequentially fitting smaller-dimensional linear models (one for each tensor factor) until convergence. This intuition behind the estimation of \mathcal{B} is not restricted to the TK, CP, OP and TR formats, but can also help guide estimation algorithms for other formats such as the hierarchical Tucker and the tensor tree formats [58], [59].

While the OP format has the advantage of parsimony, it does not allow for the level of recovery to be adjusted through a tensor rank (as will be illustrated in Section III and Fig. 6). The CP format is a more attractive alternative, since it is the natural

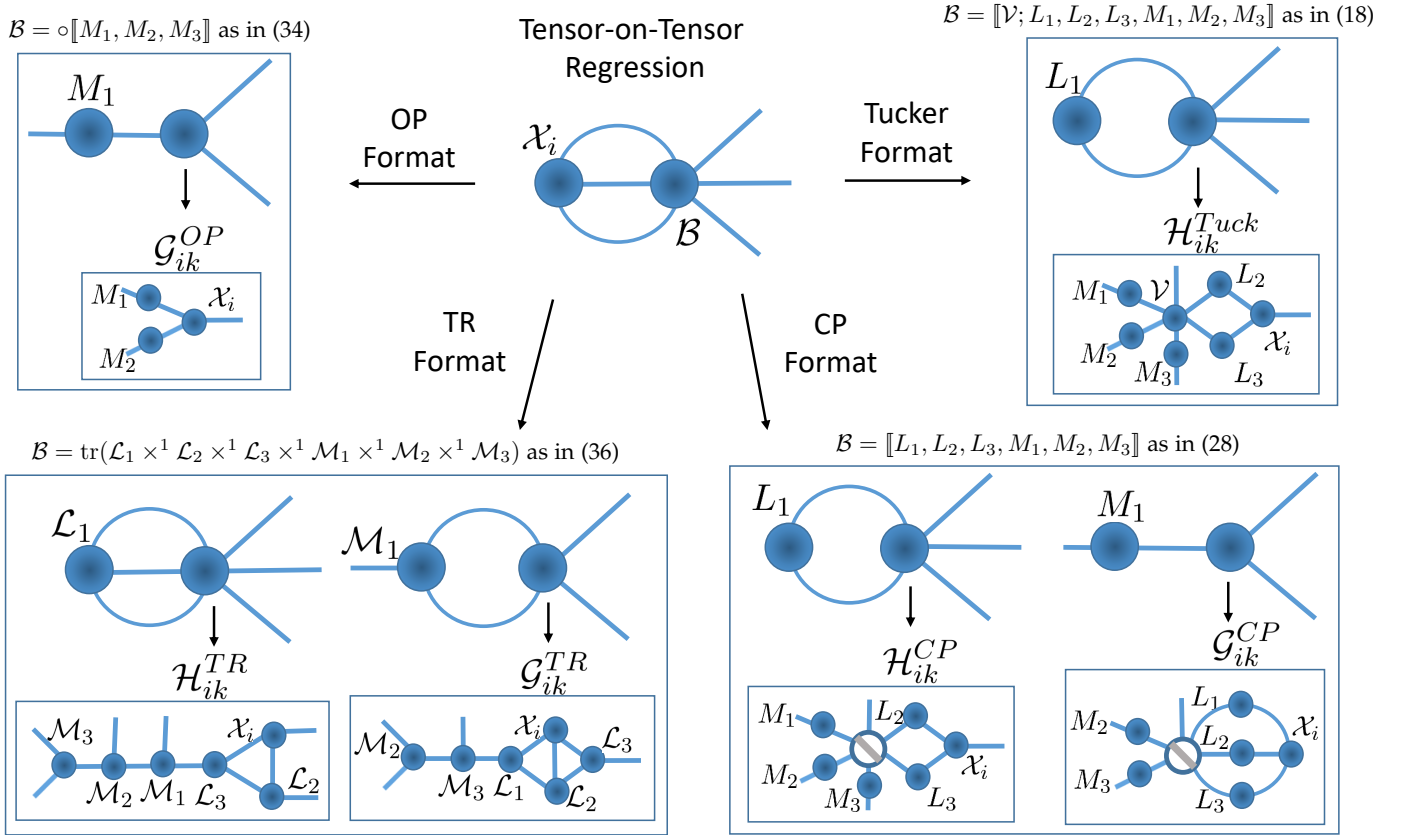


Fig. 5. Equivalent tensor-network diagrams for $(\mathcal{X}_i, \mathcal{B})$ when $p = l = 3$, which can be expressed in multiple ways depending on the tensor factor to be estimated and the type of low-rank on \mathcal{B} (which are illustrated in Fig. 4). By choosing the tensors \mathcal{G}_{ik} and \mathcal{H}_{ik} , the tensors M_1 and M_1 can be estimated using multivariate multiple linear regression, and the tensors L_1 and \mathcal{L}_1 can be estimated using multiple linear regression, respectively. In these cases, matricized versions of \mathcal{G}_{ik} and \mathcal{H}_{ik} are part of the design matrix.

generalization of the low-rank matrix format (a tensor with CP rank k is the sum of k tensors with CP rank 1). However, the CP format can be too restrictive in some scenarios, such as when the tensor modes have very different sizes. In such cases, the Tucker format provides a more appealing alternative. Moreover, a Tucker-formatted tensor has the interpretation of being a core tensor that is stretched on each mode by a tall matrix. However, its disadvantage is that the core tensor has the same number of modes as the original tensor, making it impractical in very high-order tensor scenarios. In such situations, the TR format is preferred because each additional tensor-mode requires only one additional tensor factor.

3) *Estimation of σ^2* : In all cases, the estimation of Σ_k involves finding the sum of squared errors along the k -mode S_k , as in equations (26) and (30). Given the estimated $\hat{\Sigma}_k$ and S_k , the estimate of σ^2 is very cheap and given as

$$\hat{\sigma}^2 = \frac{1}{nm} \text{tr}(\hat{\Sigma}_k S_k). \quad (39)$$

Thus $\hat{\sigma}^2$ is obtained alternatively within each iteration. Moreover, the log-likelihood function evaluated at the current estimated values is greatly simplified based on $\hat{\sigma}^2$ as

$$\ell = -\frac{nm}{2} \left[1 + \log(2\pi\hat{\sigma}^2) + \sum_{k=1}^p \log |\hat{\Sigma}_k|/m_k \right].$$

4) *Initialization and convergence*: For local optimality, we need the two conditions that the log-likelihood ℓ is jointly continuous and that the set $\{\boldsymbol{\theta} : \ell(\boldsymbol{\theta}) \geq \ell(\boldsymbol{\theta}^{(0)})\}$, for a set of initial values $\boldsymbol{\theta}^{(0)}$, is compact [53]. These conditions are satisfied because of the TVN distributional assumption on our errors, as long as the initial values satisfy the constraints on the parameters. We initialized $\Sigma_k = I_{m_k}$ and the tensor factor entries in \mathcal{B} with draws from the $\mathcal{U}(0, 1)$ distribution. With the TK format, M_k has the constraint $M_k' \Sigma_k^{-1} M_k = I_{d_k}$ for $k = 1, \dots, p$, so we used $\Sigma_k^{\frac{1}{2}} U$ as its initializer, with U having the left singular vectors of a random matrix of the same order as M_k . We also suggest using identity matrices to initialize $\Sigma_1, \dots, \Sigma_p$ and σ^2 can be initialized with 1. Our algorithms are declared to converge when we have negligible changes in the loglikelihood, as simplified in Section II-C3. A different criteria is the difference in norm $\|\mathcal{B}\| + \|\sigma^2 \Sigma\|$, where $\|\sigma^2 \Sigma\| = \sigma \prod_{k=1}^p \|\Sigma_k\|$ and $\|\mathcal{B}\|$ simplifies as per format:

- for \mathcal{B}_{TK} , with A^q as the Q matrix from the LQ decomposition of A [44], we have $\|\mathcal{B}_{TK}\| = \|\llbracket \mathcal{V}; L_1^q, \dots, L_l^q, M_1^q, \dots, M_p^q \rrbracket\|$.

- for \mathcal{B}_{CP} , $\|\mathcal{B}_{CP}\|^2 = \sum_{k,l=1}^R \{diag(\boldsymbol{\lambda})[*_{i=1}^l(L'_i L_i)] * [*_{i=1}^p(M'_i M_i)]\}(k,l)$, where “*” is the Hadamard, or entry-wise product [44].
- for \mathcal{B}_{OP} , $\|\mathcal{B}_{OP}\| = \prod_{i=1}^p \|M_i\|$.

D. Properties of our estimators

1) *Computational complexity*: We derive the computational complexity of our estimation algorithms. Recall that in all cases the response $\mathcal{Y}_i \in \mathbb{R}^{\times_{k=1}^p m_k}$ and the covariate $\mathcal{X}_i \in \mathbb{R}^{\times_{k=1}^l h_k}$ where l and p are considered fixed. WLOG, we assume that $m_1 = \max\{m_1, \dots, m_p\}$ and $h_1 = \max\{h_1, \dots, h_l\}$.

Theorem II.3. *The computational complexity of our ToTR algorithms when \mathcal{B} has*

- 1) *the TK format of Section II-C2a, with $d = \prod_{q=1}^l d_q$, $d_{-1} = d/d_1$, $c = \prod_{q=1}^l c_q$, $d_1 = \max\{d_1, \dots, d_p\}$ and $c_1 = \max\{c_1, \dots, c_l\}$ and implemented in Algorithm 1 is $\mathcal{O}(nhc_1 + n^2c + n^2m_1d_{-1} + nm_1^2d_{-1}) + \mathcal{O}(nmd_1) + \mathcal{O}(ncdh_1 + nc_1^2h_1^2d + h_1^3c_1^3) + \mathcal{O}(m_1^3 + nmm_1)$.*
- 2) *the CP format of Section II-C2b and implemented in Algorithm 2 is $\mathcal{O}(nh_1^2r^2 + nrm + rm_1^2 + m_1^3 + h_1^3r^3 + nrh + m_1r^2 + nmm_1)$.*
- 3) *the TR format, as described in Section II-C2d and with $g_0g_1 = \max\{g_{k-1}g_k : k = 1, 2, \dots, p\}$, $s_0s_1 = \max\{s_{k-1}s_k : k = 1, 2, \dots, l\}$, $g = \max\{g_0, g_1\}$, $g_0g_1 \leq m_1$ is $\mathcal{O}(mg_1g_0g_p + hns_s_l + mh_1^2s_0^2s_1^2 + h_1^3s_0^3s_1^3) + \mathcal{O}(hs_1s_0s_l + m_1^3 + g_0^3g_1^3 + nmm_1)$.*

Proof. See Sections S1-G1 - S1-G4 for the proofs. \square

In all cases we have the term $\mathcal{O}(nmm_1)$, which is the complexity of obtaining the sum of square errors S_k of equation (26) across the largest tensor-response mode, and it is necessary for obtaining the scale matrices $\Sigma_1, \dots, \Sigma_p$. In many cases this term will dominate the computational complexity. However, $\mathcal{O}(nmm_1)$ is considerably smaller than $\mathcal{O}(nm^2)$, which would be the case where our complexity increases quadratically with the dimensionality of the tensor response. We also note that in all cases, the cubic terms are WRT the tensor ranks, which can be considered negligible because such ranks are often chosen to be small, in the spirit of scientific parsimony. Finally, for the TK format, some of the factors can assumed to be identity matrices, allowing us to further reduce the complexity. (See Section S1-G3 for the computational complexity of the OP format under specific conditions.)

2) *Asymptotic sampling distributions*: We now derive the asymptotic distributions of our model-estimated parameters, specifically, the linear component and the covariance component (Section S1-M).

We first explore the limiting distribution of the estimated linear components $\text{vec}(\widehat{\mathcal{B}})$, which in all cases is multivariate normal with mean $\text{vec}(\mathcal{B})$ satisfying the same low-rank format of $\text{vec}(\widehat{\mathcal{B}})$. For the Tucker format, we first show that the vectorized core tensor $\text{vec}(\widehat{\mathcal{V}})$ follows a non-singular multivariate normal distribution, and therefore by Slutsky's theorem $\text{vec}(\widehat{\mathcal{B}})$ follows a singular multivariate normal distribution, where the singularity of the covariance matrix constraints the limiting distribution to the original low-rank Tucker format. For the CP, TR and OP cases we first show that the low-rank format factors in \mathcal{B} are jointly normally distributed. Therefore, by the Delta method the estimated tensors $\widehat{\mathcal{B}}$ in vectorized form are asymptotic normally distributed. In this case the resulting multivariate normal distribution is also singular, but these are only approximations to the CP, TR or OP formats and not constraints on the limiting distributions like it is the case for the Tucker format.

For the remainder of this paper, we define $h \doteq \prod_{i=1}^l h_i$, $M \doteq \otimes_{i=p}^1 M_i$ and $L \doteq \otimes_{i=l}^1 L_i$. We first assume that (15) holds without an intercept.

Theorem II.4. *Let (15) hold with $\mathcal{B} \equiv \mathcal{B}_{TK}$ of Tucker format as in (18) and let $X = [\text{vec}(\mathcal{X}_1) \dots \text{vec}(\mathcal{X}_n)]$ and $\widehat{\mathcal{B}}_{TK} = [\widehat{\mathcal{V}}; \widehat{L}_1, \widehat{L}_2, \dots, \widehat{L}_l, \widehat{M}_1, \widehat{M}_2, \dots, \widehat{M}_p]$. Then as $n \rightarrow \infty$*

$$\text{vec}(\widehat{\mathcal{B}}_{TK}) \xrightarrow{d} \mathcal{N}_{mh}(\text{vec}(\mathcal{B}_{TK}), \sigma^2(MM') \otimes (P_L(XX')^{-1}P_L)),$$

where $P_L = \otimes_{i=l}^1 P_i$ and $P_i = L_i(L'_i L_i)^{-1}L'_i$.

Proof. See Section S1-H. \square

The limiting distribution in Theorem II.4 is TVN when XX' has a Kronecker structure: examples include factorial designs and B-splines [60]. Here we present one such case.

Corollary II.1. *When $\widehat{\mathcal{B}}_{TK}$ is used to estimate a balanced TANOVA with q units for each factor combination, then for $\mathbf{s} = [h_1, h_2, \dots, h_l, m_1, m_2, \dots, m_p]'$, as $n \rightarrow \infty$*

$$\widehat{\mathcal{B}}_{TK} \xrightarrow{d} \mathcal{N}_{\mathbf{s}}(\mathcal{B}, \frac{\sigma^2}{q} P_1, P_2, \dots, P_l, M_1 M'_1, M_2 M'_2, \dots, M_p M'_p).$$

Proof. Here $XX' = qI_h$ and so the variance-covariance matrix in the limiting distribution of Theorem II.4 is $(\sigma^2/q)(MM') \otimes (\otimes_{i=l}^1 P_i)$, which is Kronecker-separable. The result follows from Definition II.2. \square

The CP format case is similar to Theorem II.4.

Theorem II.5. Consider (15) with $\mathcal{B} \equiv \mathcal{B}_{CP}$ as in (28) and the ML estimator $\widehat{\mathcal{B}}_{CP} = [\widehat{L}_1, \widehat{L}_2, \dots, \widehat{L}_l, \widehat{M}_1, \widehat{M}_2, \dots, \widehat{M}_p]$. Then

$$\text{vec}(\widehat{\mathcal{B}}_{CP}) \xrightarrow{d} \mathcal{N}_{mh} \left(\text{vec}(\mathcal{B}_{CP}), J_{CP} R_{CP} (\mathbf{I}_n \otimes \Sigma) R'_{CP} J'_{CP} \right)$$

as $n \rightarrow \infty$. Here J_{CP} is a Jacobian matrix and is given along with the block matrix R_{CP} in Section S1-I.

Proof. See Section S1-I. □

The sampling distributions of \mathcal{B} under the OP or TR formats are similar to the CP case, and are in theorem S1.2 of Section S1-J.

Theorem II.6. For a model with intercept, as in (13), Theorems II.4 and II.5 also hold after centering the covariates.

Proof. See Section S1-L. □

Section S1-M also discusses inference on the scale components $\widehat{\Sigma}_1, \widehat{\Sigma}_2, \dots, \widehat{\Sigma}_p$. Theorem S1.3 establishes the asymptotic independence of the scale and the linear components, we find the Fisher information matrix WRT the scale parameters, and establish its singularity. Our results on the asymptotic distribution of the scale components are not unique to our regression methodology but also generally hold for the TVN distribution.

E. Model selection or rank determination

For the CP, TR and TK formats, we determine optimal ranks using the Bayesian information criterion (BIC) [61], [62]. This calculation requires the loglikelihood that we simplified in Section II-C3. Section S1-F provides more details on rank determination (equivalently, model selection) and on the total number of calculations needed to obtain the BIC.

III. EXPERIMENTAL EVALUATIONS

We study estimation performance of the scale parameters and the low-rank linear component \mathcal{B} using simulation experiments on different ToTR models. Section III-A assesses the consistency of our estimators, and Section III-B evaluates the amounts of recovery that different low-rank formats have of \mathcal{B} , and the impact of noise on discrimination in a TANOVA framework.

A. A TANOVA(2,2) model with low-rank formats

We simulated observations from the matrix-on-matrix regression (MoMR) model

$$Y_{ijk} = \langle X_{ij} | \mathcal{B} \rangle + E_{ijk}, \quad E_{ijk} \stackrel{iid}{\sim} \mathcal{N}_{[6,7]'}(0, \sigma^2 \Sigma_1, \Sigma_2) \quad (40)$$

where $i = 1, 2, 3, 4$, $j = 1, 2, 3, 4, 5$ and X_{ij} is a 4×5 matrix with 1 at the (i, j) th position and zeroes everywhere else. We set $\sigma^2 = 1$ and obtained Σ_1 and Σ_2 independently from Wishart distributions, that is, we obtained $\Sigma_1 \sim \mathcal{W}_6(6, I_6)$ and $\Sigma_2 \sim \mathcal{W}_7(7, I_7)$ before scaling each by their $(1, 1)$ th element. We obtained realizations from four MoMR models, one each for \mathcal{B} of TK, CP, TR and OP formats, and fit appropriate models to the data using the ML estimation procedures described in Section II-C. To study consistency properties of our estimators, we used $k = 1, 4, 7, 10$ and 13, meaning that our sample sizes ranged over $n \in \{20, 80, 140, 200, 260\}$. An unstructured \mathcal{B} in this experiment would have $4 \times 5 \times 6 \times 7 = 840$ entries, but \mathcal{B} has only 59 unconstrained parameters with the OP format and 45 unconstrained parameters when it is of CP format of rank 2. This number is only 60 when \mathcal{B} has TK format with rank (2,2,2,2) and 70 when it is of the TR format with rank (2,2,2,2). Thus, our lower-rank simulation framework had at least 91% fewer unconstrained parameters in \mathcal{B} . We simulated data from (S34) using \mathcal{B} , σ^2 , Σ_1 and Σ_2 and estimated the parameters for each replication. Fig. 6 displays the Frobenius norm of the difference between the true and estimated parameters, and shows that as sample size increases, $(\widehat{\mathcal{B}}, \widehat{\sigma}^2, \widehat{\Sigma}_1, \widehat{\Sigma}_2)$ approach the true parameters $(\mathcal{B}, \sigma^2, \Sigma_1, \Sigma_2)$, demonstrating consistency of the estimators.

B. Evaluating recovery and discrimination

We simulated 600 observations from the MoMR model

$$Y_{ijk} = \langle X_{ij} | \mathcal{B} \rangle + E_{ijk}, \quad E_{ijk} \stackrel{iid}{\sim} \mathcal{N}_{[87,106]'}(0, \sigma^2 \Sigma_1, \Sigma_2), \quad (41)$$

where $i = 1, 2, 3, 4$, $j = 1, 2, 3$, X_{ij} is a 4×3 matrix with 1 at the (i, j) th position and zero elsewhere, and $\Upsilon_{ij} = \langle X_{ij} | \mathcal{B} \rangle$ corresponds to the pixel-wise logit transformation of the j th additive color (Red, Green, Blue) of the i th Andean camelid (Guanaco, Llama, Vicuña, Alpaca) images of Fig. 7(a). We set Σ_1 and Σ_2 to be AR(1) correlation matrices with coefficients 0.1 and -0.1 respectively, and $\sigma^2 = 1$. Sans constraints, we have $3 \times 4 \times 87 \times 106 = 110664$ parameters in \mathcal{B} .

We fit (41) separately for TR-, TK-, CP- and OP-formatted \mathcal{B} , with ranks set to have similar number of unconstrained parameters in \mathcal{B} . The TR format with rank (3,3,5,3) had 2958 such parameters, the TK format with rank (4,4,9,9) had 3061 parameters, the CP format with rank 15 had 3001 parameters in \mathcal{B} , while the relatively inflexible OP format had 666 parameters. In all cases, the dimension of \mathcal{B} was reduced by over 97%. The estimated tensor \mathcal{B} in each case corresponds to the

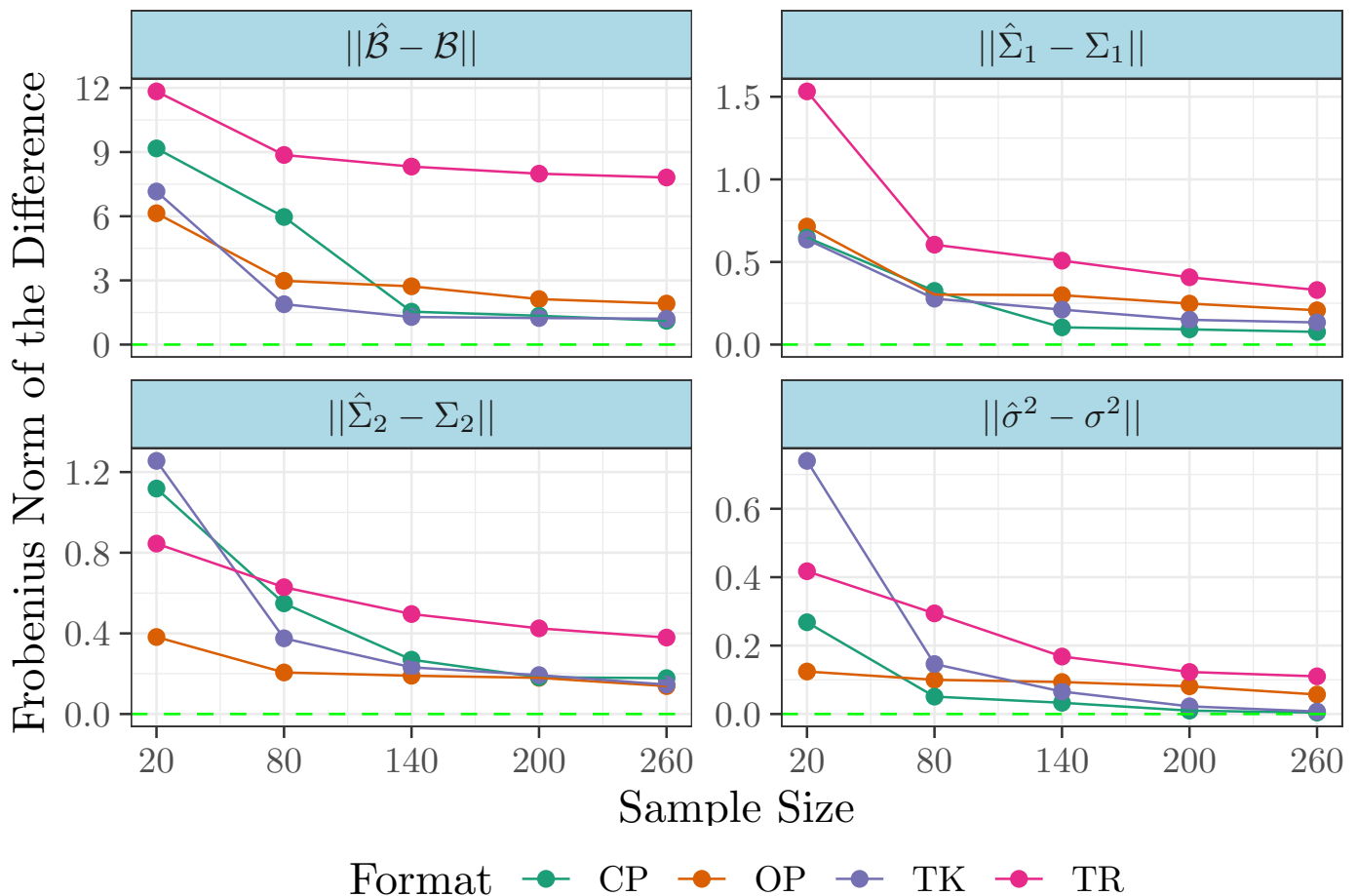


Fig. 6. Performance of the four models presented in Section III-A, each corresponding to a different format on \mathcal{B} . Each plot corresponds to the Frobenius norm of the difference between an estimated and true population parameter, against the sample size. We observe that in all cases, an increase in sample size leads to more accurate estimates.

estimated color images of the four Andean camelids. Fig. 7(a) shows varying success of these four formats in recovering the underlying camelid image (true \mathcal{B}). The OP-estimated images are the least-resolved, with the reduced number of parameters for \mathcal{B} inadequate for recovery. But the other formats can adjust for the quantum of reduction in parameters through their ranks. We illustrate this aspect by fitting (41) with \mathcal{B} having the TK, CP and TR formats with optimal rank chosen by BIC, following Section II-E. Fig. 7(a) shows very good recovery of \mathcal{B} by these BIC-optimized $\hat{\mathcal{B}}$ s, with unappreciable visual differences in all cases. In contrast, the model fit with unstructured \mathcal{B} and diagonal Σ , has a BIC of 1.64×10^7 , while fitting a model with a similar \mathcal{B} but Kronecker-separable Σ has a BIC of 1.63×10^7 . The CP, TK and TR formats therefore outperform these two alternatives when the ranks are tuned.

The TANOVA(2,2) formulation of (41) enables us to test

$$\begin{aligned} H_0 : \mathcal{P}_1 = \mathcal{P}_2 = \mathcal{P}_3 = \mathcal{P}_4 \quad \text{vs.} \\ H_a : \mathcal{P}_i \neq \mathcal{P}_{i^*}, \text{ for some } i \neq i^* \in \{1, 2, 3, 4\} \end{aligned} \quad (42)$$

where \mathcal{P}_i is a third-order tensor of size $3 \times 87 \times 106$ that contains the RGB slices of the i th Andean camelid image. The usual Wilks' Λ statistic [63] is $\Lambda = |\hat{\Sigma}_R|/|\hat{\Sigma}_T|$, where $\hat{\Sigma}_R$ is the sample covariance matrix of the residuals and $\hat{\Sigma}_T$ is the sample covariance matrix of the simpler model's residuals, which finds a common mean across all camelids. (Section S2 details the calculation of $\hat{\Sigma}_R$ and $\hat{\Sigma}_T$.) We illustrate the role of σ^2 and the low-rank OP, TR, CP or TK formats in distinguishing the four camelids, as measured by the Wilks' Λ test statistic, in Fig. 7(b), for $\sigma = 2, 4, 6, 8, 10$. The value of Λ increases with σ^2 , meaning that larger variances decrease the power of our test. Further, the CP, TR and TK formats yield lower-valued (more significant) test statistics than OP. This finding illustrates the limits of the less-flexible OP format relative to the others in recovering \mathcal{B} . Nevertheless, OP joins the other three formats in consistency of estimation and discrimination, as illustrated by Wilks' Λ .

IV. REAL DATA APPLICATIONS

Having evaluated performance of our reduced-rank ToTR methodology, we apply it to the datasets of Section I-A.

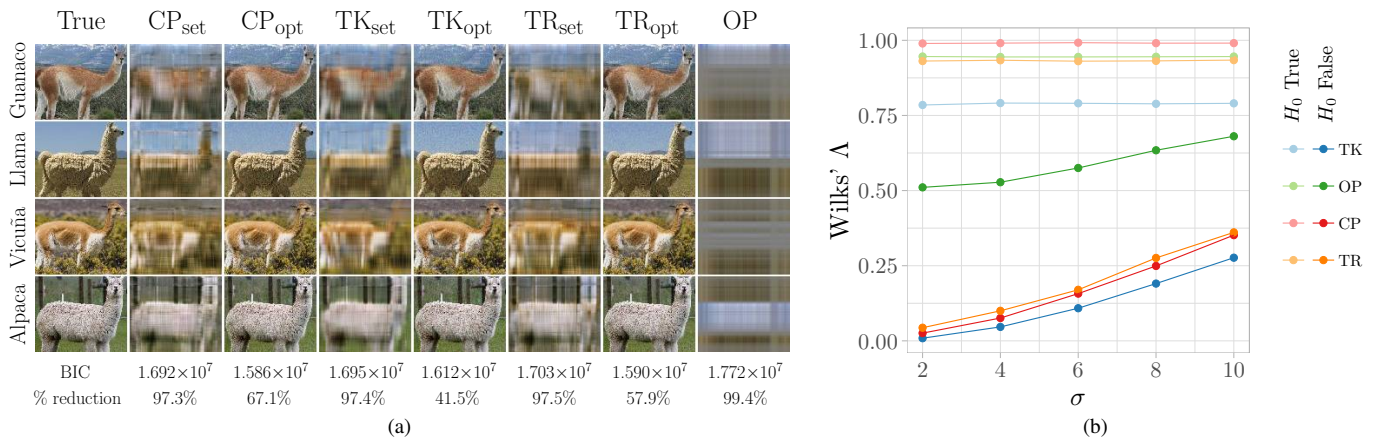


Fig. 7. (a) Results of fitting seven TANOVA(2,2) models on data simulated from (41). One model was fit assuming the OP format, and two models were fit for each of the TK, CP and TR formats: one with set ranks and another one with optimal ranks, as chosen by BIC. The two factors are the type of andean camelid (Guanaco, Llama, Vicuña, Alpaca) and the type of additive color RGB (red, green, blue). The Guanaco, Llama and Alpaca images are from Wikipedia Commons and the Vicuña image is from Encyclopædia Britannica. It is evident that while one cannot adjust the OP rank, increased rank for the TR, TK and CP formats result in more image restoration. (b) Monte-Carlo 95th quantiles of the Wilks' Λ statistics that test the set of hypothesis in equation (42), for the OP, CP, TR and TK formats, five values of scalar variance σ^2 in the x-axis, and for both true and false null hypotheses. Large variabilities lead to larger test statistics when H_0 is false, leading to weaker evidence against the null hypothesis. In all cases, CP, TR and TK formatting leads to more significant statistics when compared to the OP, even when the ranks are not optimal.

A. A TANOVA(1,5) model for cerebral activity

Section I-A1 laid out a TANOVA model involving 30 fMRI volumes of voxel-wise changes in activation from a baseline, each volume corresponding to one of ten words connoting death, positive or negative affects, for each of 17 subjects. For the j th subject we have a fifth-order tensor \mathcal{Y}_j of order $3 \times 10 \times 43 \times 56 \times 20$, where the first two modes correspond to the three kinds of word stimulus and the individual words, and the other modes correspond to the dimensions of the image volume. The j th subject has status given by \mathbf{x}_j that is a 2D unit vector with 1 at position i that is 1 for attempter or 2 for ideator. We model these responses and covariates as

$$\mathcal{Y}_j = \langle \mathbf{x}_j | \mathcal{B} \rangle + \mathcal{E}_j, \quad \mathcal{E}_j \stackrel{iid}{\sim} \mathcal{N}_{\mathbf{m}_1}(0, \sigma^2 \Sigma_1, \Sigma_2, \Sigma_3, \Sigma_4, \Sigma_5),$$

where $\mathbf{m}_1 = [3, 10, 43, 56, 20]'$ and $j = 1, \dots, 17$. We let \mathcal{B} have the TK format $[[\mathcal{V}; L_1, M_1, M_2, M_3, M_4, M_5]]$ with rank $(2, 3, 6, 15, 20, 7)$ chosen by BIC from 256 candidate ranks, and where $M'_k \Sigma_k^{-1} M_k = I_{d_k}$, $k = 1, 2, 3, 4, 5$. The 77578 parameters to be estimated in our \mathcal{B} represent an over 97.3% reduction over that of the unconstrained \mathcal{B} of size $2 \times 3 \times 10 \times 43 \times 56 \times 20$, or 2889600 parameters. (Our use of a TK format exploits its nicer distributional properties for easier inference, and therefore we only use this format here.) We set Σ_1 (specifying relationships between word types) to be unconstrained, Σ_2 (covariances between same kinds of words) to have an equicorrelation structure and $\Sigma_3, \Sigma_4, \Sigma_5$ with AR(1) correlations to capture spatial context in the image volume. Fitting the model with unstructured \mathcal{B} and diagonal Σ yielded a BIC of 210 million, while the fitted model with a similar \mathcal{B} but Kronecker-separable Σ reported a BIC of 164 million. In contrast, our TK model with Kronecker-separable covariance outperformed these two alternatives with a BIC of 127 million.

Our primary interest here is to find regions of significant interaction between word type and subject suicide attempter/ideator status to determine markers for suicide risk assessment and intervention. The interaction estimate can be expressed as $\hat{\mathcal{B}}_* = \hat{\mathcal{B}} \times_1 \mathbf{c}'_1 \times_2 C_2 \times_3 \mathbf{c}'_3$, where \mathbf{c}'_1 is a contrast vector that finds differences between suicide attempter/ideation status, C_2 is a contrast matrix for differences across word type and \mathbf{c}'_3 is a contrast vector that averages the ten words of each type. These contrast matrices and vectors are given in (S30). From Theorem II.4,

$$\hat{\mathcal{B}}_* \stackrel{d}{\rightarrow} \mathcal{N}_{\mathbf{m}_2}(\mathcal{B}_*, \tau^2 C_2 M_1 M'_1 C'_2, M_3 M'_3, M_4 M'_4, M_5 M'_5),$$

where $\mathbf{m}_2 = [3, 20, 43, 56]'$, $\mathcal{B}_* = \mathcal{B} \times_1 \mathbf{c}'_1 \times_2 C_2 \times_3 \mathbf{c}'_3$ and τ^2 is as in Section S3-A. Using the asymptotic distribution of $\hat{\mathcal{B}}_*$, we marginally standardize it to obtain $\hat{\mathcal{Z}}_*$ as shown in (S33), which also follows the TVN distribution but with correlation matrices as scale parameters. In Section S3-A we detail its derivation, interpretation and asymptotic distribution. For the i th level interaction, consider the set of hypotheses at the (k, l, m) th voxel

$$H_o : \mathcal{B}_*(i, k, l, m) = 0 \quad \text{vs} \quad H_a : \mathcal{B}_*(i, k, l, m) \neq 0.$$

Under the null hypothesis of no i th interaction effect at the (k, l, m) th voxel, the marginal distribution of $\hat{\mathcal{Z}}_*(i, k, l, m)$ is asymptotically $N(0, 1)$. Fig. 8 displays 3D maps of the brain with significant values of $\hat{\mathcal{Z}}_*$ overlaid for each of the three pairs of interactions. Significant voxels were decided using cluster thresholding [64] ($\alpha = 0.05$), with clusters of at least 12 contiguous (under a second-order neighborhood specification) voxels, with this minimum cluster size determined by the

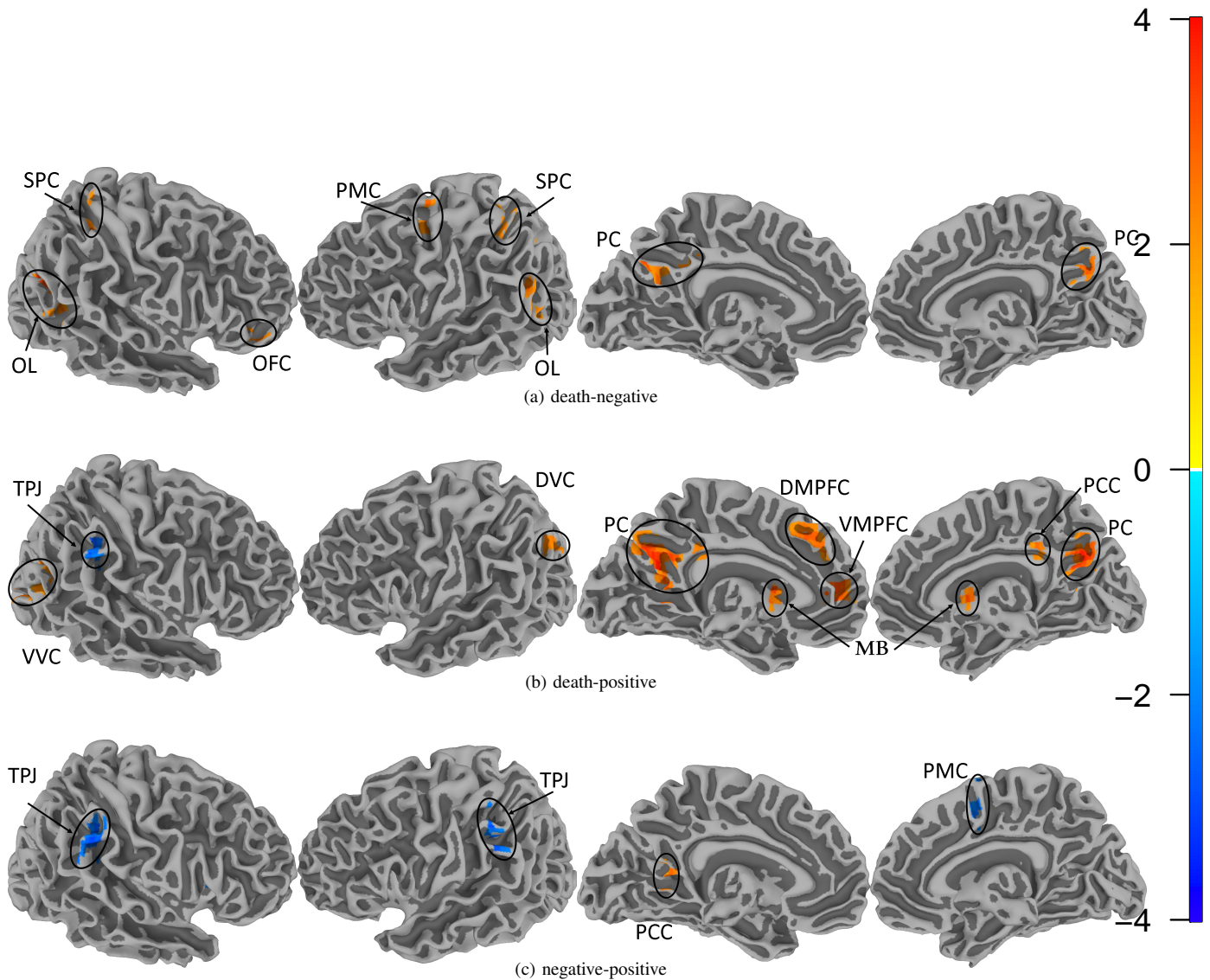


Fig. 8. The test statistic \hat{Z}_* of the interaction between subject's attempter/ideator status and (a) death-negative, (b) death-positive and (c) negative-positive words at voxels identified significant by cluster thresholding at the 5% level. These voxels are in the precuneus (PC), temporal-parietal junction (TPJ), orbital frontal cortex (OFC), premotor cortex (PMC), superior parietal cortex (SPC), ventral visual cortex (VVC), dorsal visual cortex (DVC), dorsal medial frontal cortex (DMPFC), ventral medial prefrontal cortex (VMPFC), mammillary bodies (MB), posterior cingulate cortex (PCC) and occipital lobe (OL).

Analysis for Neuroimaging (AFNI) software [65], [66]. There are many methods [67]–[73] for significance detection in fMRI studies but we use cluster thresholding here as an illustration and also because it is the most popular method. We now briefly discuss the results.

Fig. 8(a) identifies significant interactions between death- and negative-connoting words on the one hand and suicide attempters vis-a-vis ideators on the other. All significant interactions are positive and dominated by the precuneus and the orbital frontal cortex. The precuneus is associated with depression and rumination [74]–[76], while the orbital frontal cortex is associated with the influence that emotions and feelings have on decision-making [77], as well as with suicide attempters' reactions to external stimuli [78]. Both regions are also associated with the Default Mode Network (DMN) that plays a role in representing emotions [79]. These results indicate more differential rumination and emotions (between attempters and ideators) caused by death-related words, as compared to negative-connoting words. These findings are reinforced by the significance detected in the occipital lobe, the premotor cortex (PMC) and the superior parietal cortical regions that are related to working memory and depression [80]–[82]. Fig. 8(b) displays significant interactions between the positive and death-related words and suicide attempters and ideators. The precuneus is more pronounced here relative to Fig. 8(a), indicating that death-related words are more salient than words that have negative and positive connotations among attempters vis-a-vis ideators. This observation is reinforced with the detected significance in the dorsal and ventral visual medial prefrontal cortex, the mammillary bodies, and the posterior cingulate cortex (PCC) that are all involved in processing emotional information [83], [84]. The PCC is also involved in memory, emotion, and decision-making [85], [86] and is connected to the temporal-parietal junction [87] which is

involved with emotions and perception [88], [89]. High \widehat{Z}_* values in the ventral and dorsal visual cortices are commensurate with their association with working memory tasks [90]. Also, the low values of \widehat{Z}_* in the temporal parietal junction point to needed additional processing of death-related versus positive-connoting words among attempters relative to ideators. Fig. 8(c) shows significant interactions between negative and positive-emoting words and suicide attempters and ideators. The low values in the left and right temporal-parietal junctions and the PMC indicate that words conveying negative thoughts don't need as much processing as do positive-connoting words among attempters relative to ideators. The significant association of the PCC in both Figs. 8(b) and (c) supports our hypothesis that death-related words are more salient than negative or positive words in differentiating attempters from ideators. In summary, the two groups of subjects have positive- and negative-connoting words result in neurally similar significant brain regions when compared to death-related words, which show further significance in areas associated with the processing of emotional feelings and planning. Our conclusions here are on an experiment with only 9 attempters and 8 ideators and so are preliminary, but are interpretable, providing some confidence in the practical reductions afforded by TANOVA when coupled with the use of the Tucker-formatted \mathcal{B} for this application.

B. A TANOVA(3,3) model for the LFW face database

We return to the LFW database of Section I-A2 that is a compendium of over 13,000 face images. Using the steps detailed in Section S3-B, we selected 605 images with unambiguous genders, age group and ethnic origin, and such that there are at most 33 images for each factor combination. This dataset was also used by [29] with the goal of classification, leading to a vector-variate response of attributes and tensor-valued covariates of color images, for which a CP format was assumed. In contrast, our objective is to distinguish the characteristics of different attributes, leading to a TANOVA(3,3) model with color images as the response and gender, ethnic origin and gender as covariates. Our model is as per (15) and specifically

$$\mathcal{Y}_{ijkl} = \langle \mathcal{X}_{ijk} | \mathcal{B} \rangle + \mathcal{E}_{ijkl}, \quad \mathcal{E}_{ijkl} \sim \mathcal{N}_{\mathbf{m}_3}(0, \sigma^2 \Sigma_1, \Sigma_2, \Sigma_3),$$

where $i = 1, 2$, $j = 1, 2, 3$, $k = 1, 2, 3, 4$, $l = 1, \dots, n_{ijk}$, $\mathbf{m}_3 = [151, 111, 3]'$, and the (i, j, k, l) th response \mathcal{Y}_{ijkl} is the color image of size $151 \times 111 \times 3$ for the l th person of the i th gender, j th ethnic origin and k th age group. Here $\mathcal{X}_{ijk} = \mathbf{e}_i^2 \circ \mathbf{e}_j^3 \circ \mathbf{e}_k^4$ is the tensor-valued covariate for a TANOVA(3,3) model with $(h_1, h_2, h_3) = (2, 3, 4)$, as described in Section II-B2, encoding the genders \times ethnic-origin \times age-group attributes of \mathcal{Y}_{ijkl} . The corresponding TANOVA parameter \mathcal{B} is of size $2 \times 3 \times 4 \times 151 \times 111 \times 3$

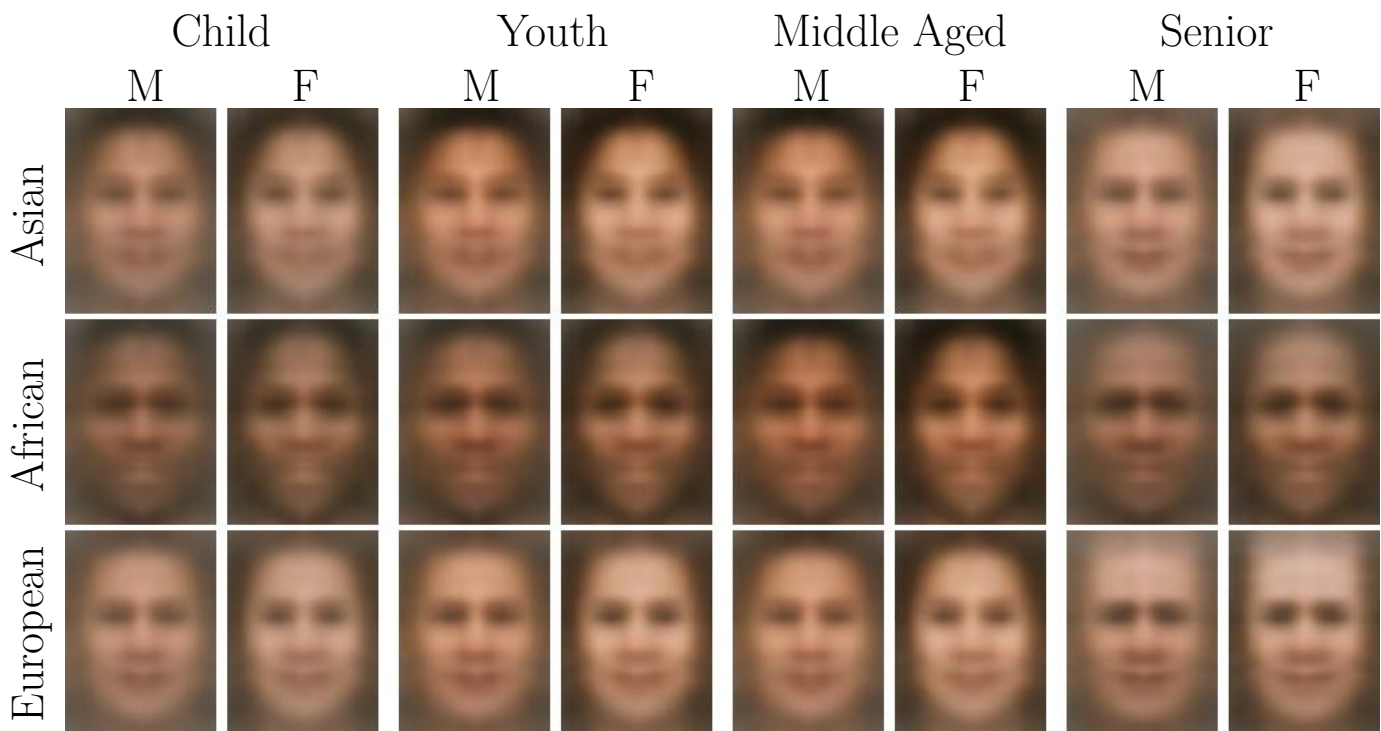


Fig. 9. Different slices of the resulting factorized tensor \mathcal{B} that results from fitting a TANOVA(3,3) model on the LFW dataset using the TT format. The results are compressed mean images across genders (male, female), ethnic origin (Asian, African, European) and age groups (child, youth, middle aged and senior) from 605 central LFW images. We can observe that the TT format preserved vital information regarding the factor-combination of age group, gender and ethnic-origin.

and contains all the group means. We constrained \mathcal{B} to have a tensor train (TT) format of TR rank $(1, 3, 3, 4, 10, 3)$, chosen using BIC out of a total of 64 candidate ranks. (In terms of the BIC, the TT format also bested the TK, CP and OP formats.) The number of parameters involved in \mathcal{B} is 6393 due to the TT restriction, which is a reduction in the number of unconstrained

parameters of around 99% from the unconstrained \mathcal{B} that has more than 1.2 million parameters. Fig. 9 displays the estimated $\hat{\mathcal{B}}$, from where we observe that the TT format preserved visual information regarding ethnic origin, gender, and age-group. Fitting the model with unstructured \mathcal{B} and diagonal Σ resulted in a BIC of 1.02×10^9 , while the fitted model with a similar \mathcal{B} but Kronecker-separable Σ reported a BIC of -1.22×10^7 . In contrast, our TT model with Kronecker-separable covariance outperformed these alternatives with a BIC of -1.87×10^7 .

V. DISCUSSION

We have provided a multivariate regression and ANOVA framework that exploits the tensor-valued structure of the explanatory and response variables using four different low-rank formats on the regression coefficient and a Kronecker-separable structure on the covariance matrix. These structures are imposed for context but more so for practical reasons, as the number of parameters involved in the classical MVMLR model grows exponentially with the tensor dimensions. Different structures can be compared between each other using criteria such as BIC. We provided algorithms for ML estimation, derived their computational complexity, and evaluated them via simulation experiments. We also studied the asymptotic properties of our estimators and applied our methodology to identify brain regions associated with suicide attempt or ideation status and death-negative- or positive-connoting words. Finally, we also used our methods to distinguish facial characteristics in the LFW dataset.

There are several other avenues for further investigation. For instance, we can perform additional dimension reduction by adding an L_1 penalty on the likelihood optimization. Also, the number of parameters in the intercept can potentially grow when the tensor response is high-dimensional, which motivates specifying a low-rank structure on the intercept term. Similarly, the independent and identically distributed assumption on the errors is not feasible when external factors group data-points into units that are similar to one another. For these cases, a mixed-effects model is more appropriate. Also, [28] recently demonstrated that in the scalar-on-tensor regression case, the use of the CP or TK format can induce a block structure along the direction of the modes of the tensor, a phenomenon that we also saw in Fig. III-A when the ranks were set, but that went away when BIC was allowed to tune these ranks. Some of our further investigations (Section S4) support this latter finding in a 2D regression framework, however additional investigations and palliative measures may be needed. Further, it would be worth investigating generalization of the Kronecker separable structure of the dispersion matrix or the normality assumption to incorporate more general distributional forms. Finally, it would be interesting to study the exact distribution of Wilks' Λ statistic or other statistic that can be used for testing hypothesis in our TANOVA framework without the need to do simulation. These are some issues that may benefit from further attention and that we leave for future work.

ACKNOWLEDGMENTS

The authors are very grateful to B. Klindinst and A. Willette of the Program of Neuroscience and the Department of Food Sciences and Human Nutrition at Iowa State University for help with the interpretation of Fig. 8. This research was supported in part by the National Institute of Justice (NIJ) under Grants No. 2015-DN-BX-K056 and 2018-R2-CX-0034. The research of the second author was also supported in part by the National Institute of Biomedical Imaging and Bioengineering (NIBIB) of the National Institutes of Health (NIH) under Grant R21EB016212, and the United States Department of Agriculture (USDA) National Institute of Food and Agriculture (NIFA) Hatch project IOW03617. The content of this paper is however solely the responsibility of the authors and does not represent the official views of the NIJ, the NIBIB, the NIH, the NIFA or the USDA.

SUPPLEMENTARY APPENDIX

S1. SUPPLEMENT TO SECTION II

A. Some Matrix Algebra Properties

In this section we provide identities and detail notation used in the main paper, in preparation for the proof of Lemma II.1 and Theorem II.1. While the $\text{vec}(\cdot)$ operator stacks the columns of a matrix into a vector, the commutation matrix $K_{k,l} \in \mathbb{R}^{kl \times kl}$ matches the elements of $\text{vec}(A)$ and $\text{vec}(A')$,

$$\text{vec}(A') = K_{k,l} \text{vec}(A), \quad A \in \mathbb{R}^{k \times l}. \quad (\text{S1})$$

The commutation matrix plays a critical role in tensor algebra, as it allows us to reshape tensors inside their vectorization. If A is a symmetric $n \times n$ matrix, then $\text{vec}(A)$ has n^2 elements of which $n(n-1)/2$ are repetitions, while the half-vectorization $\text{vech}(A)$ contains the $n(n+1)/2$ unique elements of A , since it does not take into account the elements above the diagonal. The duplication matrix D_n maps the elements of $\text{vec}(A)$ and $\text{vech}(A)$ as $D_n \text{vech}(A) = \text{vec}(A)$, and is a full-column rank matrix of size $n^2 \times (n(n+1)/2)$. The following is from [91]:

Property S1.1. Let $A_1 \in \mathbb{R}^{m \times n}$ and $A_2 \in \mathbb{R}^{p \times q}$ and $K_{\cdot,\cdot}$ be a commutation matrix. Then

a. $K_{\cdot,\cdot}$ is orthogonal and flipping the arguments results in its transpose. That is,

$$K'_{m,n} = K_{m,n}^{-1} = K_{n,m}.$$

b. $K_{\cdot, \cdot}$ can be used to change the order of the Kronecker product. That is,

$$K_{p,m}(A_1 \otimes A_2)K_{n,q} = A_2 \otimes A_1.$$

c. $K_{\cdot, \cdot}$ can be used to split the Kronecker product inside the vectorization. That is,

$$\text{vec}(A_1 \otimes A_2) = R_{A_1} \text{vec}(A_2), \quad R_{A_1} = (I_n \otimes K_{q,m})(\text{vec } A_1 \otimes I_q).$$

The Kronecker product (\otimes) between A and B results in the following block matrix:

$$A \otimes B = \begin{bmatrix} A(1,1)B & \dots & A(1,m)B \\ \vdots & \ddots & \vdots \\ A(n,1)B & \dots & A(n,m)B \end{bmatrix}. \quad (\text{S2})$$

The following properties follow recursively from the two-matrix cases in [92].

Property S1.2. Let A_1, A_2, \dots, A_p be matrices of any size and $\Sigma_1, \Sigma_2, \dots, \Sigma_p$ be positive definite matrices of any size. Then

- $\left| \bigotimes_{i=p}^1 \Sigma_i \right| = \prod_{i=1}^p |\Sigma_{-i}|^{m_{-i}}, \quad m_{-i} = m/m_i$
- $\left(\bigotimes_{i=p}^1 \Sigma_i \right)^{-1} = \left(\bigotimes_{i=p}^1 \Sigma_i^{-1} \right), \quad \left(\bigotimes_{i=p}^1 A_i \right)' = \left(\bigotimes_{i=p}^1 A_i' \right).$
- $\bigotimes_{i=p}^1 A_i = \left(\bigotimes_{i=p}^{l+1} A_i \right) \otimes \left(\bigotimes_{i=l}^1 A_i \right), \quad l = 2, \dots, p-2.$
- $\left(\bigotimes_{i=p}^1 A_i \right) \left(\bigotimes_{i=p}^1 B_i \right) = \bigotimes_{i=p}^1 (A_i B_i), \quad \text{where } A_i \text{ has as many columns as the rows of } B_i.$

B. Some Tensor Algebra Properties

The vectorization, k th-mode matricization and the k th canonical matricization of a p -th order tensor \mathcal{X} of size $m_1 \times m_2 \times \dots \times m_p$ as defined in Table I and Equation (4) are

$$\text{vec}(\mathcal{X}) = \sum_{i_1=1}^{m_1} \dots \sum_{i_p=1}^{m_p} \mathcal{X}(i_1 \dots i_p) \left(\bigotimes_{q=p}^1 e_{i_q}^{m_q} \right), \quad (\text{S3})$$

$$\mathcal{X}_{(k)} = \sum_{i_1=1}^{m_1} \dots \sum_{i_p=1}^{m_p} \mathcal{X}(i_1 \dots i_p) e_{i_k}^{m_k} \left(\bigotimes_{\substack{q=p \\ q \neq k}}^1 e_{i_q}^{m_q} \right)', \quad (\text{S4})$$

and

$$\mathcal{X}_{\langle k \rangle} = \sum_{i_1=1}^{m_1} \dots \sum_{i_p=1}^{m_p} \mathcal{X}(i_1 \dots i_p) \left(\bigotimes_{q=k}^1 e_{i_q}^{m_q} \right) \left(\bigotimes_{q=p}^{k+1} e_{i_q}^{m_q} \right)', \quad (\text{S5})$$

respectively. To illustrate these reshapings, consider the third-order tensor $\mathcal{X} \in \mathbb{R}^{3 \times 4 \times 2}$ illustrated in Fig. S1 and that was also

$$\mathcal{X} = \begin{array}{|c|c|c|c|c|} \hline & 13 & 16 & 19 & 22 \\ \hline 1 & 14 & 4 & 17 & 7 & 20 & 10 & 23 \\ \hline 2 & 15 & 5 & 18 & 8 & 21 & 11 & 24 \\ \hline 3 & & 6 & 9 & 12 & & & \\ \hline \end{array}$$

Fig. S1. A third order tensor $\mathcal{X} \in \mathbb{R}^{3 \times 4 \times 2}$ with elements 1 through 24.

used in [38].

The k th-mode matricizations are

$$\mathcal{X}_{(1)} = \begin{bmatrix} 1 & 4 & 7 & 10 & 13 & 16 & 19 & 22 \\ 2 & 5 & 8 & 11 & 14 & 17 & 20 & 23 \\ 3 & 6 & 9 & 12 & 15 & 18 & 21 & 24 \end{bmatrix}, \quad \mathcal{X}_{(2)} = \begin{bmatrix} 1 & 2 & 3 & 13 & 14 & 15 \\ 4 & 5 & 6 & 16 & 17 & 18 \\ 7 & 8 & 9 & 19 & 20 & 21 \\ 10 & 11 & 12 & 22 & 23 & 24 \end{bmatrix},$$

$$\mathcal{X}_{(3)} = \begin{bmatrix} 1 & 2 & 3 & 4 & 5 & 6 & 7 & 8 & 9 & 10 & 11 & 12 \\ 13 & 14 & 15 & 16 & 17 & 18 & 19 & 20 & 21 & 22 & 23 & 24 \end{bmatrix}$$

and the k canonical matricizations are

$$\mathcal{X}_{\langle 1 \rangle} = \mathcal{X}_{(1)}, \quad \mathcal{X}_{\langle 2 \rangle} = \mathcal{X}'_{(3)}, \quad \mathcal{X}_{\langle 3 \rangle} = \text{vec}(\mathcal{X}) = [1 \ 2 \ \dots \ 24]'$$

The last-mode with first-mode contraction, denoted as \times^1 and defined in Table II and Equation (5), is used to define the TR format in equation (11). One special case of this contraction is the matrix product between X and Y , which contracts the columns of X with the rows of Y , and can be expressed as $X \times^1 Y$. In Fig. S2 we further illustrate this contraction, for the \mathcal{X} of Figure S1.

$$\mathcal{X} \times^1 \begin{bmatrix} 1 & 2 \\ 1 & 2 \end{bmatrix} = \begin{array}{|c|c|c|c|} \hline & 28 & 40 & 52 & 64 \\ \hline 14 & 32 & 20 & 44 & 26 & 56 & 32 & 68 \\ \hline 16 & 36 & 22 & 48 & 28 & 60 & 34 & 72 \\ \hline 18 & & 24 & 30 & 36 & & & \\ \hline \end{array}$$

Fig. S2. The third order tensor that results from applying the last-mode with first-mode contraction between \mathcal{X} and Y , where \mathcal{X} is as in Figure S1.

We can reshape tensors by manipulating the vector outer product (\circ) applied to unit basis vectors, as in Equation (2). If $\{e_k^{m_k}\}_{k=1}^p$ are unit basis vectors, then $\bigotimes_{k=p}^1 e_k^{m_k}$ is also so, and so

$$\left(\bigotimes_{k=p}^1 e_k^{m_k} \right)' \left(\bigotimes_{k=p}^1 e_k^{m_k} \right) = \bigotimes_{k=p}^1 (e_k^{m_k'} e_k^{m_k}) = 1. \quad (\text{S6})$$

Equation (S6) is helpful in simplifying matrix products between matricized tensors.

C. Proof of Lemma II.1

Proof.

(a) We have

$$\begin{aligned} \mathcal{X}'_{\langle p-1 \rangle} &= \sum_{i_1=1}^{m_1} \dots \sum_{i_p=1}^{m_p} \mathcal{X}(i_1, i_2, \dots, i_p) \left(\left(\bigotimes_{q=p-1}^1 e_{i_q}^{m_q} \right) (e_{i_p}^{m_p})' \right)' \\ &= \sum_{i_1=1}^{m_1} \dots \sum_{i_p=1}^{m_p} \mathcal{X}(i_1, i_2, \dots, i_p) \left((e_{i_p}^{m_p}) \left(\bigotimes_{q=p-1}^1 e_{i_q}^{m_q} \right)' \right) = \mathcal{X}_{(p)}. \end{aligned}$$

(b) For any $l = 1, 2, \dots, p$, we have

$$\begin{aligned} \text{vec}(\mathcal{X}_{\langle l \rangle}) &= \sum_{i_1=1}^{m_1} \dots \sum_{i_p=1}^{m_p} \mathcal{X}(i_1, i_2, \dots, i_p) \text{vec} \left(\left(\bigotimes_{q=l}^1 e_{i_q}^{m_q} \right) \left(\bigotimes_{q=p}^{l+1} e_{i_q}^{m_q} \right)' \right) \\ &= \sum_{i_1=1}^{m_1} \dots \sum_{i_p=1}^{m_p} \mathcal{X}(i_1, i_2, \dots, i_p) \left(\bigotimes_{q=p}^1 e_{i_q}^{m_q} \right) = \text{vec}(\mathcal{X}). \end{aligned}$$

(c) Using the definition of vectorization in Table I, we have

$$\begin{aligned} (\text{vec } \mathcal{X})' (\text{vec } \mathcal{Y}) &= \left[\sum_{i_1=1}^{m_1} \dots \sum_{i_p=1}^{m_p} \mathcal{X}(i_1, i_2, \dots, i_p) \left(\bigotimes_{q=p}^1 e_{i_q}^{m_q} \right)' \right] \left[\sum_{i_1=1}^{m_1} \dots \sum_{i_p=1}^{m_p} \mathcal{Y}(i_1, i_2, \dots, i_p) \left(\bigotimes_{q=p}^1 e_{i_q}^{m_q} \right) \right] \\ &= \sum_{i_1=1}^{m_1} \dots \sum_{i_p=1}^{m_p} \mathcal{X}(i_1, i_2, \dots, i_p) \mathcal{Y}(i_1, i_2, \dots, i_p) \left(\bigotimes_{q=p}^1 e_{i_q}^{m_q} \right)' \left(\bigotimes_{q=p}^1 e_{i_q}^{m_q} \right) \\ &= \sum_{i_1=1}^{m_1} \dots \sum_{i_p=1}^{m_p} \mathcal{X}(i_1, i_2, \dots, i_p) \mathcal{Y}(i_1, i_2, \dots, i_p) = \langle \mathcal{X}, \mathcal{Y} \rangle. \end{aligned}$$

Similarly if $\mathbf{i} = [i_1, \dots, i_p]'$ then

$$\begin{aligned} \text{tr}(\mathcal{X}_{(k)}\mathcal{Y}'_{(k)}) &= \text{tr} \left\{ \left[\sum_{i_1=1}^{m_1} \dots \sum_{i_p=1}^{m_p} \mathcal{X}(\mathbf{i})(e_{i_k}^{m_k}) \left(\bigotimes_{\substack{q=p \\ q \neq k}}^1 e_{i_q}^{m_q} \right)' \right] \left[\sum_{i_1=1}^{m_1} \dots \sum_{i_p=1}^{m_p} \mathcal{Y}(\mathbf{i}) \left(\bigotimes_{\substack{q=p \\ q \neq k}}^1 e_{i_q}^{m_q} \right) (e_{i_k}^{m_k})' \right] \right\} \\ &= \sum_{i_1=1}^{m_1} \dots \sum_{i_p=1}^{m_p} \mathcal{X}(i_1, i_2, \dots, i_p) \mathcal{Y}(i_1, i_2, \dots, i_p) \text{tr} \left\{ e_{i_k}^{m_k} \left(\bigotimes_{\substack{q=p \\ q \neq k}}^1 e_{i_q}^{m_q} \right)' \left(\bigotimes_{\substack{q=p \\ q \neq k}}^1 e_{i_q}^{m_q} \right) (e_{i_k}^{m_k})' \right\} \\ &= \sum_{i_1=1}^{m_1} \dots \sum_{i_p=1}^{m_p} \mathcal{X}(i_1, i_2, \dots, i_p) \mathcal{Y}(i_1, i_2, \dots, i_p) = \langle \mathcal{X}, \mathcal{Y} \rangle. \end{aligned}$$

(d)

$$\begin{aligned} \text{vec}[\mathcal{X}; A_1, \dots, A_p] &= \sum_{i_1=1}^{m_1} \dots \sum_{i_p=1}^{m_p} \mathcal{X}(i_1, i_2, \dots, i_p) \text{vec} \left(\begin{smallmatrix} p \\ \circ \\ q=1 \end{smallmatrix} A_q(:, i_q) \right) \\ &= \sum_{i_1=1}^{m_1} \dots \sum_{i_p=1}^{m_p} \mathcal{X}(i_1, i_2, \dots, i_p) \left(\bigotimes_{q=p}^1 A_q(:, i_q) \right) = \left(\bigotimes_{q=p}^1 A_q \right) \text{vec}(\mathcal{X}). \end{aligned}$$

(e) We have for $\mathbf{i} = [i_1, \dots, i_p]'$ and $\mathbf{j} = [j_1, \dots, j_q]'$ that

$$\begin{aligned} \mathcal{B}'_{\langle p \rangle} \text{vec} \mathcal{X} &= \left[\sum_{i_1=1}^{m_1} \dots \sum_{i_p=1}^{m_p} \sum_{j_1=1}^{h_1} \dots \sum_{j_q=1}^{h_q} \mathcal{B}([i'j']') \left(\left(\bigotimes_{k=q}^1 e_{j_k}^{h_k} \right) \left(\bigotimes_{k=p}^1 e_{i_k}^{m_k} \right)' \right) \right] \left[\sum_{i_1=1}^{m_1} \dots \sum_{i_p=1}^{m_p} \mathcal{X}(\mathbf{i}) \left(\bigotimes_{k=p}^1 e_{i_k}^{m_k} \right) \right] \\ &= \sum_{i_1=1}^{m_1} \dots \sum_{i_p=1}^{m_p} \sum_{j_1=1}^{h_1} \dots \sum_{j_q=1}^{h_q} \mathcal{B}([i'j']') \mathcal{X}(\mathbf{i}) \left(\bigotimes_{k=q}^1 e_{j_k}^{h_k} \right) \left(\bigotimes_{k=p}^1 e_{i_k}^{m_k} \right)' \left(\bigotimes_{k=p}^1 e_{i_k}^{m_k} \right) \\ &= \sum_{i_1=1}^{m_1} \dots \sum_{i_p=1}^{m_p} \sum_{j_1=1}^{h_1} \dots \sum_{j_q=1}^{h_q} \mathcal{B}([i'j']') \mathcal{X}(\mathbf{i}) \left(\bigotimes_{k=q}^1 e_{j_k}^{h_k} \right) = \text{vec} \langle \mathcal{X} | \mathcal{B} \rangle. \end{aligned}$$

(f) Because of Lemma II.1(a) and Lemma II.1(b) and the commutation matrix, if $\mathcal{Y} \in \mathbb{R}^{m_1 \times m_2 \times \dots \times m_k}$, then

$$\text{vec}(\mathcal{Y}) = \text{vec}(\mathcal{Y}_{\langle k-1 \rangle}) = \text{vec}(\mathcal{Y}'_{(k)}) = K_{m_k, \prod_{i=1}^{k-1} m_i} \text{vec}(\mathcal{Y}_{(k)}). \quad (\text{S7})$$

Therefore, if we let $\mathcal{X}^{(j_{k+1}, \dots, j_p)} \in \mathbb{R}^{m_1 \times m_2 \times \dots \times m_k}$ be the sub-tensor of \mathcal{X} defined as $\mathcal{X}^{(j_{k+1}, \dots, j_p)} = \mathcal{X}(:, \dots, :, j_{k+1}, \dots, j_p)$, then from (S7),

$$\begin{aligned} \text{vec}(\mathcal{X}) &= \begin{bmatrix} \text{vec} \mathcal{X}^{(1, \dots, 1, 1)} \\ \text{vec} \mathcal{X}^{(1, \dots, 1, 2)} \\ \vdots \\ \text{vec} \mathcal{X}^{(m_{k+1}, \dots, m_p)} \end{bmatrix} = \begin{bmatrix} K_{m_k, \prod_{i=1}^{k-1} m_i} \text{vec}(\mathcal{X}'_{(k)}^{(1, \dots, 1, 1)}) \\ K_{m_k, \prod_{i=1}^{k-1} m_i} \text{vec}(\mathcal{X}'_{(k)}^{(1, \dots, 1, 2)}) \\ \vdots \\ K_{m_k, \prod_{i=1}^{k-1} m_i} \text{vec}(\mathcal{X}'_{(k)}^{(m_{k+1}, \dots, m_p)}) \end{bmatrix} \\ &= K'_{(k)} \text{vec}(\mathcal{X}_{(k)}). \end{aligned}$$

The result follows by left-multiplying both sides by the orthogonal matrix $K_{(k)}$. \square

D. Proof of Theorem II.1

Proof.

(a) We have based on property S1.2

$$\begin{aligned} (\circ[M_1, M_2, \dots, M_p])_{\langle p \rangle} &= \sum_{i_1=1}^{m_1} \sum_{j_1=1}^{h_1} \dots \sum_{i_p=1}^{m_p} \sum_{j_p=1}^{h_p} \left(\prod_{q=1}^p M_q(i_q, j_q) \right) \left\{ \left(\begin{smallmatrix} p \\ \circ \\ q=1 \end{smallmatrix} e_{j_q}^{h_q} \right) \circ \left(\begin{smallmatrix} p \\ \circ \\ q=1 \end{smallmatrix} e_{i_q}^{m_q} \right) \right\}_{\langle p \rangle} \\ &= \sum_{i_1=1}^{m_1} \sum_{j_1=1}^{h_1} \dots \sum_{i_p=1}^{m_p} \sum_{j_p=1}^{h_p} \left(\prod_{q=1}^p M_q(i_q, j_q) \right) \left\{ \left(\bigotimes_{q=p}^1 e_{j_q}^{h_q} \right) \left(\bigotimes_{q=p}^1 e_{i_q}^{m_q} \right)' \right\} \\ &= \bigotimes_{q=p}^1 \left(\sum_{j_q=1}^{h_q} \sum_{i_q=1}^{m_q} M_q(i_q, j_q) e_{j_q}^{h_q} e_{i_q}^{m_q} \right) = \bigotimes_{q=p}^1 M'_q. \end{aligned}$$

(b) Because of Theorem II.1(a) and Lemma II.1(e),

$$\text{vec}\langle \mathcal{X} | \circ \llbracket M_1, M_2 \dots, M_p \rrbracket \rangle = (\circ \llbracket M_1, M_2 \dots, M_p \rrbracket)_{<p>}' \text{vec}(\mathcal{X}) = \left(\bigotimes_{q=p}^1 M_q \right) \text{vec}(\mathcal{X}) = \text{vec} \llbracket \mathcal{X}; M_1, \dots, M_p \rrbracket.$$

Therefore $\llbracket \mathcal{X}; M_1, \dots, M_p \rrbracket$ and $\langle \mathcal{X} | \circ \llbracket M_1, M_2 \dots, M_p \rrbracket \rangle$ are of the same size and vectorization, and must be the same.

(c) Using definition II.1 and property S1.2

$$\begin{aligned} \circ \llbracket M_1, M_2 \dots, M_p \rrbracket_{(S \times S^c)} &= \sum_{i_1=1}^{m_1} \sum_{j_1=1}^{h_1} \dots \sum_{i_p=1}^{m_p} \sum_{j_p=1}^{h_p} \left(\prod_{q=1}^p M_q(i_q, j_q) \right) \left\{ \left(e_{j_k}^{h_k} \otimes e_{i_k}^{m_k} \right) \left(\bigotimes_{q=p, q \neq k}^1 e_{j_q}^{h_q} \otimes \bigotimes_{q=p, q \neq k}^1 e_{i_q}^{m_q} \right)' \right\} \\ &= (\text{vec } M'_k) (\text{vec} \circ \llbracket M_1, M_2 \dots, M_{k-1}, M_{k+1}, \dots, M_p \rrbracket)'. \end{aligned}$$

□

E. Some matrices involved in our methodology

In this Section we provide and simplify some expressions involved in Sections II-C and II-D2. If \mathcal{V} is a tensor of size $r \times r \times \dots \times r$, then its super-diagonal $\mathbf{v} \in \mathbb{R}^r$ contains the elements with coincident indices in each dimension of \mathcal{V} , such that

$$\mathbf{v}(i) = \mathcal{V}(i, i, \dots, i). \quad (\text{S8})$$

We assume vectors are their own super-diagonals. Now we provide simplifications for the expressions involved in the CP format using the Hadamard (or element-wise) matrix-product (*), which is computationally more efficient than the traditional matrix product.

1) *The CP format: Simplifying Equation (31)*: First, let \mathbf{w}_i be the super-diagonal of $\llbracket \mathcal{X}_i; L'_1, L'_2 \dots, L'_l \rrbracket$, as defined in equation (S8), and let W_i be the $r \times r$ diagonal matrix with diagonal elements in \mathbf{w}_i . Then the matrix G_{ik}^{CP} in (29) can be written as

$$G_{ik}^{CP} = W_i \left(\bigodot_{q=p, q \neq k}^1 M_q \right)', \quad (\text{S9})$$

where \odot is the Khatri-Rao matrix product of [92]. This formulation allows us to simplify the matrix $\sum_{i=1}^n G_{ik}^{CP} \Sigma_{-k}^{-1} G_{ik}^{CP'}$ from Equation (31) using Proposition 3.2 from [44] as

$$\sum_{i=1}^n G_{ik}^{CP} \Sigma_{-k}^{-1} G_{ik}^{CP'} = \left[\sum_{i=1}^n \mathbf{w}_i \mathbf{w}_i' \right] * \left[\begin{smallmatrix} p \\ * \\ q=1, q \neq k \end{smallmatrix} (M'_k \Sigma_k^{-1} M_k) \right]. \quad (\text{S10})$$

Further, we can simplify equation (31) based on equation (S10) and the following identity

$$\mathcal{Y}_{i(k)} \Sigma_{-k}^{-1} G_{ik}^{CP'} = [\mathbf{y}_{1i} \dots \mathbf{y}_{m_k i}]' W_i,$$

where \mathbf{y}_{si} is the super-diagonal of $\llbracket \mathcal{Y}_{si}; M'_1 \Sigma_1^{-1}, \dots, M'_{k-1} \Sigma_{k-1}^{-1}, M'_{k+1} \Sigma_{k+1}^{-1}, \dots, M'_p \Sigma_p^{-1} \rrbracket$, and \mathcal{Y}_{si} is the tensor of size $m_1 \times \dots \times m_{k-1} \times m_{k+1} \times \dots \times m_p$ obtained upon fixing the k -th mode of \mathcal{Y}_i at the position s . After having estimated \widehat{M}_k in equation (31), we can also simplify S_k as

$$S_k = \sum_{i=1}^n \mathcal{Y}_{i(k)} \Sigma_{-k}^{-1} \mathcal{Y}'_{i(k)} - \widehat{M}_k \left(\sum_{i=1}^n G_{ik}^{CP} \Sigma_{-k}^{-1} G_{ik}^{CP'} \right) \widehat{M}_k',$$

where $\sum_{i=1}^n G_{ik}^{CP} \Sigma_{-k}^{-1} G_{ik}^{CP'}$ is already simplified in equation (S10).

Simplifying Equation (33): The matrix $\sum_{i=1}^n H_{ik}^{CP} \Sigma^{-1} H_{ik}^{CP'}$ from equation (33) can be written as $\mathcal{H}_{<2>}^2$, which is the 2-canonical matricization of the tensor \mathcal{H}^2 of size $h_k \times r \times h_k \times r$, with sub-tensors

$$\mathcal{H}^2(s, :, t, :) = \left(\begin{smallmatrix} p \\ * \\ k=1 \end{smallmatrix} M'_k \Sigma_k^{-1} M_k \right) * \left(\sum_{i=1}^n \mathbf{w}_{si} \mathbf{w}'_{ti} \right) \quad \text{for all } s, t = 1, 2, \dots, h_k,$$

where $\mathbf{w}_{si} \in \mathbb{R}^r$ is the super-diagonal of $\llbracket \mathcal{X}_{si}; L'_1, \dots, L'_{k-1}, L'_{k+1}, \dots, L'_l \rrbracket$, and \mathcal{X}_{si} is the tensor of size $h_1 \times \dots \times h_{k-1} \times h_{k+1} \times \dots \times h_l$ obtained upon fixing the k -th mode of \mathcal{X}_i at the position s . Finally, equation (33) can be greatly simplified using the above simplification along with the following identity

$$H_{ik}^{CP} \Sigma^{-1} \text{vec}(\mathcal{Y}_i) = [(\mathbf{w}_{1i} * \mathbf{y}_i)' \dots (\mathbf{w}_{h_k i} * \mathbf{y}_i)']',$$

where \mathbf{y}_i is the super-diagonal of $\llbracket \mathcal{Y}_i; M'_1 \Sigma_1^{-1}, \dots, M'_p \Sigma_p^{-1} \rrbracket$.

2) *The TR format*: To define the matrices G_{ik}^{TR} for $k = 1, 2, \dots, l$, let

$$\mathcal{B}_{-\mathcal{M}_k} = \mathcal{M}_{k+1} \times^1 \dots \times^1 \mathcal{M}_p \times^1 \mathcal{L}_1 \times^1 \dots \times^1 \mathcal{L}_l \times^1 \mathcal{M}_1 \times^1 \dots \times^1 \mathcal{M}_{k-1}, \quad (\text{S11})$$

be the $(p+1)$ th order TT-formatted tensor of dimension $(g_k \times m_{k+1} \times \dots \times m_p \times h_1 \times \dots \times h_l \times m_1 \times \dots \times m_{k-1} \times g_{k-1})$ that is generated similar to the TR tensor in Equation (36), but is missing the TR factor \mathcal{M}_k . The tensor $\mathcal{B}_{-\mathcal{M}_k}$ in Equation (S11) is defined for the cases where $k = 2, 3, \dots, p-1$, however $\mathcal{B}_{-\mathcal{M}_1}$ and $\mathcal{B}_{-\mathcal{M}_p}$ are similar: the tensor $\mathcal{B}_{-\mathcal{M}_p}$ has dimensions $(g_p \times h_1 \times \dots \times h_l \times m_1 \times \dots \times m_{p-1} \times g_{p-1})$ because \mathcal{L}_1 is the first factor in the train, and the tensor $\mathcal{B}_{-\mathcal{M}_1}$ has dimensions $(g_1 \times m_2 \times \dots \times m_p \times h_1 \times \dots \times h_l \times g_0)$ because \mathcal{L}_l is the last factor in the train. We define the matrix G_{ik}^{TR} involved in Equation (37) as

$$G_{ik}^{TR} = \left\{ \mathcal{X}_i \times_{1,2,\dots,l}^{p-k+2,p-k+3,\dots,p-k+l+1} \mathcal{B}_{-\mathcal{M}_k} \right\}_{(\mathcal{R} \times \mathcal{C})},$$

where $\mathcal{R} = \{1, p+1\}$, and \mathcal{C} is the ordered set of size $p-1$ that indexes the modes of size (m_1, m_2, \dots, m_p) , but skipping m_k and in reverse order (so that the order of the modes matches with the columns of $\mathcal{Y}_{i(k)}$ in Equation (37)). Similarly, to define the matrices H_{ik}^{TR} for $k = 1, 2, \dots, l$, let

$$\mathcal{B}_{-\mathcal{L}_k} = \mathcal{L}_{k+1} \times^1 \dots \times^1 \mathcal{L}_l \times^1 \mathcal{M}_1 \times^1 \dots \times^1 \mathcal{M}_p \times^1 \mathcal{L}_1 \times^1 \dots \times^1 \mathcal{L}_{k-1}, \quad (\text{S12})$$

be the $(p+1)$ -th order TT-formatted tensor of dimensions $(s_k \times h_{k+1} \times \dots \times h_l \times m_1 \times \dots \times m_p \times h_1 \times \dots \times h_{k-1} \times s_{k-1})$ that is generated similar to the TR tensor in Equation (36), but is missing the TR factor \mathcal{L}_k . The tensor $\mathcal{B}_{-\mathcal{L}_k}$ in (S12) is defined for the cases where $k = 2, 3, \dots, l-1$, however $\mathcal{B}_{-\mathcal{L}_1}$ and $\mathcal{B}_{-\mathcal{L}_l}$ are similar: the tensor $\mathcal{B}_{-\mathcal{L}_l}$ has dimensions $(s_l \times m_1 \times \dots \times m_p \times h_1 \times \dots \times h_{l-1} \times s_{l-1})$ because \mathcal{M}_1 is the first factor in the train, and the tensor $\mathcal{B}_{-\mathcal{L}_1}$ has dimensions $(s_1 \times h_2 \times \dots \times h_l \times m_1 \times \dots \times m_p \times s_0)$ because \mathcal{M}_p is the last factor in the train. We define the matrix H_{ik}^{TR} involved in Equation (38) as

$$H_{ik}^{TR} = \left\{ \mathcal{X}_i \times_{1,\dots,k-1,k+1,\dots,l}^{l+p+2-k,\dots,l+p,2,\dots,l-k+1} \mathcal{B}_{-\mathcal{L}^{(k)}} \right\}_{(\mathcal{R} \times \mathcal{C})}, \quad (\text{S13})$$

where $\mathcal{R} = \{2, 1, p+3\}$, and $\mathcal{C} = \{p+2, p+1, \dots, 3\}$ is the ordered set of size $p-1$ that indexes the modes of size (m_1, m_2, \dots, m_p) . Note that we define the contraction in Equation (S13) as $(\times_{2,\dots,l}^{2,\dots,l})$ when $k=1$ and as $(\times_{1,\dots,l-1}^{p+2,\dots,l+p})$ when $k=l$.

F. Rank determination and number of parameters

In Section II-E we propose choosing ranks using the BIC, defined as

$$BIC = K \log(n) - 2\ell,$$

where n is the sample size and ℓ is the loglikelihood that we simplified in Section II-C3. We decompose the total number of parameters K as $K = K_\Sigma + K_{\mathcal{B}}$, where K_Σ is the number of parameters involved in the covariance matrix and $K_{\mathcal{B}}$ is the total of parameters involved in the low-rank format of \mathcal{B} . The value of K_Σ depends on the correlation structure that is imposed on all the scale matrices $\Sigma_1, \dots, \Sigma_p$. For the general unconstrained model of (15), we have

$$K_\Sigma = 1 + \sum_{k=1}^p \left(\frac{m_k(m_k+1)}{2} - 1 \right)$$

to account for σ^2 as well as for the constraint that $\Sigma_k(1,1) = 1$ for all $k = 1, 2, \dots, p$. To determine $K_{\mathcal{B}}$ for the constrained cases, we need to consider each low-rank format separately:

- For \mathcal{B}_{TK} as in equation (18) we have

$$K_{\mathcal{B}} = \prod_{j=1}^l c_k \prod_{j=1}^p d_k + \sum_{k=1}^l \left(h_k c_k - \frac{c_k(c_k+1)}{2} \right) + \sum_{k=1}^p \left(m_k d_k - \frac{d_k(d_k+1)}{2} \right)$$

to account for the parameters involved in \mathcal{V} as well as those involved in each $L_1, \dots, L_l, M_1, \dots, M_p$ and their orthogonality constraints.

- For \mathcal{B}_{CP} as in equation (28) we have

$$K_{\mathcal{B}} = R \times \left(\sum_{k=1}^l h_k + \sum_{k=1}^p m_k - l - p + 1 \right)$$

to account for each $L_1, \dots, L_l, M_1, \dots, M_p$ and their column-scale constraints.

- For \mathcal{B}_{TR} as in equation (36) we have

$$K_{\mathcal{B}} = \sum_{k=1}^l s_{k-1} h_k s_k + \sum_{k=1}^p g_{k-1} m_k g_k - l - p + 1$$

to account for each $\mathcal{L}_1, \dots, \mathcal{L}_l, \mathcal{M}_1, \dots, \mathcal{M}_p$ and their scale indeterminacy.

- For \mathcal{B}_{OP} as in equation (34) we have

$$K_B = \sum_{k=1}^p h_k m_k - p + 1$$

to account for each M_1, \dots, M_p and their scale indeterminacy.

G. Computational Complexity and Proof of Theorem II.3

1) Computational complexity for the Tucker format:

Proof. The complexity is expressed in terms of four terms, which corresponds to lines 4, 6, 8 and 11 in Algorithm 1, respectively. We now derive the complexity of each of these lines:

Line 4: The computational complexity of line 4 corresponds to implementing equation (25) by obtaining:

- 4a) $\llbracket \mathcal{Y}_i; I_{m_1}, M'_2 \Sigma_2^{-1}, \dots, M'_p \Sigma_p^{-1} \rrbracket$ for all $i = 1, 2, \dots, n$, which will be dominated later by 6a)
- 4b) $\mathcal{W}_i = \llbracket \mathcal{X}_i; L'_1, L'_2, \dots, L'_p \rrbracket$ for all $i = 1, 2, \dots, n$, which has $\mathcal{O}(nhc_1)$ complexity.
- 4c) $W'(WW')^{-1}W$ where $W = [\text{vec}(\mathcal{W}_1), \dots, \text{vec}(\mathcal{W}_n)]$, with $\mathcal{O}(n^2c)$ complexity.
- 4d) Q_1 of eq. (24), the product $\Sigma_1^{-1/2}Q_1$ and the truncated singular value decomposition of $\Sigma_1^{-1/2}Q_1$, which have $\mathcal{O}(n^2m_1d_{-1} + nm_1^2d_{-1})$ complexity.

Line 6: The computational complexity of line 6 corresponds to implementing equation (23) by obtaining:

- 6a) $\mathcal{Z}_i = \llbracket \mathcal{Y}_i; M'_1 \Sigma_1^{-1}, M'_2 \Sigma_2^{-1}, \dots, M'_p \Sigma_p^{-1} \rrbracket$ for all $i = 1, 2, \dots, n$, which has $\mathcal{O}(nmd_1)$ complexity.
- 6b) W^- , which is the generalized inverse of W . This computation is dominated by 4c).
- 6c) $[\text{vec}(\mathcal{Z}_1), \dots, \text{vec}(\mathcal{Z}_n)]W^{-'}$, which has $\mathcal{O}(cnd)$ complexity and will be dominated by 8b).

Line 8: The computational complexity of line 8 corresponds to implementing equation (21) by obtaining:

- 8a) $\mathcal{G}_i = \llbracket \mathcal{X}_i; I_{h_1}, L'_2, \dots, L'_p \rrbracket$, which is dominated by 4b).
- 8b) $\mathcal{H}_i = \mathcal{G}_i \times_{2, \dots, l}^{\dots, l} \mathcal{V}$ for all $i = 1, 2, \dots, n$, which has $\mathcal{O}(ncdh_1)$ complexity.
- 8c) $\mathcal{H}_{i<2>} \mathcal{H}'_{i<2>}$ and $\mathcal{H}_{i<2>} \text{vec}(\mathcal{Z}_i)$ for all $i = 1, 2, \dots, n$ to form matrices in equation (21), with $\mathcal{O}(nc_1^2 h_1^2 d)$ complexity.
- 8d) inverse and final product in equation (21), with complexity $\mathcal{O}(h_1^3 c_1^3)$.

Line 11: The computational complexity of line 11 corresponds to implementing equation (27) by obtaining:

- 11a) inverse of $\Sigma_1, \Sigma_2, \dots, \Sigma_p$, with complexity $\mathcal{O}(m_1^3)$.
- 11b) $\langle \mathcal{W}_i | \mathcal{V} \rangle$ for all $i = 1, 2, \dots, n$ with complexity $\mathcal{O}(ndc_1 h_1)$ given \mathcal{H}_i of 8b), and is dominated by 8b).
- 11c) $\llbracket \langle \mathcal{W}_i | \mathcal{V} \rangle; M_1, M_2, \dots, M_p \rrbracket$ for all $i = 1, 2, \dots, n$, which is dominated by 6a).
- 11d) $\sum_{i=1}^n \mathcal{Y}_{i(k)} \Sigma_{-k}^{-1} \mathcal{Y}'_{i(k)}$ with complexity $\mathcal{O}(nmm_1)$.

□

2) Computational complexity for the CP format:

Proof. The complexity is expressed in terms of two terms, which corresponds to lines 4 and 7 in Algorithm 2, respectively. We now derive the complexity of each of these lines:

Line 4: The computational complexity of line 4 corresponds to implementing equation (33), and based on the simplifications detailed in Section S1-E1. This involves obtaining:

- 4a) the vectors of super-diagonals w_{si} , which are computationally dominated by 7b).
- 4b) $\sum_{i=1}^n w_{si} w'_{ii}$ for all $s, t = 1, 2, \dots, h_1$, with complexity $\mathcal{O}(nh_1^2 r^2)$.
- 4c) $\mathcal{M}_q = \circ_{k=1}^p M_k[:, q]$ for all $q = 1, 2, \dots, r$, with complexity $\mathcal{O}(mr)$. This is dominated by 4d).
- 4d) $\mathbf{y}_i(q) = \langle \mathcal{Y}_i, \mathcal{M}_q \rangle$ for all $i = 1, 2, \dots, n$, and $q = 1, 2, \dots, r$, with complexity $\mathcal{O}(nrm)$.
- 4e) $w_{si} * \mathbf{y}'_i$ for all $s = 1, 2, \dots, h_1$ and $i = 1, 2, \dots, n$, with complexity $\mathcal{O}(nrh_1)$. This is dominated by 4b).
- 4f) $*_{k=1}^p M'_k \Sigma_k^{-1} M_k$ with computational complexity $\mathcal{O}(rm_1^2 + m_1^3)$
- 4g) The final inversion and matrix-vector product of equation (33) with complexity $\mathcal{O}(h_1^3 r^3)$.

Line 7: The computational complexity of line 7 corresponds to implementing equation (31), which is simplified in Section S1-E1. This involves obtaining:

- 7a) $\mathcal{L}_q = \circ_{k=1}^l L_k[:, q]$ for all $q = 1, 2, \dots, r$, with complexity $\mathcal{O}(hr)$. This is dominated by 7b).
- 7b) $w_i(q) = \langle \mathcal{X}_i, \mathcal{L}_q \rangle$ for all $i = 1, 2, \dots, n$ and $q = 1, 2, \dots, r$, with complexity $\mathcal{O}(nrh)$.
- 7c) the vectors of super-diagonals \mathbf{y}_{si} , which are computationally dominated by 4d).
- 7d) The inverse and matrix product of equation (31) has complexity $\mathcal{O}(m_1 r^2 + r^3)$, and $\mathcal{O}(r^3)$ is dominated by 4g).
- 7e) $\sum_{i=1}^n \mathcal{Y}_{i(k)} \Sigma_{-k}^{-1} \mathcal{Y}'_{i(k)}$ with complexity $\mathcal{O}(nmm_1)$.

□

3) *Computational complexity for the OP format:* Unlike the CP and Tucker cases, the complexity of the OP format depends on the order of the tensor response and covariate modes. Therefore, finding the exact complexity will depend on many special cases unless a restriction is imposed. Here we will assume that for all $k = 1, 2, \dots, p$, $m_k = h_k$. This means that all the matrix factors M_k are square. This way, the order of the modes will not matter anymore and we can assume without generality that m_1 is the size of the largest mode.

Theorem S1.1. *The computational complexity of implementing the OP format is*

$$\mathcal{O}(nmm_1 + m_1^3).$$

Proof. The computational complexity of line 4 corresponds to implementing equation (31), but where G_{ik}^{CP} is replaced with the G_{ik}^{OP} of Section II-C2c.

- 4a) Computing G_{ik}^{OP} for each $k = 1, 2, \dots, p$ and for all $i = 1, 2, \dots, n$ with $\mathcal{O}(nmm_1)$ complexity.
- 4b) $\sum_{i=1}^n \mathcal{Y}_{i(k)} \Sigma_{-1}^{-1} G_{ik}^{OP'}$, $\sum_{i=1}^n G_{ik}^{OP} \Sigma_{-k}^{-1} G_{ik}^{OP'}$ and $\sum_{i=1}^n \mathcal{Y}_{i(k)} \Sigma_{-k}^{-1} \mathcal{Y}'_{i(k)}$ all have $\mathcal{O}(nmm_1)$ complexity.
- 4c) The inverse and matrix product of equation (31) has complexity $\mathcal{O}(m_1^3)$.

□

4) *Computational complexity for the TR format:*

Proof. The complexity is expressed in terms of two terms, which corresponds to lines 4 and 7 in Algorithm 2, respectively. We now derive the complexity of each of these lines:

Line 4: The computational complexity of line 4 corresponds to implementing equation (31), which is implemented in equation (33) when the H_{ik}^{TR} of Section S1-E2 is used instead of H_{ik}^{CP} . This involves obtaining:

- 4a) $\mathcal{M} = \mathcal{M}_1 \times^1 \mathcal{M}_2 \times \dots \times^1 \mathcal{M}_p$ with complexity $\mathcal{O}(mg_1g_0g_p)$.
- 4b) $\mathcal{L}_{-1} = \mathcal{L}_2 \times^1 \mathcal{L}_2 \times \dots \times^1 \mathcal{L}_l$, which is dominated by 7a).
- 4c) $\mathcal{D}_i = \mathcal{L}_{-1} \times_{2, \dots, l}^{2, \dots, l} \mathcal{X}_i$ for all $i = 1, 2, \dots, n$ with complexity $\mathcal{O}(hns_1s_l)$, dominated by $\mathcal{O}(hns_1s_l)$.
- 4d) $\mathcal{M} \times^1 \mathcal{D}_i$ for all $i = 1, 2, \dots, n$ with complexity $\mathcal{O}(nmh_1s_1s_0s_1)$. This is dominated by 4e).
- 4e) The final inversion and matrix-vector product of equation (33) with complexity $\mathcal{O}(nmh_1^2s_0^2s_1^2 + h_1^3s_0^3s_1^3)$.

Line 7: The computational complexity of line 4 corresponds to solving equation (37), which is implemented in equation (33) when the G_{ik}^{TR} of Section S1-E2 is used instead of G_{ik}^{CP} . This involves obtaining:

- 7a) $\mathcal{L} = \mathcal{L}_1 \times^1 \mathcal{L}_2 \times \dots \times^1 \mathcal{L}_l$ with complexity $\mathcal{O}(hs_1s_0s_l)$.
- 7b) $H_i = \mathcal{L} \times_{2, \dots, h+1}^{1, \dots, h} \mathcal{X}_i$ for all $i = 1, 2, \dots, n$ with complexity $\mathcal{O}(hns_0s_l)$, dominated by 4c).
- 7c) $\mathcal{M}_{-1} = \mathcal{M}_2 \times^1 \mathcal{M}_3 \times \dots \times^1 \mathcal{M}_p$, which is dominated by 4a).
- 7d) $\mathcal{M}_{-1} \times^1 H_i$ for all $i = 1, 2, \dots, n$ with complexity $\mathcal{O}(nm_{-1}g_0g_1g_p)$. This is dominated by 7e).
- 7e) $\sum_{i=1}^n \mathcal{Y}_{i(k)} \Sigma_{-k}^{-1} G_{ik}^{TR'}$ and $\sum_{i=1}^n G_{ik}^{TR} \Sigma_{-k}^{-1} G_{ik}^{TR'}$, with complexity $\mathcal{O}(nm_{-1}g_0g_1(g_0g_1 + m_1) + m_1^3)$. The first term in the sum is dominated by 7g).
- 7f) The final inversion and matrix-vector product of equation (31) with complexity $\mathcal{O}(g_0^3g_1^3)$.
- 7g) $\sum_{i=1}^n \mathcal{Y}_{i(k)} \Sigma_{-k}^{-1} \mathcal{Y}'_{i(k)}$ with complexity $\mathcal{O}(nmm_1)$.

□

H. Proof of Theorem II.4

Proof. Based on Lemma II.1(d) and Equation (23), we obtain

$$\text{vec}(\widehat{\mathcal{V}}) = [M' \Sigma^{-1} \otimes W^{-'}] \text{vec}(Y'), \quad (\text{S14})$$

where

$$\text{vec}(Y') \sim \mathcal{N}_{n \times m}((M \otimes W') \text{vec}(\mathcal{V}), \sigma^2 \Sigma \otimes I_n). \quad (\text{S15})$$

Furthermore, because $W^{-} = X'(XX')^{-1}L(L'L)^{-1}$ and both $W^{-'}W'$ and $M'\Sigma^{-1}M$ are identity matrices, we obtain based on (S14) and (S15) that

$$\text{vec}(\widehat{\mathcal{V}}) \sim \mathcal{N}_q\left(\text{vec}(\mathcal{V}), \sigma^2 I_m \otimes ((L'L)^{-1}L'(XX')^{-1}L(L'L)^{-1})\right), \quad (\text{S16})$$

where q is the product of the modes of the Tucker rank. Now, because \widehat{M}_k and \widehat{L}_k are MLEs and they are identifiable given the rest, as $n \rightarrow \infty$ $\widehat{M}_k \xrightarrow{P} M_k$ and $\widehat{L}_k \xrightarrow{P} L_k$, and therefore

$$\left(\bigotimes_{k=p}^1 \widehat{M}_k\right) \otimes \left(\bigotimes_{k=l}^1 \widehat{L}_k\right) \xrightarrow{P} M \otimes L. \quad (\text{S17})$$

The rest of the proof follows by left-multiplying the $\text{vec}(\widehat{\mathcal{V}})$ of (S16) by the left hand side of (S17) and applying Slutsky's Theorem. □

I. Proof of Theorem II.5

Before proving Theorem II.5 we state some of the matrices involved in it. First, let

$$\widehat{\boldsymbol{\theta}}_{CP} = [\text{vec}(\widehat{\mathcal{L}}_1)' \text{vec}(\widehat{\mathcal{L}}_2)' \dots \text{vec}(\widehat{\mathcal{L}}_l)' \text{vec}(\widehat{\mathcal{M}}_1)' \text{vec}(\widehat{\mathcal{M}}_2)' \dots \text{vec}(\widehat{\mathcal{M}}_p)']'.$$

Then the Jacobian matrix $J_{CP} = \frac{\partial}{\partial \widehat{\boldsymbol{\theta}}_{CP}} \text{vec}(\widehat{\mathcal{B}}_{CP})$ is a block matrix with blocks as per Lemma S1.1(a). Furthermore, we have

$$R_{CP} = [A'_1 A'_2 \dots A'_l B'_1 B'_2 \dots B'_p]', \quad (\text{S18})$$

where for all $k = 1, 2, \dots, l$,

$$A_k = [S_{1k}^{-1} H_{1k}^{CP} \Sigma^{-1} \dots S_{1k}^{-1} H_{nk}^{CP} \Sigma^{-1}], \quad S_{1k} = \sum_{i=1}^n H_{ik}^{CP} \Sigma^{-1} H_{ik}^{CP'} \quad (\text{S19})$$

and for all $k = 1, 2, \dots, p$,

$$B_k = ([S_{2k}^{-1} G_{1k}^{CP} \Sigma^{-1} \dots S_{2k}^{-1} G_{nk}^{CP} \Sigma^{-1}] \otimes \mathbf{I}_{m_k}) (I_n \otimes K_{(k)}), \quad S_{2k} = \sum_{i=1}^n G_{ik}^{CP} \Sigma^{-1} G_{ik}^{CP'}, \quad (\text{S20})$$

where $K_{(k)}$ is given in Lemma II.1(f) and the matrices S_{1k} and S_{2k} are simplified in Section S1-E1. Now we can prove Theorem II.5.

Proof. From Equations (31) and (33), we obtain that $\text{vec}(\widehat{\mathcal{L}}_k) = A_k \mathbf{y}$ and $\text{vec}(\widehat{\mathcal{M}}_k) = B_k \mathbf{y}$, and thus

$$\widehat{\boldsymbol{\theta}}_{CP} = R_{CP} \mathbf{y}. \quad (\text{S21})$$

Further, from our normality and independence assumptions,

$$\mathbf{y} = \begin{bmatrix} \text{vec}(\mathcal{Y}_1) \\ \dots \\ \text{vec}(\mathcal{Y}_n) \end{bmatrix} \sim \mathcal{N}_{m \times n} \left(\begin{bmatrix} \text{vec}(\langle \mathcal{X}_1 | \mathcal{B} \rangle) \\ \dots \\ \text{vec}(\langle \mathcal{X}_n | \mathcal{B} \rangle) \end{bmatrix}, \mathbf{I}_n \otimes \Sigma \right), \quad (\text{S22})$$

and from (S21) and (S22),

$$\widehat{\boldsymbol{\theta}}_{CP} \sim \mathcal{N}_{R \times (\sum_{i=1}^p m_i + \sum_{i=1}^l h_i)} \left(\boldsymbol{\theta}_{CP}, R_{CP} (\mathbf{I}_n \otimes \Sigma) R'_{CP} \right).$$

Now consider the transformation $g: \mathbb{R}^{R \times (\sum_{i=1}^p m_i + \sum_{i=1}^l h_i)} \rightarrow \mathbb{R}^{m \times h}$ such that $g(\widehat{\boldsymbol{\theta}}_{CP}) = \text{vec}(\widehat{\mathcal{B}}_{CP})$. The Jacobian matrix of this transformation is J_{CP} . Using the multivariate extension of Taylor's Theorem as in Theorem 5.2.3 in [93], we obtain

$$g(\widehat{\boldsymbol{\theta}}_{CP}) \stackrel{d}{\rightarrow} \mathcal{N}_{m \times h} \left(g(\boldsymbol{\theta}_{CP}), J_{CP} R_{CP} (\mathbf{I}_n \otimes \Sigma) R'_{CP} J'_{CP} \right),$$

where $g(\widehat{\boldsymbol{\theta}}_{CP}) = \text{vec}(\widehat{\mathcal{B}}_{CP})$ and $g(\boldsymbol{\theta}_{CP}) = \text{vec}(\mathcal{B}_{CP})$. \square

J. The OP and TR cases

We now state and prove some results on inference for the OP and TR format:

Theorem S1.2.

(a) Consider Equation (15) with $\mathcal{B} = \mathcal{B}_{TR}$ as in (36) with its analogue $\widehat{\mathcal{B}}_{TR}$ and

$$\widehat{\boldsymbol{\theta}}_{TR} = [\text{vec}(\widehat{\mathcal{L}}_1)' \text{vec}(\widehat{\mathcal{L}}_2)' \dots \text{vec}(\widehat{\mathcal{L}}_l)' \text{vec}(\widehat{\mathcal{M}}_{1(2)})' \text{vec}(\widehat{\mathcal{M}}_{2(2)})' \dots \text{vec}(\widehat{\mathcal{M}}_{3(2)})']'.$$

Then as $n \rightarrow \infty$,

$$\text{vec}(\widehat{\mathcal{B}}_{TR}) \stackrel{d}{\rightarrow} \mathcal{N}_{m \times h} \left(\text{vec}(\mathcal{B}_{TR}), J_{TR} R_{TR} (\mathbf{I}_n \otimes \Sigma) R'_{TR} J'_{TR} \right),$$

where $J_{TR} = \frac{\partial \text{vec}(\widehat{\mathcal{B}}_{TR})}{\partial \widehat{\boldsymbol{\theta}}_{TR}}$ is a block matrix with blocks given in Lemma S1.1(b) and R_{TR} is equal to R_{CP} in equation (S18) after replacing $(G_{ik}^{CP}, H_{ik}^{CP})$ with $(G_{ik}^{TR}, H_{ik}^{TR})$.

(b) Now let Equation (15) have $\mathcal{B} = \circ[[M_1, \dots, M_p]]$ with its analogue $\widehat{\mathcal{B}}_{OP}$ and

$$\widehat{\boldsymbol{\theta}}_{OP} = [\text{vec}(\widehat{\mathcal{M}}_1)' \text{vec}(\widehat{\mathcal{M}}_2)' \dots \text{vec}(\widehat{\mathcal{M}}_p)']',$$

Then as $n \rightarrow \infty$,

$$\text{vec}(\widehat{\mathcal{B}}_{OP}) \stackrel{d}{\rightarrow} \mathcal{N}_{m \times h} \left(\text{vec}(\mathcal{B}_{OP}), J_{OP} R_{OP} (\mathbf{I}_n \otimes \Sigma) R'_{OP} J'_{OP} \right),$$

where $J_{OP} = \frac{\partial \text{vec}(\widehat{\mathcal{B}}_{OP})}{\partial \widehat{\boldsymbol{\theta}}_{OP}}$ is a block matrix with blocks given in Lemma S1.1(c) and $R_{OP} = [B'_1 B'_2 \dots B'_p]'$, where B_k is given in equation (S20) for all $k = 1, \dots, p$ after replacing G_{ik}^{CP} with G_{ik}^{OP} .

Proof.

The proof of both parts is similar to that of Theorem II.5 and thus omitted. \square

K. Jacobian matrices

The Jacobians needed in Theorems II.5 and S1.2 are block matrices, where each block is given in the following lemma

Lemma S1.1.

(a) Let $\mathcal{B}_{CP} = \llbracket M_1, M_2, \dots, M_p \rrbracket \in \mathbb{R}^{m_1 \times m_2 \times \dots \times m_p}$. Then for $k = 1, 2, \dots, p$,

$$\frac{\partial \text{vec}(\mathcal{B}_{CP})}{\partial \text{vec}(M_k)} = K'_{(k)}(T_k^{CP} \otimes I_{m_k}), \text{ where } T_k^{CP} = \bigoplus_{q=p, q \neq k}^1 M_q.$$

(b) Let $\mathcal{B}_{TR} = \text{tr}(\mathcal{M}_1 \times^1 \mathcal{M}_2 \times^1 \dots \times^1 \mathcal{M}_p) \in \mathbb{R}^{m_1 \times m_2 \times \dots \times m_p}$. Then for $k = 1, 2, \dots, p$,

$$\frac{\partial \text{vec}(\mathcal{B}_{TR})}{\partial \text{vec}(\mathcal{M}_{k(2)})} = K'_{(k)}(T_k^{TR'} \otimes I_{m_k}),$$

where

$$T_k^{TR} = \text{tr}(\mathcal{M}_{k+1} \times^1 \dots \times^1 \mathcal{M}_p \times^1 \mathcal{M}_1 \times^1 \dots \times^1 \dots \times^1 \mathcal{M}_{k-1})_{(\{1, p+1\} \times \{2, 3, \dots, p\})}.$$

(c) Let $\mathcal{B}_{OP} = \circ \llbracket M_1, M_2, \dots, M_p \rrbracket \in \mathbb{R}^{m_1 \times \dots \times m_p \times n_1 \times \dots \times n_p}$. Then for $k = 1, 2, \dots, p$,

$$\frac{\partial \text{vec}(\mathcal{B}_{OP})}{\partial \text{vec}(M'_k)} = K'_{(p+k)} K'_{(k+1)} \left((\text{vec} \circ \llbracket M_1, \dots, M_{k-1}, M_{k+1}, \dots, M_p \rrbracket) \otimes I_{m_k n_k} \right).$$

Proof.

(a) First, because $\mathcal{B}_{CP(k)} = M_k T_k^{CP'}$, we have

$$\frac{\partial \text{vec}(\mathcal{B}_{CP(k)})}{\partial \text{vec}(M_k)} = T_k^{CP} \otimes I_{m_k}.$$

The result follows from Lemma II.1(f).

(b) The derivation of this results follows a similar path as in part (a) because $\mathcal{B}_{TR(k)} = M_{k(2)} T_k^{TR}$.

(c) Let \mathcal{S} be as in Theorem II.1(c). Then the vectorization of (10) results in

$$\frac{\partial \text{vec}(\mathcal{B}_{OP(\mathcal{S} \times \mathcal{S}^c)})}{\partial \text{vec}(M'_k)} = \left((\text{vec} \circ \llbracket M_1, \dots, M_{k-1}, M_{k+1}, \dots, M_p \rrbracket) \otimes I_{m_k n_k} \right).$$

The result follows from $\text{vec}(\mathcal{B}_{OP(\mathcal{R} \times \mathcal{E})}) = K_{(k+1)} K_{(p+k)} \text{vec}(\mathcal{B}_{OP})$, where $K_{(k)}$ is orthogonal as in Lemma II.1(f). \square

L. Proof of Theorem II.6

Proof. Based on Section II-C1, the estimation of \mathcal{B} when the intercept is present can be performed by centering the covariates and responses. Let $C_n = I_n - \frac{1}{n} \mathbf{1}_n \mathbf{1}'_n$. For the Tucker case in Theorem II.4, let $Y_c = [(\text{vec } \mathcal{Y}_1^c) (\text{vec } \mathcal{Y}_2^c) \dots (\text{vec } \mathcal{Y}_n^c)]$, where $\mathcal{Y}_i^c = \mathcal{Y}_i - \bar{\mathcal{Y}}$. Then $\text{vec}(Y'_c) = (I_m \otimes C_n) \text{vec}(Y')$, and similar to Equation (S14),

$$\text{vec}(\hat{\mathcal{V}}) = [M' \Sigma^{-1} \otimes W^{+'}] (I_m \otimes C_n) \text{vec}(Y') = [M' \Sigma^{-1} \otimes W^{+'}] \text{vec}(Y'),$$

where the last equality follows because $X \mathbf{1}_n = \mathbf{0}$ when the covariates are centered, and therefore $W^{+'} \mathbf{1}_n = \mathbf{0}$ also. The remaining results follow using the same steps as in the proof of Theorem II.4, but with centered covariates. For the CP case as in Theorem II.5, if $\mathbf{y}_c = [(\text{vec } \mathcal{Y}_1^c)' (\text{vec } \mathcal{Y}_2^c)' \dots (\text{vec } \mathcal{Y}_n^c)']'$ are the centered responses, then $\mathbf{y}_c = (C_n \otimes I_m) \mathbf{y}$, and similar to Equation (S21),

$$\hat{\boldsymbol{\theta}}_{CP} = R_{CP} (C_n \otimes I_m) \mathbf{y} = R_{CP} \mathbf{y},$$

where the last step follows because $R_{CP} (\mathbf{1}_n \otimes I_m) = \mathbf{0}$. The rest results by following the same steps as in the proof of Theorem II.5, but with centered covariates. The proof of the TR and OP cases are similar and thus omitted. \square

M. Distribution of the scale components

The final inference result is on the distribution of the estimated scale matrices $\widehat{\Sigma}_1, \widehat{\Sigma}_2, \dots, \widehat{\Sigma}_p$. We obtain the Fisher information matrix and show that it is singular.

Theorem S1.3. *Let $\theta_\Sigma = [(\text{vech } \Sigma_1)', \text{vech } \Sigma_2', \dots, \text{vech } \Sigma_p']'$, where $\Sigma_1, \Sigma_2, \dots, \Sigma_p$ are scale matrices with no restrictions on their proportionality, and vech is the half-vectorization mapping, as discussed further in Section S1. Then*

- (a) *The joint linear components $\begin{bmatrix} \text{vec}(\widehat{\Upsilon}) \\ \text{vec}(\widehat{\mathcal{B}}) \end{bmatrix}$ and $\widehat{\theta}_\Sigma$ are asymptotically independent regardless of the format of $\widehat{\mathcal{B}}$.*
- (b) *The Fisher information with respect to θ_Σ , denoted as \mathbb{I}_Σ , is a block matrix with k th block diagonal matrices ($k = 1, 2, \dots, p$) given by*

$$\mathbb{E} \left(- \frac{\partial^2 \ell(\Sigma_k)}{\partial(\text{vech } \Sigma_k) \partial(\text{vech } \Sigma_k)'} \right) = \frac{nm-k}{2} D'_{m_k} (\Sigma_k^{-1} \otimes \Sigma_k^{-1}) D_{m_k} \quad (\text{S23})$$

and (k, l) th block matrices for $k \neq l$, $k, l = 1, 2, \dots, p$, given as

$$\mathbb{E} \left(- \frac{\partial^2 \ell(\Sigma_k, \Sigma_l)}{\partial(\text{vech } \Sigma_k) \partial(\text{vech } \Sigma_l)'} \right) = \frac{nm-kl}{2} D'_{m_k} (\text{vec}(\Sigma_k^{-1}) \text{vec}(\Sigma_l^{-1})') D_{m_l}, \quad (\text{S24})$$

where D_{m_k} is the duplication matrix of Section S1 and $m_{-kl} = \prod_{i=1, i \neq k, i \neq l}^p m_i$.

- (c) *The Fisher information \mathbb{I}_Σ is singular.*

Proof.

- (a) This statement follows upon expressing the Equation (13) as the MVMLR regression model $\text{vec}(\mathcal{Y}_i) = \text{vec}(\Upsilon) + \mathcal{B}'_{\langle l \rangle} \text{vec}(\mathcal{X}_i) + e_i$, and then applying Theorem 15.4 in [91].
- (b) Equation (13) with $\sigma^2 = 1$ can be expressed as

$$\mathcal{Z}_i = \mathcal{Y}_i - \langle \mathcal{X}_i | \mathcal{B} \rangle \stackrel{iid}{\sim} N_{m_1, m_2, \dots, m_p}(0, \Sigma_1, \Sigma_2, \dots, \Sigma_p), \quad i = 1, 2, \dots, n. \quad (\text{S25})$$

We will start by finding the diagonal of the block Fisher information matrix. We know from Theorem II.2(c) that

$$\mathcal{Z}_{i(k)} \sim \mathcal{N}_{m_k, m_{-k}}(0, \Sigma_k, \Sigma_{-k}) \quad (\text{S26})$$

for $k = 1, \dots, p$. We find the second differential of the loglikelihood of $\mathcal{Z}_{i(k)}$ in (S26) with respect to Σ_k only as

$$\begin{aligned} \ell(\Sigma_k) &= -\frac{m-k}{2} \log |\Sigma_k| - \frac{1}{2} \text{tr}(\Sigma_k^{-1} \mathcal{Z}_{i(k)} \Sigma_{-k}^{-1} \mathcal{Z}'_{i(k)}), \\ \partial \ell(\Sigma_k) &= -\frac{m-k}{2} \text{tr}(\Sigma_k^{-1} \partial \Sigma_k) + \frac{1}{2} \text{tr}(\Sigma_k^{-1} \partial \Sigma_k \Sigma_k^{-1} \mathcal{Z}_{i(k)} \Sigma_{-k}^{-1} \mathcal{Z}'_{i(k)}), \\ \partial^2 \ell(\Sigma_k) &= \frac{m-k}{2} \text{tr}(\Sigma_k^{-1} \partial \Sigma_k \Sigma_k^{-1} \partial \Sigma_k) - \text{tr}(\Sigma_k^{-1} \partial \Sigma_k \Sigma_k^{-1} \partial \Sigma_k \Sigma_k^{-1} \mathcal{Z}_{i(k)} \Sigma_{-k}^{-1} \mathcal{Z}'_{i(k)}). \end{aligned} \quad (\text{S27})$$

Now, based on Equation (S26), $\mathcal{Z}_{i(k)} \Sigma_{-k}^{-1} \mathcal{Z}'_{i(k)} \sim \mathcal{W}_{m_k}(m_{-k}, \Sigma_k)$, where \mathcal{W} denotes the Wishart distribution on $m_k \times m_k$ -dimension random matrices and m_{-k} degrees of freedom. Therefore $\mathbb{E}(\mathcal{Z}_{i(k)} \Sigma_{-k}^{-1} \mathcal{Z}'_{i(k)}) = m_{-k} \Sigma_k$. Thus using the duplication matrix and expressing the matrix trace as a vector inner product in Lemmas II.1(c) and II.1(d)

$$\mathbb{E}(-\partial^2 \ell(\Sigma_k)) = \frac{m-k}{2} \text{tr}(\Sigma_k^{-1} \partial \Sigma_k \Sigma_k^{-1} \partial \Sigma_k) = \partial(\text{vech } \Sigma_k)' \left(\frac{m-k}{2} D'_{m_{-k}} (\Sigma_k \otimes \Sigma_k) D_{m_{-k}} \right) \partial(\text{vech } \Sigma_k).$$

Now we find the element in the $(2,1)$ th position of the block-Fisher information matrix. Finding this element is enough to find the rest of the Fisher information matrix because the order of the scale matrices in the TVN distribution can be permuted in concordance with the modes of the random tensor. Let $\Sigma_{-12} = \bigotimes_{i=p}^3 \Sigma_i$ and $m_{-12} = \prod_{i=3}^p m_i$. Then based on the distribution of $\mathcal{Z}_{i(1)}$ in (S26) we can write the log likelihood as

$$\begin{aligned} \ell(\Sigma_1, \Sigma_2) &= -\frac{1}{2} \text{tr} [(\Sigma_{-12}^{-1} \otimes \Sigma_2^{-1}) \mathcal{Z}'_{i(1)} \Sigma_1^{-1} \mathcal{Z}_{i(1)}] \quad (\text{by Property S1.2c.}) \\ &= -\frac{1}{2} \text{vec}(\Sigma_{-12}^{-1} \otimes \Sigma_2^{-1})' (\mathcal{Z}_{i(1)} \otimes \mathcal{Z}_{i(1)})' \text{vec}(\Sigma_1^{-1}) \quad (\text{by Lemmas II.1(c) and II.1(d)}) \\ &= -\frac{1}{2} \text{vec}(\Sigma_2^{-1})' R'_{\Sigma_{-12}^{-1}} (\mathcal{Z}_{i(1)} \otimes \mathcal{Z}_{i(1)})' \text{vec}(\Sigma_1^{-1}), \quad (\text{by Property S1.1c.}) \end{aligned} \quad (\text{S28})$$

Furthermore, if $X \sim N_{m_1, m_2}(0, \Sigma_1, \Sigma_2)$, $J^{k,l}$ is a single-entry matrix (with 1 at the position (k, l) and 0 everywhere else) and $\Sigma_1^{1/2}[k, i] = \sigma_{ki}^1$, $\Sigma_2^{1/2}[j, l] = \sigma_{jl}^2$, then for $Z \sim N_{p,r}(0, I_p, I_r)$,

$$\begin{aligned}
\mathbb{E}(X \otimes X) &= (\Sigma_1^{1/2} \otimes \Sigma_1^{1/2}) \mathbb{E}(Z \otimes Z) (\Sigma_2^{1/2} \otimes \Sigma_2^{1/2}) = (\Sigma_1^{1/2} \otimes \Sigma_1^{1/2}) \{J^{k,l}\}_{k,l} (\Sigma_2^{1/2} \otimes \Sigma_2^{1/2}) \\
&= \left\{ \sum_{i=1}^p \sum_{j=1}^r \sigma_{ki}^1 \Sigma_1^{1/2} J^{i,j} \Sigma_2^{1/2} \sigma_{jl}^2 \right\}_{k,l} \\
&= \left\{ \sum_{i=1}^p \sum_{j=1}^r \sigma_{ki}^1 \Sigma_1^{1/2}[:, i] \Sigma_2^{1/2}[j, :] \sigma_{jl}^2 \right\}_{k,l} \\
&= \left\{ \left(\sum_{i=1}^p \sigma_{ki}^1 \Sigma_1^{1/2}[:, i] \right) \left(\sum_{j=1}^r \Sigma_2^{1/2}[j, :] \sigma_{jl}^2 \right) \right\}_{k,l} \\
&= \left\{ \left[\sigma_{k1}^1 I_p \dots \sigma_{kp}^1 I_p \right] \text{vec}(\Sigma_1^{1/2}) \text{vec}(\Sigma_2^{1/2})' \begin{bmatrix} \sigma_{1l}^2 I_r \\ \vdots \\ \sigma_{rl}^2 I_r \end{bmatrix} \right\}_{k,l} \\
&= (\Sigma_1^{1/2} \otimes I_p) \text{vec}(\Sigma_1^{1/2}) \text{vec}(\Sigma_2^{1/2})' (\Sigma_2^{1/2} \otimes I_r) = \text{vec}(\Sigma_1) \text{vec}(\Sigma_2)'.
\end{aligned} \tag{S29}$$

To differentiate the negative loglikelihood of (S28), we use that if Σ is non-singular then, $\frac{\partial \text{vec} \Sigma^{-1}}{\partial \text{vec} \Sigma} = -(\Sigma^{-1} \otimes \Sigma^{-1})$, which follows from vectorizing both sides of $\partial \Sigma^{-1} = -\Sigma^{-1} \partial \Sigma \Sigma^{-1}$. From application of this operation to both sides of (S28) and taking expectation of (S29) results in

$$\begin{aligned}
-\mathbb{E} \left(\frac{\partial^2 \ell(\Sigma_1, \Sigma_2)}{\partial (\text{vec} \Sigma_2) \partial (\text{vec} \Sigma_1)'} \right) &= \frac{1}{2} (\Sigma_2^{-1} \otimes \Sigma_2^{-1}) R'_{\Sigma_{-12}} \left\{ \mathbb{E}(\mathcal{Z}_{i(1)} \otimes \mathcal{Z}_{i(1)}) \right\}' (\Sigma_1^{-1} \otimes \Sigma_1^{-1}) \\
&= \frac{1}{2} (\Sigma_2^{-1} \otimes \Sigma_2^{-1}) R'_{\Sigma_{-12}} \left\{ (\text{vec} \Sigma_1) (\text{vec}(\Sigma_{-12} \otimes \Sigma_2))' \right\}' (\Sigma_1^{-1} \otimes \Sigma_1^{-1}) \\
&= \frac{1}{2} (\Sigma_2^{-1} \otimes \Sigma_2^{-1}) R'_{\Sigma_{-12}} \text{vec}(\Sigma_{-12} \otimes \Sigma_2) (\text{vec} \Sigma_1^{-1})' \\
&= \frac{1}{2} (\Sigma_2^{-1} \otimes \Sigma_2^{-1}) R'_{\Sigma_{-12}} R_{\Sigma_{-12}} (\text{vec} \Sigma_2) (\text{vec} \Sigma_1^{-1})' \quad (\text{Lemma S1.1c}) \\
&= \frac{m_{-12}}{2} (\Sigma_2^{-1} \otimes \Sigma_2^{-1}) (\text{vec} \Sigma_2) (\text{vec} \Sigma_1^{-1})' \quad (\text{see below}) \\
&= \frac{m_{-12}}{2} (\text{vec} \Sigma_2^{-1}) (\text{vec} \Sigma_1^{-1})'.
\end{aligned}$$

The rest follows by multiplying D'_{m_1} on the left and D_{m_2} on the right. The following term simplifies greatly using Property S1.1 of the commutation matrix and Property S1.2 of the Kronecker product:

$$\begin{aligned}
R'_{\Sigma_{-12}} R_{\Sigma_{-12}} &= \left(((\text{vec} \Sigma_{-12}^{-1})' \otimes I_{m_2}) (I_{m_{-12}} \otimes K_{m_{-12}, m_2}) (I_{m_{-12}} \otimes K_{m_2, m_{-12}}) (\text{vec} \Sigma_{-12} \otimes I_{m_2}) \right) \otimes I_{m_2} \\
&= \left(((\text{vec} \Sigma_{-12}^{-1})' \otimes I_{m_2}) (I_{m_2 \times m_{-12}^2}) (\text{vec} \Sigma_{-12} \otimes I_{m_2}) \right) \otimes I_{m_2} \\
&= \text{tr}(\Sigma_{-12}^{-1} \Sigma_{-12}) \otimes I_{m_2^2} = m_{-12} I_{m_2^2}.
\end{aligned}$$

(c) Let $\mathbb{I}_{\Sigma_{12}}$ denote the first four block matrices of the Fisher information,

$$\mathbb{I}_{\Sigma_{12}} = \frac{nm_{-12}}{2} \begin{bmatrix} m_2 D'_{m_1} (\Sigma_1^{-1} \otimes \Sigma_1^{-1}) D_{m_1} & D'_{m_1} (\text{vec}(\Sigma_1^{-1}) \text{vec}(\Sigma_2^{-1})') D_{m_2} \\ D'_{m_2} (\text{vec}(\Sigma_2^{-1}) \text{vec}(\Sigma_1^{-1})') D_{m_1} & m_1 D'_{m_2} (\Sigma_2^{-1} \otimes \Sigma_2^{-1}) D_{m_2} \end{bmatrix} = \begin{bmatrix} A & B \\ B' & C \end{bmatrix}.$$

Using the result of Section 3.8 of [91], where E^- denotes the Moore-Penrose inverse of E , we obtain:

$$A^{-1} = \frac{2}{nm_{-1}} D_{m_1}^- (\Sigma_1 \otimes \Sigma_1) D_{m_1}', \quad C^{-1} = \frac{2}{nm_{-2}} D_{m_2}^- (\Sigma_2 \otimes \Sigma_2) D_{m_2}',$$

and

$$BC^{-1}B' = \frac{nm_{-1}}{2m_1} D'_{m_1} (\text{vec} \Sigma_1^{-1}) (\text{vec} \Sigma_1^{-1})' D_{m_1}.$$

Using these results we obtain

$$\begin{aligned}
\text{tr}(A^{-1}BC^{-1}B') &= \frac{1}{m_1} \text{tr} \left(D_{m_1}^- (\Sigma_1 \otimes \Sigma_1) D_{m_1}' D_{m_1}' (\text{vec} \Sigma_1^{-1}) (\text{vec} \Sigma_1^{-1})' D_{m_1} \right) \\
&= \frac{1}{m_1} \text{tr} \left(D_{m_1}^- (\text{vec} \Sigma_1) (\text{vec} \Sigma_1^{-1})' D_{m_1} \right) = \frac{m_1}{m_1} = 1.
\end{aligned}$$

This last result implies that for the Schur complement of $\mathbb{I}_{\Sigma_{12}}$, namely $S = (A - BC^{-1}B')$, it follows that $S[A^{-1}D'_{m_1}(\text{vec } \Sigma_1^{-1})] = \mathbf{0}$, which means that the S has a non-trivial kernel, and therefore is singular. So $\mathbb{I}_{\Sigma_{12}}$ is singular [94], and consequently so is \mathbb{I}_{Σ} . \square

S2. SUPPLEMENT TO SECTION III

To calculate Wilks' Lambda statistic $\Lambda = |\widehat{\Sigma}_R|/|\widehat{\Sigma}_T|$ we need $\widehat{\Sigma}_R$, which is the sample covariance matrix of the residuals after fitting (41), and is formally expressed as

$$\widehat{\Sigma}_R = \sum_{i=1}^4 \sum_{j=1}^3 \sum_{k=1}^{50} \text{vec}(Y_{ijk} - \langle X_{ij} | \widehat{\mathcal{B}} \rangle) \text{vec}(Y_{ijk} - \langle X_{ij} | \widehat{\mathcal{B}} \rangle)',$$

with appropriate \mathcal{B} and $\widehat{\mathcal{B}}$ is its estimate. The matrix $\widehat{\Sigma}_T$ is the sample covariance matrix of the simpler model's residuals, which finds a common mean across all camelids, and is formally written as

$$\widehat{\Sigma}_T = \sum_{i=1}^4 \sum_{j=1}^3 \sum_{k=1}^{50} \text{vec}(Y_{ijk} - \langle \mathbf{x}_j | \widehat{\mathcal{B}}^* \rangle) \text{vec}(Y_{ijk} - \langle \mathbf{x}_j | \widehat{\mathcal{B}}^* \rangle)',$$

where $\mathbf{x}_j^* \in \mathbb{R}^3$ has 1 in position i and zeroes elsewhere. The tensor $\widehat{\mathcal{B}}^*$ is the low-rank estimator of \mathcal{B}^* , both of size $3 \times 87 \times 106$, and contains the grand-camelid mean image. The tensor \mathcal{B} is of order 4 while \mathcal{B}^* is of order 3, and therefore considerations must be considered when choosing the ranks of \mathcal{B}^* . We chose the same CP rank for both \mathcal{B} and \mathcal{B}^* , and the rank of \mathcal{B}^* was chosen to concord to the corresponding dimensions of \mathcal{B} in the TK and TR cases. The matrices $\widehat{\Sigma}_R$ and $\widehat{\Sigma}_T$ are non-negative definite of size 9222×9222 and rank 600, so the Wilks' Lambda statistic calculation involves the generalized determinant, which is the product of the non-zero eigenvalues.

S3. SUPPLEMENT TO SECTION IV

This section will need the following lemma, which identifies the distribution of the Tucker product of a random TVN tensor.

Lemma S3.1. *If $\mathbf{Y} \sim \mathcal{N}_m(0, \Sigma_1, \Sigma_2, \dots, \Sigma_p)$ and $M_k \in \mathbb{R}^{n_k \times m_k}$ for all $k = 1, 2, \dots, p$, then $\mathbf{X} = \llbracket \mathbf{Y}; M_1, M_2, \dots, M_p \rrbracket \sim \mathcal{N}_{[n_1, n_2, \dots, n_p]}(0, M_1 \Sigma_1 M_1', M_2 \Sigma_2 M_2', \dots, M_p \Sigma_p M_p')$.*

Proof. From Lemma II.1(d) $\text{vec}(\mathbf{X}) = (\bigotimes_{k=p}^1 M_k) \text{vec}(\mathbf{Y})$, and therefore based on the properties of the MVN distribution and Property S1.2(d),

$$\text{vec}(\mathbf{X}) \sim \mathcal{N}_{n_1 \times \dots \times n_p}(0, \bigotimes_{k=p}^1 (M_k \Sigma_k M_k')).$$

The remainder of the proof follows from and Definition II.2. \square

A. Supplement to Section IV-A

In Section IV-A we are interested in doing inference on the interaction between word type and subject suicide attempter/ideator status to determine markers for suicide risk assessment and intervention. The 3-level interaction is given as $\widehat{\mathcal{B}}_* = \widehat{\mathcal{B}} \times_1 \mathbf{c}'_1 \times_2 C_2 \times_3 \mathbf{c}'_3$, where $\mathbf{c}_1 = (1, -1)'$ is a contrast vector that finds differences between suicide attempter/ideation status, $\mathbf{c}_3 = (1, 1, \dots, 1)'/10$ a contrast vector that averages the 10 words of each word type, and

$$C_2 = \begin{bmatrix} 1 & 0 & -1 \\ 1 & -1 & 0 \\ 0 & -1 & 1 \end{bmatrix} \quad (\text{S30})$$

is a contrast matrix for differences across word type. The tensor $\widehat{\mathcal{B}}_*$ contains all the interactions; for instance, the first row of C_2 finds differences between the first and third word types, so the first level interaction $\widehat{\mathcal{B}}_*(1, :, :, :)$

$$\frac{1}{10} \sum_{k=1}^{10} \left(\widehat{\mathcal{B}}(1, 1, k, :, :, :) - \widehat{\mathcal{B}}(1, 3, k, :, :, :) - \widehat{\mathcal{B}}(2, 1, k, :, :, :) + \widehat{\mathcal{B}}(2, 3, k, :, :, :) \right),$$

identifies regions of significant differences in how death- and negative-connoted words affect suicide ideators and attempters. Similarly, the second row of C_2 finds differences between the first two word types, so the second level interaction $\widehat{\mathcal{B}}_*(2, :, :, :)$ is

$$\frac{1}{10} \sum_{k=1}^{10} \left(\widehat{\mathcal{B}}(1, 1, k, :, :, :) - \widehat{\mathcal{B}}(1, 2, k, :, :, :) - \widehat{\mathcal{B}}(2, 1, k, :, :, :) + \widehat{\mathcal{B}}(2, 2, k, :, :, :) \right),$$

and its significant regions correspond to locations with a significant difference in how the contrast between death-related and positive-connoting words affect suicide ideators and attempters. Finally, the third row of C_2 finds differences between the first and third word types and so the third-level interaction $\widehat{\mathcal{B}}_*(3, :, :, :)$ is

$$\frac{1}{10} \sum_{k=1}^{10} \left(\widehat{\mathcal{B}}(1, 3, k, :, :, :) - \widehat{\mathcal{B}}(1, 2, k, :, :, :) - \widehat{\mathcal{B}}(2, 3, k, :, :, :) + \widehat{\mathcal{B}}(2, 2, k, :, :, :) \right),$$

and its significant regions correspond to locations with a significant difference in how the contrast between negative- and positive-connoting words affect suicide ideators and attempters.

To obtain the asymptotic distribution of the estimate $\widehat{\mathcal{B}}$ we use Theorem II.4 and Definition II.2, to obtain that as $n \rightarrow \infty$,

$$\widehat{\mathcal{B}} \xrightarrow{d} \mathcal{N}_{2,3,10,43,56,20}(\mathcal{B}, \sigma^2 P_1 (XX')^{-1} P_1, M_1 M_1', M_2 M_2', M_3 M_3', M_4 M_4', M_5 M_5'), \quad (\text{S31})$$

where XX' is a diagonal matrix with two non-zero entries (9, 8). From (S31), (S30) and Lemma S3.1, the asymptotic distribution of $\widehat{\mathcal{B}}_*$ is

$$\widehat{\mathcal{B}}_* \xrightarrow{d} \mathcal{N}_{3,20,43,56}(\mathcal{B}_*, \tau^2 C_2 M_1 M_1' C_2', M_3 M_3', M_4 M_4', M_5 M_5'), \quad (\text{S32})$$

where $\tau^2 = \sigma^2 \times (\mathbf{c}'_1 P_1 (XX')^{-1} P_1 \mathbf{c}_1) \times (\mathbf{c}'_3 M_2 M_2' \mathbf{c}_3)$ and $\mathcal{B}_* = \mathcal{B} \times_1 \mathbf{c}'_1 \times_2 C_2 \times_3 \mathbf{c}'_3$. Using (IV-A), we marginally standardize $\widehat{\mathcal{B}}_*$ using the Tucker product and Lemma S3.1 to obtain

$$\widehat{\mathcal{Z}}_* = \llbracket \widehat{\mathcal{B}}_*; \mathbf{d}_2(\tau^2 C_2 M_1 M_1' C_2'), \mathbf{d}_2(M_3 M_3'), \mathbf{d}_2(M_4 M_4'), \mathbf{d}_2(M_5 M_5') \rrbracket, \quad (\text{S33})$$

where $\mathbf{d}_2(A)$ is a diagonal matrix of the inverse square roots of the diagonal entries of A . Then $\widehat{\mathcal{Z}}_*(i, \cdot, \cdot, \cdot)$ has the TVN distribution, with correlation matrices as scale parameters.

B. Supplement to Section IV-B

The ethnic origin and age-group assignments of these images are from the classifier of [10] that provided values of attributes that are positive for its presence and negative otherwise, along with magnitudes that describe the degree to which the attribute is present or absent (these magnitudes cannot be compared between different attributes). Since these attributes are for all age groups and ethnic origins, we have ambiguous classification for a large majority of the images. We removed ambiguities in age group and ethnic origin by selecting images where (for each factor) the maximum attribute is positive and the other attributes are negative. The genders were as per [9]’s manual assignments of each image. We considered images only of male or female genders, and discarded those that have no or both gender assignments. Although these two filters reduced the number of images to 5,472, they were very imbalanced, as 37% of them corresponded to only one of the $2 \times 3 \times 4 = 24$ factor-combinations (senior males of European ethnicity). While our TANOVA model can handle imbalance, it can provide inaccurate information for the underrepresented factor-combinations. Therefore, we randomly selected at most 33 images for each factor combination, reducing the sample size from 5,472 to 605.

We used the inner $151 \times 111 \times 3$ portion of the original $250 \times 250 \times 3$ voxels where the third dimension corresponds to the color intensities in RGB format, and the logit transformation was applied to every value to match the statespace of the normal distribution.

S4. SUPPLEMENT TO SECTION V

[28] recently reported blocking behavior in the direction of the modes of \mathcal{B} when estimating it via low-rank CP and TK formats and in the context of a scalar-on-tensor regression framework. We provide a limited evaluation to see if this behavior is also exhibited in ToTR, for instance, in imaging applications, when we use BIC to tune the ranks. Our evaluation is in the context of the balanced TANOVA(1,2) model

$$Y_i = \langle \mathbf{x}_i | \mathcal{B} \rangle + E_i, \quad E_i \stackrel{iid}{\sim} \mathcal{N}_{[61,76]'}(0, \sigma^2, \Sigma_1, \Sigma_2), \quad (\text{S34})$$

with \mathcal{B} being a 3-way tensor of size $2 \times 61 \times 76$, which we chose from the inner 61×76 portion (eliminating all rows and columns consisting only of background pixels) of the 128×128 digitized Hoffman phantom of [95] and recently adapted by [73] for use in fMRI simulation experiments. The original phantom [95] is a digitized representation of the brain, and the inner (61×76) portion of this phantom formed the first layer (*i.e.*, $\mathcal{B}[1, :, :]$) of our \mathcal{B} , with the background pixels having value 0, the light foreground pixels having value 1 and the darker foreground pixels having value 2. The second layer $\mathcal{B}[2, :, :]$ had the same values as $\mathcal{B}[1, :, :]$, except for the 138 “truly activated pixels” in two disjoint regions that were introduced by [73] to evaluate activation detection methods in simulation settings. At these pixels, $\mathcal{B}[2, :, :]$ had the value 3. (Fig. S3, top block, displays the two layers of \mathcal{B} .) The vector \mathbf{x}_i (where $i = 1, 2, \dots, 6$) is a 2D binary vector that indicates which of the two phantom images corresponds to $\mathbb{E}(Y_i)$. We let (Σ_1, Σ_2) be AR(1) correlation matrices with coefficients $(\rho_1, \rho_2) \in \{(0.25, 0.35), (0.6, 0.8)\}$ to represent cases with low and high correlations among the errors and set $\sigma \in \{0.2, 0.4, 0.6, 0.8, 1\}$, for five different noise settings. Fig. S3 (top row of middle and bottom blocks) shows sample realizations of the model under lower (middle block)

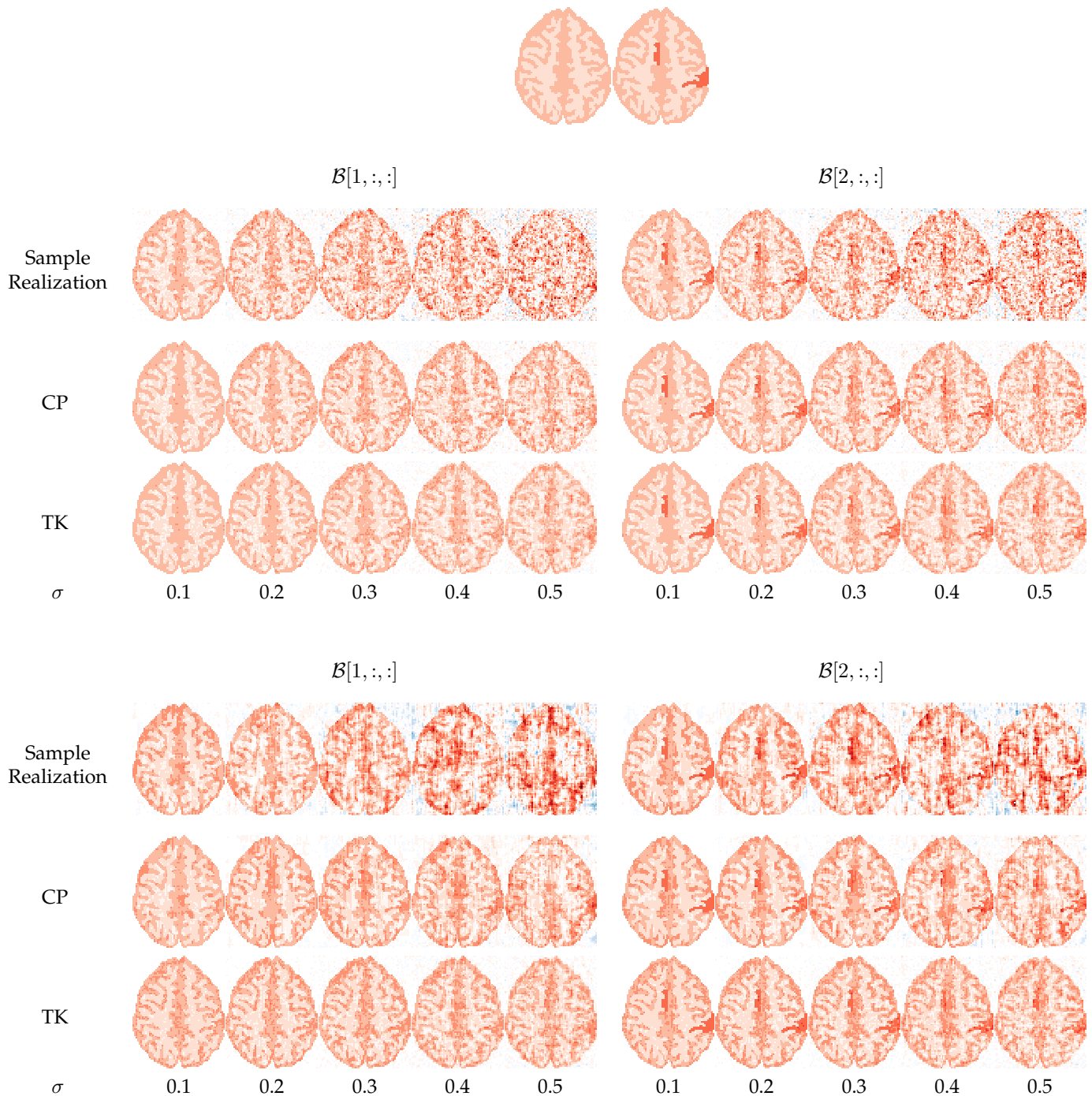


Fig. S3. The top block displays the modified Hoffman's phantom [73] that formed our true \mathcal{B} in the experiments of Section reevaluation-arxiv. The second block displays a sample realization (first row) and the $\hat{\mathcal{B}}$ (left block corresponds to the first layer of \mathcal{B} , right block corresponds to the second layer of \mathcal{B}) using the CP (second row) and TK (third row) formats, with optimal ranks estimated by BIC, for $\sigma = 0.1, 0.2, 0.3, 0.4, 0.5$, with data generated having modest AR(1) correlations: $\rho_1 = 0.25, \rho_2 = 0.35$. The bottom block is similar to the middle block, but it displays performance in the high AR(1) correlations case: here, $\rho_1 = 0.6, \rho_2 = 0.8$. We see that although increasing variance and AR(1) correlation lead to noisier sample realizations and parameter estimates, the anatomy of brain structure, and the activation is largely recovered by both formats, even when we have only three realizations under each setting.

and high correlations (bottom block) cases. We estimated \mathcal{B} assuming CP and TK formats, with ranks tuned using BIC, as per Section II-E, and displayed these $\hat{\mathcal{B}}$ s in the second and third rows of the middle and lower blocks of Fig. S3. These estimates show good recovery in \mathcal{B} in all cases, of both the putative anatomical and activation regions, even though it is understandable that this performance depreciates with higher noise and intra-brain correlation coefficients. Lower σ s yield larger optimal ranks for both TK and CP, while increasing the AR(1) coefficients increases the model complexity. The figures also indicate that there

is not much appreciable blocking effect in the direction of the modes of the tensor. We however, observed blocking behavior, earlier with the CP and TK (and also TR) formats when the ranks were set (Figure III-A), but not when we allowed BIC to choose these ranks. We also did not observe such patterns with the TR format and BIC-tuned ranks in Fig. 9, even though we achieved a parameter reduction of over 99%. Therefore, while further investigations are needed, our initial evaluations here show that our BIC-optimized reduced-rank (CP and TK) format ToTR and TANOVA do not induce unwanted directional effects, therefore showing promise in imaging and other applications.

REFERENCES

- [1] R. A. Johnson and D. W. Wichern, *Applied multivariate statistical analysis*. Pearson, 2008.
- [2] R. Tibshirani, "Regression Shrinkage and Selection Via the Lasso," *Journal of the Royal Statistical Society: Series B (Methodological)*, vol. 58, no. 1, pp. 267–288, Jan. 1996.
- [3] J. Friedman, T. Hastie, and R. Tibshirani, "Sparse inverse covariance estimation with the graphical lasso," *Biostatistics*, vol. 9, no. 3, pp. 432–441, Jul. 2008.
- [4] R. D. Cook, B. Li, and F. Chiaromonte, "Envelope models for parsimonious and efficient multivariate linear regression," *Statistica Sinica*, vol. 20, no. 3, pp. 927–960, 2010.
- [5] A. Mukherjee and J. Zhu, "Reduced rank ridge regression and its kernel extensions," *Statistical Analysis and Data Mining*, vol. 4, no. 6, pp. 612–622, Dec. 2011.
- [6] K. A. Busch, J. Fawcett, and D. G. Jacobs, "Clinical correlates of inpatient suicide," *Journal of Clinical Psychiatry*, vol. 64, 2003.
- [7] M. A. Just, L. Pan, V. L. Cherkassky, D. McMakin, C. Cha, M. K. Nock, and D. Brent, "Machine learning of neural representations of suicide and emotion concepts identifies suicidal youth," *Nature Human Behaviour*, vol. 1, pp. 911–919, 2017.
- [8] G. B. Huang, M. Ramesh, T. Berg, and E. Learned-Miller, "Labeled faces in the wild: A database for studying face recognition in unconstrained environments," University of Massachusetts, Amherst, Tech. Rep., October 2007.
- [9] M. Afifi and A. Abdelhamed, "Afif4: Deep gender classification based on adaboost-based fusion of isolated facial features and foggy faces," *Journal of Visual Communication and Image Representation*, vol. 62, pp. 77 – 86, 2019.
- [10] N. Kumar, A. C. Berg, P. N. Belhumeur, and S. K. Nayar, "Attribute and simile classifiers for face verification," in *2009 IEEE 12th International Conference on Computer Vision*, Sep. 2009, pp. 365–372.
- [11] X. Bi, X. Tang, Y. Yuan, Y. Zhang, and A. Qu, "Tensors in statistics," *Annual Review of Statistics and Its Application*, vol. 8, no. 1, pp. 345–368, 2021.
- [12] Y. Panagakis, J. Kossaifi, G. G. Chrysos, J. Oldfield, M. A. Nicolaou, A. Anandkumar, and S. Zafeiriou, "Tensor methods in computer vision and deep learning," *Proceedings of the IEEE*, vol. 109, no. 5, pp. 863–890, 2021.
- [13] P. Hoff, "Multilinear tensor regression for longitudinal relational data," *The Annals of Applied Statistics*, vol. 9, 11 2014.
- [14] W. W. Sun and L. Li, "STORE: sparse tensor response regression and neuroimaging analysis," *The Journal of Machine Learning Research*, vol. 18, no. 1, pp. 4908–4944, Jan. 2017.
- [15] L. Li and X. Zhang, "Parsimonious tensor response regression," *Journal of the American Statistical Association*, vol. 112, no. 519, pp. 1131–1146, 2017.
- [16] W. Guo, I. Kotsia, and I. Patras, "Tensor learning for regression," *IEEE Transactions on Image Processing*, vol. 21, no. 2, pp. 816–827, 2012.
- [17] Y. Fu, J. Gao, X. Hong, and D. Tien, "Tensor regression based on linked multiway parameter analysis," in *2014 IEEE International Conference on Data Mining*, 2014, pp. 821–826.
- [18] H. Zhou, L. Li, and H. Zhu, "Tensor regression with applications in neuroimaging data analysis," *Journal of the American Statistical Association*, vol. 108, no. 502, pp. 540–552, 12 2013.
- [19] X. Li, H. Zhou, and L. Li, "Tucker tensor regression and neuroimaging analysis," *Statistics in Biosciences*, Mar 2018.
- [20] C. Li and H. Zhang, "Tensor quantile regression with application to association between neuroimages and human intelligence," *Annals of Applied Statistics*, vol. 15, no. 3, pp. 1455–1477, 2021.
- [21] G. Rabusseau and H. Kadri, "Low-Rank Regression with Tensor Responses," *Advances in Neural Information Processing Systems*, no. 29, p. 15, 2016.
- [22] R. Guhaniyogi, S. Qamar, and D. B. Dunson, "Bayesian tensor regression," *Journal of Machine Learning Research*, vol. 18, no. 79, pp. 1–31, 2017.
- [23] T. Ahmed, H. Raja, and W. U. Bajwa, "Tensor regression using low-rank and sparse Tucker decompositions," *SIAM Journal on Mathematics of Data Science*, vol. 2, no. 4, pp. 944–966, 2020.
- [24] D. Kong, B. An, J. Zhang, and H. Zhu, "L2rm: Low-rank linear regression models for high-dimensional matrix responses," *Journal of the American Statistical Association*, vol. 115, no. 529, pp. 403–424, 2020.
- [25] Y. Zhou, R. K. W. Wong, and K. He, "Tensor Linear Regression: Degeneracy and Solution," *IEEE Access*, vol. 9, 2021.
- [26] Y. Deng, X. Tang, and A. Qu, "Correlation tensor decomposition and its application in spatial imaging data," *Journal of the American Statistical Association*, vol. 0, no. 0, pp. 1–17, 2021.
- [27] J. C. Poythress, J. Ahn, and C. Park, "Low-rank, orthogonally decomposable tensor regression with application to visual stimulus decoding of fmri data," *Journal of Computational and Graphical Statistics*, vol. 0, no. 0, pp. 1–14, 2021.
- [28] G. Papadogeorgou, Z. Zhang, and D. B. Dunson, "Soft tensor regression," *Journal of Machine Learning Research*, vol. 22, no. 219, pp. 1–53, 2021. [Online]. Available: <http://jmlr.org/papers/v22/20-476.html>
- [29] E. Lock, "Tensor-on-tensor regression," *Journal of Computational and Graphical Statistics*, 01 2017.
- [30] J. D. Carroll and J.-J. Chang, "Analysis of individual differences in multidimensional scaling via an n-way generalization of "Eckart-Young" decomposition," *Psychometrika*, vol. 35, no. 3, 1970.
- [31] R. A. Harshman, "Foundations of the parafac procedure: Models and conditions for an explanatory" multi-modal factor analysis," *UCLA Working Papers in Phonetics*, no. 16, 1970.
- [32] Y. Liu, J. Liu, and C. Zhu, "Low-Rank Tensor Train Coefficient Array Estimation for Tensor-on-Tensor Regression," *IEEE Transactions on Neural Networks and Learning Systems*, vol. 31, Dec. 2020.
- [33] C. Llosa, "Tensor on tensor regression with tensor normal errors and tensor network states on the regression parameter," *Iowa State University Creative Components*, vol. 82, Jan. 2018. [Online]. Available: <https://lib.dr.iastate.edu/creativecomponents/82>
- [34] W. Zhao, K. M. Kendrick, F. Chen, H. Li, and T. Feng, "Neural circuitry involved in quitting after repeated failures: role of the cingulate and temporal parietal junction," *Scientific Reports*, vol. 6, no. 1, p. 24713, Apr. 2016.
- [35] I. Oseledets, "Tensor-train decomposition," *SIAM Journal on Scientific Computing*, vol. 33, no. 5, pp. 2295–2317, 2011.
- [36] G. Brandi and T. Di Matteo, "Predicting multidimensional data via tensor learning," *Journal of Computational Science*, vol. 53, p. 101372, 2021.
- [37] L. R. Tucker, "Some mathematical notes on three-mode factor analysis," *Psychometrika*, vol. 31, no. 3, pp. 279–311, Sep 1966.
- [38] T. G. Kolda and B. W. Bader, "Tensor decompositions and applications," *SIAM Review*, vol. 51, no. 3, pp. 455–500, September 2009.
- [39] M. Bahri, Y. Panagakis, and S. Zafeiriou, "Robust Kronecker-Decomposable Component Analysis for Low-Rank Modeling," in *2017 IEEE International Conference on Computer Vision (ICCV)*, Oct. 2017, pp. 3372–3381.
- [40] P. Hoff, "Separable covariance arrays via the Tucker product, with applications to multivariate relational data," *Bayesian Analysis*, vol. 6, no. 2, pp. 179–196, 06 2011.

- [41] D. Akdemir and A. Gupta, "Array variate random variables with multiway kronecker delta covariance matrix structure," *Journal of Algebraic Statistics*, vol. 2, pp. 98–113, 01 2011.
- [42] M. Ohlson, M. R. Ahmad, and D. von Rosen, "The multilinear normal distribution: Introduction and some basic properties," *Journal of Multivariate Analysis*, vol. 113, pp. 37 – 47, 2013.
- [43] A. M. Manceur and P. Dutilleul, "Maximum likelihood estimation for the tensor normal distribution: Algorithm, minimum sample size, and empirical bias and dispersion," *Journal of Computational and Applied Mathematics*, vol. 239, pp. 37 – 49, 2013.
- [44] T. G. Kolda, "Multilinear operators for higher-order decompositions." Sandia National Laboratories, Tech. Rep. SAND2006-2081, 923081, Apr. 2006.
- [45] A. Cichocki, N. Lee, I. Oseledets, A.-H. Phan, Q. Zhao, and D. P. Mandic, "Tensor networks for dimensionality reduction and large-scale optimization: Part 1 low-rank tensor decompositions," *Foundations and Trends® in Machine Learning*, vol. 9, no. 4-5, 2016.
- [46] L. De Lathauwer, B. De Moor, and J. Vandewalle, "A multilinear singular value decomposition," *SIAM Journal on Matrix Analysis and Applications*, vol. 21, no. 4, pp. 1253–1278, 2000.
- [47] D. Gerard and P. Hoff, "A higher-order LQ decomposition for separable covariance models," *Linear Algebra and its Applications*, vol. 505, pp. 57 – 84, 2016.
- [48] R. Orús, "A practical introduction to tensor networks: Matrix product states and projected entangled pair states," *Annals of Physics*, vol. 349, pp. 117 – 158, 2014.
- [49] G. Z. Thompson, R. Maitra, W. Q. Meeker, and A. F. Bastawros, "Classification With the Matrix-Variate-t Distribution," *Journal of Computational and Graphical Statistics*, vol. 29, no. 3, Jul. 2020.
- [50] A. Gupta and D. Nagar, *Matrix Variate Distributions*. Taylor & Francis, 1999.
- [51] M. M. Wolf, F. Verstraete, M. B. Hastings, and J. I. Cirac, "Area laws in quantum systems: Mutual information and correlations," *Physical review letters*, vol. 100, p. 070502, 03 2008.
- [52] M. S. Srivastava, T. von Rosen, and D. von Rosen, "Models with a kronecker product covariance structure: Estimation and testing," *Mathematical Methods of Statistics*, vol. 17, no. 4, Dec 2008.
- [53] J. de Leeuw, "Block-relaxation algorithms in statistics," in *Information Systems and Data Analysis*. Berlin, Heidelberg: Springer Berlin Heidelberg, 1994, pp. 308–324.
- [54] H. Abdi, "Singular value decomposition (svd) and generalized singular value decomposition (gsvd)," *Encyclopedia of Measurement and Statistics.*, 01 2007.
- [55] H. Glanz and L. Carvalho, "An expectation maximization algorithm for the matrix normal distribution with an application in remote sensing," *Journal of Multivariate Analysis*, vol. 167, 2018.
- [56] C. Viroli, "On matrix-variate regression analysis," *Journal of Multivariate Analysis*, vol. 111, pp. 296 – 309, 2012.
- [57] S. Ding and R. Cook, "Matrix-variate regressions and envelope models," *Journal of the Royal Statistical Society: Series B (Statistical Methodology)*, vol. 80, 05 2016.
- [58] W. Hackbusch and S. Kühn, "A new scheme for the tensor representation," *Journal of Fourier Analysis and Applications*, vol. 15, pp. 706–722, 10 2009.
- [59] L. Grasedyck, "Hierarchical singular value decomposition of tensors," *SIAM Journal on Matrix Analysis and Applications*, vol. 31, no. 4, pp. 2029–2054, 2010.
- [60] I. D. Currie, M. Durban, and P. H. C. Eilers, "Generalized Linear Array Models with Applications to Multidimensional Smoothing," *Journal of the Royal Statistical Society. Series B (Statistical Methodology)*, vol. 68, no. 2, pp. 259–280, 2006.
- [61] R. Kashyap, "A bayesian comparison of different classes of dynamic models using empirical data," *IEEE Transactions on Automatic Control*, vol. 22, no. 5, pp. 715–727, 1977.
- [62] G. Schwarz, "Estimating the dimension of a model," *Ann. Statist.*, vol. 6, no. 2, pp. 461–464, 03 1978.
- [63] K. V. Mardia, J. T. Kent, and J. M. Bibby, *Multivariate analysis*. New York: Academic Press, 1979.
- [64] R. Heller, D. Stanley, D. Yekutieli, N. Rubin, and Y. Benjamini, "Cluster-based analysis of fMRI data," *NeuroImage*, vol. 33, no. 2, pp. 599–608, nov 2006.
- [65] R. W. Cox, "AFNI: software for analysis and visualization of functional magnetic resonance neuroimages," *Computers and Biomedical research*, vol. 29, no. 3, pp. 162–173, 1996.
- [66] R. W. Cox and J. S. Hyde, "Software tools for analysis and visualization of fMRI data," *NMR in Biomedicine*, vol. 10, no. 4-5, pp. 171–178, 1997.
- [67] C. R. Genovese, N. A. Lazar, and T. Nichols, "Thresholding of statistical maps in functional neuroimaging using the false discovery rate," *Neuroimage*, vol. 15, pp. 870–878, 2002.
- [68] Y. Benjamini and R. Heller, "False discovery rates for spatial signals," *Journal of the American Statistical Association*, vol. 102, no. 480, pp. 1272–1281, 2007.
- [69] M. Smith and L. Fahrmeir, "Spatial Bayesian variable selection with application to ffunctional Magnetic Resonance Imaging," *Journal of the American Statistical Association*, vol. 102, no. 478, pp. 417–431, 2007.
- [70] S. M. Smith and T. E. Nichols, "Threshold-free cluster enhancement: Addressing problems of smoothing, threshold dependence and localisation in cluster inference," *Neuroimage*, vol. 44, 2009.
- [71] K. Tabelow, J. Polzehl, H. U. Voss, and V. Spokoiny, "Analyzing fMRIexperiments with structural adaptive smoothing procedures," *NeuroImage*, vol. 33, no. 1, pp. 55–62, 2006.
- [72] J. Polzehl, H. U. Voss, and K. Tabelow, "Structural adaptive segmentation for statistical parametric mapping," *NeuroImage*, vol. 52, no. 2, pp. 515–523, 2010.
- [73] I. A. Almodóvar-Rivera and R. Maitra, "FAST adaptive smoothed thresholding for improved activation detection in low-signal fMRI," *IEEE Transactions on Medical Imaging*, vol. 38, no. 12, pp. 2821–2828, 2019.
- [74] W. Cheng, E. T. Rolls, J. Qiu, D. Yang, H. Ruan, D. Wei, L. Zhao, J. Meng, P. Xie, and J. Feng, "Functional Connectivity of the Precuneus in Unmedicated Patients With Depression," *Biological Psychiatry: Cognitive Neuroscience and Neuroimaging*, vol. 3, no. 12, pp. 1040–1049, Dec. 2018.
- [75] Y. Jacob, L. S. Morris, K.-H. Huang, M. Schneider, S. Rutter, G. Verma, J. W. Murrough, and P. Balchandani, "Neural correlates of rumination in major depressive disorder: A brain network analysis," *NeuroImage: Clinical*, vol. 25, p. 102142, Jan. 2020.
- [76] H.-X. Zhou, X. Chen, Y.-Q. Shen, L. Li, N.-X. Chen, Z.-C. Zhu, F. X. Castellanos, and C.-G. Yan, "Rumination and the default mode network: Meta-analysis of brain imaging studies and implications for depression," *NeuroImage*, vol. 206, p. 116287, Feb. 2020.
- [77] A. Bechara, H. Damasio, and A. R. Damasio, "Emotion, Decision Making and the Orbitofrontal Cortex," *Cerebral Cortex*, vol. 10, no. 3, pp. 295–307, Mar. 2000.
- [78] F. Jollant, N. S. Lawrence, V. Giampietro, M. J. Brammer, M. A. Fullana, D. Drapier, P. Courtet, and M. L. Phillips, "Orbitofrontal cortex response to angry faces in men with histories of suicide attempts," *The American Journal of Psychiatry*, vol. 165, no. 6, pp. 740–748, Jun. 2008.
- [79] A. B. Satpute and K. A. Lindquist, "The Default Mode Network's Role in Discrete Emotion," *Trends in Cognitive Sciences*, vol. 23, no. 10, pp. 851–864, Oct. 2019.
- [80] S. R. Simon, M. Meunier, L. Piettre, A. M. Berardi, C. M. Segebarth, and D. Boussaoud, "Spatial attention and memory versus motor preparation: premotor cortex involvement as revealed by fMRI," *Journal of Neurophysiology*, vol. 88, no. 4, pp. 2047–2057, Oct. 2002.
- [81] M. Koenigs, A. K. Barbey, B. R. Postle, and J. Grafman, "Superior Parietal Cortex Is Critical for the Manipulation of Information in Working Memory," *Journal of Neuroscience*, vol. 29, no. 47, pp. 14 980–14 986, Nov. 2009.
- [82] J. J. Maller, R. H. S. Thomson, J. V. Rosenfeld, R. Anderson, Z. J. Daskalakis, and P. B. Fitzgerald, "Occipital bending in depression," *Brain*, vol. 137, no. 6, pp. 1830–1837, Jun. 2014.

- [83] R. Smith, R. D. Lane, A. Alkozei, J. Bao, C. Smith, A. Sanova, M. Nettles, and W. D. S. Killgore, "The role of medial prefrontal cortex in the working memory maintenance of one's own emotional responses," *Scientific Reports*, vol. 8, no. 1, p. 3460, Feb. 2018.
- [84] E. T. Rolls, "The cingulate cortex and limbic systems for action, emotion, and memory," *Handbook of Clinical Neurology*, vol. 166, pp. 23–37, 2019.
- [85] E. J. Bubb, L. Kinnavane, and J. P. Aggleton, "Hippocampal – diencephalic – cingulate networks for memory and emotion: An anatomical guide," *Brain and Neuroscience Advances*, vol. 1, 2017.
- [86] S. R. Heilbronner, B. Y. Hayden, and M. L. Platt, "Decision Salience Signals in Posterior Cingulate Cortex," *Frontiers in Neuroscience*, vol. 5, Apr. 2011.
- [87] Q. Zhao, G. Zhou, S. Xie, L. Zhang, and A. Cichocki, "Tensor ring decomposition," *CoRR*, vol. abs/1606.05535, 2016.
- [88] D. Zaitchik, C. Walker, S. Miller, P. LaViolette, E. Feczko, and B. C. Dickerson, "Mental state attribution and the temporoparietal junction: An fMRI study comparing belief, emotion, and perception," *Neuropsychologia*, vol. 48, no. 9, pp. 2528–2536, Jul. 2010.
- [89] G. Lettieri, G. Handjaras, E. Ricciardi, A. Leo, P. Papale, M. Betta, P. Pietrini, and L. Cecchetti, "Emotionotopy in the human right temporo-parietal cortex," *Nature Communications*, vol. 10, no. 1, p. 5568, Dec. 2019.
- [90] L. G. Ungerleider, S. M. Courtney, and J. V. Haxby, "A neural system for human visual working memory," *Proceedings of the National Academy of Sciences*, vol. 95, no. 3, pp. 883–890, Feb. 1998.
- [91] J. R. Magnus and H. Neudecker, *Matrix differential calculus with applications in statistics and econometrics*, third edition ed., ser. Wiley series in probability and statistics. Wiley, 2019.
- [92] K. B. Petersen and M. S. Pedersen, "The matrix cookbook," nov 2012, version 20121115.
- [93] E. L. Lehmann, *Elements of large-sample theory*, ser. Springer texts in statistics. New York: Springer, 1999.
- [94] T.-T. Lu and S.-H. Shiou, "Inverses of 2 x 2 block matrices," *Computers & Mathematics with Applications*, vol. 43, no. 1, pp. 119–129, 2002.
- [95] E. Hoffman, P. Cutler, W. Digby, and J. Mazziotta, "3-d phantom to simulate cerebral blood flow and metabolic images for pet," *IEEE Transactions on Nuclear Science*, vol. 37, no. 2, pp. 616–620, 1990.